Random Functions in Landscape Cosmology

Lerh Feng Low

A thesis submitted in fulfilment of the requirements for the degree of Doctor of Philosophy in Physics, the University of Auckland, 2021.

Abstract

String theory suggests that our universe is but one of a vast number of possible universes, with each universe corresponding to a minimum in the so-called *landscape*. Because of the complexity of the landscape, direct analysis is very difficult. In this thesis, we adopt an indirect approach: we model the landscape as a random Gaussian field, deriving baseline expectations for the landscape's properties based solely on large-number statistics. We find that many of the properties of the landscape depend on a single parameter, γ, that is related to the power spectrum of the landscape. We further calculate numerous properties of interest, such as the probability of finding a minimum with a positive vacuum energy, the slopes of the potential near such a minimum, and the inflationary slow-roll parameter η at saddles with one downhill direction. We identify regions of the parameter space where inflation is viable, as well as regions in which a universe resembling ours can occur.

Acknowledgements

With great thanks to the members of my research group during the course of my PhD: Professor Richard Easther, Drs. Shaun Hotchkiss, Mateja Gosenca, and Nathan Musoke, and future Drs. Emily Kendall, Lilian Guo, and Frank Wang.

Support from a University of Auckland Doctoral Scholarship is gratefully acknowledged.

Contents

Chapter 1

Introduction

1.1 Introduction

In the beginning, there was the Big Bang. Shortly after the Big Bang, there was inflation.[1]

The mechanism responsible for inflation is unknown. The leading framework is so-called "slow-roll inflation", with inflation driven by a single, minimally-coupled scalar field called the *inflaton*. Slow-roll inflation is described by two parameters,

$$\begin{aligned} \epsilon &= \frac{M_P^2}{2}\left(\frac{V'}{V}\right)^2 \\ \eta &= M_P^2\left|\frac{V''}{V}\right| \end{aligned} \tag{1.1}$$

where M_P is the Planck mass $\sqrt{\frac{\hbar c}{8\pi G}}$, V is the the inflaton potential, and V' is its derivative with respect to its parameters ϕ.[2] Inflation occurs when the slow-roll parameters ϵ and η are small, which happens when the first and second derivatives of the inflaton are small. Therefore the universe inflates whenever the gradient of the inflaton is small, hence the name "slow-roll".

Inflation ends once the slow-roll parameters are no longer small.[3] After rolling

[1] In this thesis, we assume inflation happened. There is strong evidence that inflation happened [40], but it remains a hypothesis.

[2] Here we use the common notation denoting the inflaton as $V(\phi)$.

[3] Strictly speaking, inflation ends once $\epsilon = 1$, and furthermore, η does not need to be small to

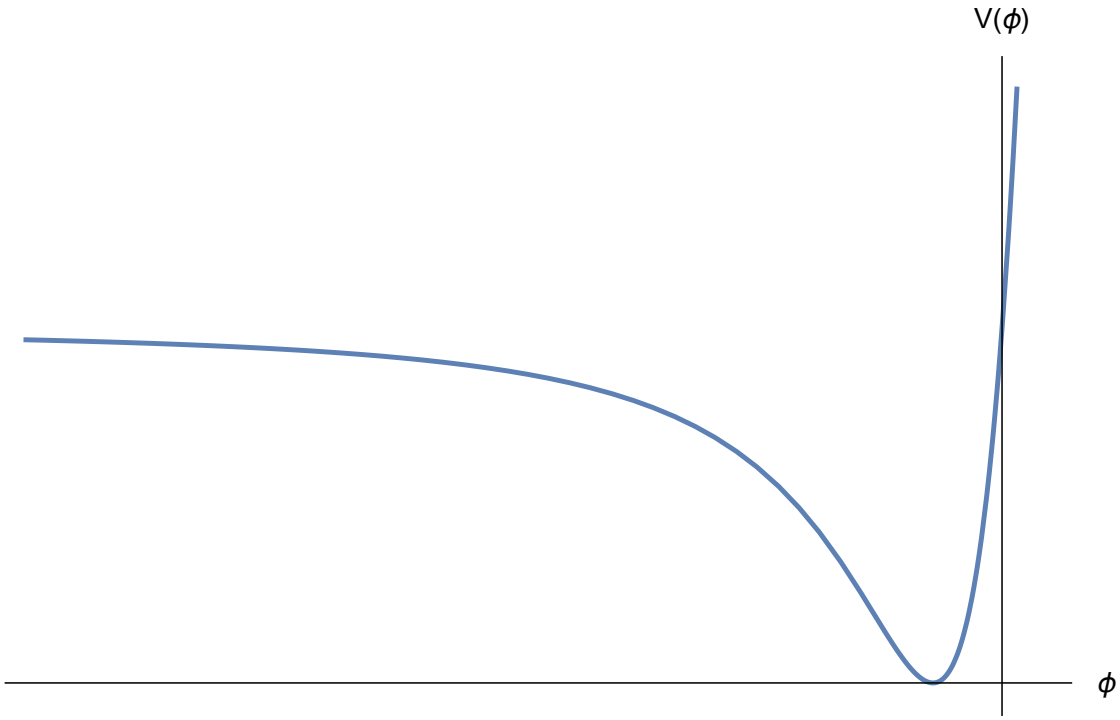

Figure 1.1: In this toy example, our universe would inflate when the inflaton $V(\phi)$ is on the left where the gradient is small, before eventually settling at the minimum. The inflaton value at this particular minimum is zero, implying that the vacuum energy is zero. (Arbitrary units)

down the inflaton potential, the universe eventually settles in a minimum (see Fig. 1.1). The value of the inflaton potential at this minimum manifests as *vacuum energy*.[4] If the vacuum energy is positive, it is repulsive, which is especially relevant because observations indicate our universe contains dark energy. If the vacuum energy is negative, then it is attractive, and the universe will eventually contract into a Big Crunch.

Although the nature of the inflaton is not well-understood, the high energy scale of inflation suggests that string theory is a natural setting in which to investigate

have inflation (see *ultra slow roll inflation* [2]). However, getting inflation with $\eta > 1$ requires tuning: without it, a large η would imply that V'' is large, and by extension V' (and therefore ϵ) varies wildly. We can have inflation with $\eta > 1$, but probably not prolonged inflation.

[4]Vacuum energy is the energy present in a vacuum. Intuitively, we might expect this to be zero, but there is no *a priori* reason it has to be zero. Indeed, if dark energy is due to a cosmological constant, there would be positive vacuum energy.

it. String theory includes 10 or 11 space-time dimensions, which is clearly at odds with the 4-dimensional universe that we observe. To make the theory compatible with observations, we need to "compactify" the extra dimensions – i.e., find a way to roll up the extra dimensions until they are small enough to evade detection. There are many different ways to perform these compactifications in string theory, not all of which are compatible with gravity. These inconsistent theories are often referred to as the "swampland", while the remainder form the "landscape". In this picture, one of the theories in the landscape is the Standard Model of our universe.

The string theory landscape is extremely (possibly intractably) complicated. The number of scalar fields ("moduli") that can be used to construct a new theory is in the hundreds, possibly thousands. Estimates for the number of minima ("vacua") range from 10^{500} to 10^{27200} [3].[5] The landscape effectively defines the "overall" laws of physics. However, the "effective" laws of physics at low energies[6] vary with position in the landscape. The vast number of vacua in the landscape has historically led string theorists to assume that there must be a vacuum with low-energy properties that correspond to our Standard Model.

Making sense of the landscape is a tantalizing prospect, because it can potentially answer some of the deepest questions imaginable. Traditionally, physics has had no good answer to the question, "Why does our universe have the laws it does?" Perhaps the only possible explanation was the Anthropic Principle – if the universe didn't have those laws, then there wouldn't exist intelligent life which can ask "why?" in the first place. This anthropic reasoning makes many people uncomfortable [5]. However, in the context of the string landscape, we can frame probabilities for why the laws of physics are what they appear to be.

Because the string landscape is so complicated, it is not easy to make sense of it. Nonetheless, there are attempts at deriving constraints on the landscape. The *swampland conjectures* [18, 19, 20, 21] attempt to delineate precise conditions that must be obeyed by all vacua in the landscape. An example is the weak gravity conjecture [6]. In our universe, gravity is by far the weakest of the four fundamental forces. The weak gravity conjecture goes further and suggests that, for a theory

[5]For comparison, an order of magnitude estimate for the number of atoms in the observable universe is 10^{80} [4].

[6]Here "low energies" refers to Large Hadron Collider scales and below – the regime which we have probed with experiments.

to be consistent, it must require that gravity is the weakest of the four forces. If the conjecture is true, it would draw a clear line separating the landscape from the swampland.

An alternative way to approach the landscape is to treat it as a purely random function, or in practice, a *random Gaussian field*. If a field F is written as a sum of Fourier components, and if those Fourier components are independent and random, then the sum of sufficiently many terms would tend towards a random Gaussian field by the Central Limit Theorem. There is no guarantee that the terms that make up the landscape are indeed random and independent, but this approach sets a baseline expectation – it depends solely on the landscape being comprised of many terms. This is the simplest choice for a random field, depending primarily on large-number statistics and without requiring any knowledge of their interactions, no matter how complicated they may be. Any significant deviation from this baseline expectation would, in turn, point to "structure" in the landscape.

The first work utilizing this 'random' approach was by Aazami & Easther [7]. The authors investigated the eigenvalues of random Hessian matrices associated with extrema of a random function. From the purely mathematical constraint that derivatives commute,[7] the Hessian matrices are symmetric. The eigenvalues of random symmetric matrices converge to a semicircle distribution in the limit of large number of dimensions, a result first derived by Wigner in the 1950s [8, 9]. The Wigner semicircle is evenly distributed around zero, implying equal numbers of positive and negative eigenvalues. In our case, we are interested in minima, which is equivalent to requiring that every eigenvalue of the Hessian at the point under consideration is positive.[8] This requires a massive deviation from the Wigner semicircle. If we assume that each eigenvalue has equal probability of being positive or negative, then because there are N eigenvalues in an N-dimensional case, we get that the probability of a minimum is 2^{-N}. Aazami and Easther argued that this simple estimate is too large: assuming that the elements of the Hessian are

[7] Mathematically, $\partial/\partial x(\partial V/\partial y) = \partial/\partial y(\partial V/\partial x)$.

[8] The work on which we build in Section 2 [54] uses the opposite sign convention, where maxima have positive eigenvalues. The difference arises from the characterisation of random density fields, for which the gravitational potential has a minimum where the density has a maximum. We will work with this convention for consistency, but will be careful to resolve any ambiguity when discussing physical results in the landscape.

random numbers drawn from identical and independent distributions, eigenvalues are very unlikely to take nearly-equal values, a phenomenon called "eigenvalue repulsion". This renders the probability of a minimum much smaller than 2^{-N}. Aazami and Easther calculated that minima are super-exponentially ($\propto e^{-N^2}$) suppressed, and therefore minima are vastly outnumbered by saddles. Chen *et al.* also described this result [10]. However, this early result was later shown to be incomplete, because the individual elements of the Hessian are not independently random [11, 32]. This leads to a density of minima that still decreases exponentially, but not super-exponentially. The result is more minima, although minima are still drastically outnumbered by saddles. [32, 33].

Following on this early work, Tye, Xu and Zhang investigated the density perturbations that might emerge from inflation driven by multiple random Gaussian fields, concluding from general arguments that the universe will likely undergo Brownian-like motion on top of the overall drift towards lower values. They found that in the case where scattering is frequent but weak, the resulting power spectrum is similar to that of single-field slow-roll inflation; but in the case where scattering is frequent and strong, much more interesting things happen, such as detectable features in the Cosmic Microwave Background (CMB) power spectrum [16]. However, this scenario also leads to an enhanced tensor-to-scalar ratio in the CMB, which is not supported by recent results [43, 57]. Another feature found by Tye, Xu and Zhang is that non-Gaussianity is suppressed, a feature observed to be generic to random Gaussian fields by Frazer & Liddle and Bjorkmo & Marsh using different methods [17, 23].

Separately, numerous papers have developed the overall problem of large excursion statistics of random matrices. Utilizing a random matrix theory approach, Bray & Dean computed the number of critical points (including both minima/maxima and saddles) as a function of their field value and their index – the number of positive or negative eigenvalues – and arrived at the intuitive result that above a certain threshold energy, almost all critical points are maxima [12]. Also utilizing random matrix theory, Dean & Majumdar investigated the probability of large deviations in the eigenvalues at critical points from the average value [13, 14] and Majumdar *et al.* calculated the probability distribution of the number of positive eigenvalues [15]. All these studies involved a large N limit, an assumption that

might not work well for the string theory landscape, where $N \sim 100$ and is not necessarily "large".

An alternative way to view the word "random" is in the context of random functions. These are random elements in the space of all possible functions. A very simple example of how one might generate a random function is to take the Taylor expansion near a critical point and draw the coefficients of the Taylor expansion from a random distribution. Papers utilizing the random function approach include Agarwal *et al.* [22] and Bjorkmo & Marsh [23, 24]. All three papers study the probability of getting inflation that yields observables matching observations, such as the probability of getting at least 60 e-folds of inflation in the landscape. Agarwal *et al.* found emergent properties in the generated random potential, and in particular the probability of getting N_e e-folds of inflation prior to a waterfall transition scales as $P(N_e) \propto -N_e^3$. This result implies that long periods of inflation are unlikely, with short bursts being the most probable; in particular the fraction of inflationary trajectories that yield 60 e-folds of accelerated growth is only about 10^{-5}. This low probability is also the conclusion of He *et al.* [25]. Nonetheless, if we examine only the regions of the random potential in which inflation lasted for 60 e-folds, Bjorkmo & Marsh found that compatibility with Planck's results is not rare [23].

Yet another approach is Dyson Brownian motion. Originally proposed by Freeman Dyson [29], the method evolves the elements of the Hessian and/or its eigenvalues stochastically with the Langevin equation. This can then be used to find the equilibrium eigenvalues (i.e., the eigenvalues at the minimum), or to calculate the universe's trajectory in the landscape as it evolves. It should be noted that the Dyson Brownian motion method is fundamentally different from the random Gaussian field method, and hence the two can yield different results. However, at large N, the two methods converge [23].

Using the Dyson Brownian motion method, Marsh *et al.* investigated the inflationary trajectories of specific universes, a problem which had previously appeared computationally prohibitive [26]. Marsh *et al.* successfully sidestepped the heavy computational costs by only realizing the potential around the specific trajectory. The Hessian matrix is then evolved via Dyson Brownian motion along the inflationary path. The conclusion was that a prolonged period of inflation is

unlikely because eigenvalue repulsion causes the gradient near a saddle to grow [26]. This result was later extended to suggest that the probable resulting power spectra from inflation are not compatible with observations [27]. Simultaneously, theoretical problems with using Dyson Brownian motion to create an inflationary trajectory (such as the fact that it does not yield the same potential value after moving in a closed loop) were discovered, leaving the reliability of the approach in question [27, 28]. Although the method might not generate fully physical inflationary trajectories, it is still useful for investigating the eigenvalues of the Hessian at a saddle: it is capable of producing the most probable eigenvalue distribution at a stationary point that agrees with other methods [34], and its predictions for cosmological observables [36] also agree with those from random functions [24]. Using the Dyson Brownian motion method to evolve the eigenvalues of a random matrix, Dias *et al.* found that as the number of dimensions is increased, the predictions for cosmological observables become sharper; furthermore, these predictions are compatible with Planck's results [35, 36].

A different kind of question to ask is if the minima are stable. Classically they are always "stable" (since the gradient is zero at the minimum), but it is in principle possible to quantum tunnel out of the minimum. Because each minimum has different effective low-energy laws of physics, if this were to happen, the universe as we know it will undoubtedly be destroyed. Tunnelling probability depends on the barrier width and height. Greene *et al.* first found that the distance between minima decreases as the number of dimensions (i.e. scalar fields) is increased, leading to the conclusion that the fraction of minima with lifetimes long enough to be metastable decreases with dimensions [30]. Masoumi and Vilenkin [31] later expanded on this result to find that the stability of a minimum is highly correlated with its energy density, with minima being much more stable at lower energy densities. This result is intuitive, for we would not expect deep (and therefore stable) minima at high energy densities where minima themselves are very rare.

Related to the question of stability is the question of how steep the slopes leading out of the minimum are. This tells us about both the end of inflation and the heights of the barriers around the minima, since gentler slopes also imply a smaller potential barrier to quantum tunnel across. This eigenvalue distribution was analyzed by Yamada & Vilenkin [34] using two different methods. The results

match the intuitive expectation that the higher the energy density of the minimum, the gentler the slopes leading out of it on average. Yamada & Vilenkin also calculate $P(min|\Lambda)$, the probability that a stationary point with a given energy density will be a minimum.

In this thesis, we represent the landscape (the 'potential') as a multidimensional random Gaussian field, which is a function of N independent variables. Within this model to investigate these questions:

1. How likely is it for a minimum to have a potential value $\Lambda > 0$, written mathematically as $P(\Lambda > 0|min)$? What fraction of minima can lead to a long-lived universe, and what is the probability distribution of the possible values of the cosmological constant in these minima?

2. How large are the eigenvalues leading into the most probable minima? This sheds light on possible quintessence scenarios in the landscape with one or more active degrees of freedom.

3. Slow-roll inflation occurs when the gradient of the potential is small. The natural place in the landscape for this to happen is a saddle with only one downhill direction (henceforth '1-saddle'). How steep is the slope leading out of typical saddles, and how does this depend on the 1-saddle's potential value Λ?

The first question tells us how likely it is that an observer in the landscape will observe dark energy.[9] The second tells us about the end of inflation and the approach to our current universe. The final question tells us about inflation itself – in particular, if we can calculate the slow-roll parameter η, we might be able to say something about how probable inflation is in the multiverse. We will start with theoretical derivations in Chapter 2, then deal with the three questions in Chapters 3–5. Finally, we will point out future work and conclude in Chapter 6.

[9]More precisely, it tells us how likely it is we observe positive vacuum energy. The observed accelerated expansion of the universe could be due to a variety of reasons, of which positive vacuum energy is but one of them. Therefore, if this probability turns out to be very low, it does not show that the universe is not expanding at an accelerating pace.

Chapter 2

Preliminaries

Random fields and functions have been widely studied in physics and mathematics, with applications in statistical mechanics [45, 46], complex dynamics [47, 48], mathematical physics [49, 51], optics [52, 53] and other fields in addition to cosmology. We will start with a mathematical derivation of the relevant theory, before examining the three research questions in detail.

2.1 Preliminaries

In many ways our approach relies on an N-dimensional generalization of Bardeen, Bond, Kaiser and Szalay's (henceforth BBKS) [54] 1985 paper. BBKS's original calculation was for 3D, which we extend to N dimensions. In very low dimensions ($N \leq 3$) it is possible to obtain exact analytical results. Conversely, in the large N limit it is also possible to derive many approximate expressions [55]. In our case, N is greater than 3 but not necessarily large.

Random fields are defined by BBKS thusly:

> An n-dimensional random field $F(r)$ is a set of random variables, one for each point r in n-dimensional real space, defined by the set of finite-dimensional joint probability distribution functions,

$$P[F(r_1), F(r_2) \dots F(r_m)]dF(r_1)dF(r_2) \dots dF(r_m) \qquad (2.1)$$

that the function F have values in the range $F(r_j)$ to $F(r_j)+dF(r_j)$ for each of the $j = 1, \ldots, m$, with m an arbitrary integer and $r_1, r_2 \ldots, r_m$ arbitrary points.

This definition is technical, but can be understood on a more intuitive level. The random field $F(r)$ maps every point r to a random value. That value depends on the probability distribution function P, which determines how probable it is that the field's value at every point is $F(r_1), F(r_2)$, etc. Different probability distribution functions yield different random fields. The particular random field we are interested in is the random Gaussian field, for which P is a multivariate Gaussian,

$$P(y_1, \ldots y_n)dy_1 \ldots dy_n = \frac{e^{-Q}}{\sqrt{(2\pi)^n \det M}} dy_i \ldots dy_n \tag{2.2}$$

where $Q = \sum y_i (M^{-1})_{ij} y_j/2$ and M is the covariance matrix $M_{ij} = \langle \Delta y_i \Delta y_j \rangle$, $\Delta y_i \equiv y_i - \langle y_i \rangle$. Note in this equation n is not the number of dimensions of the field, but rather the total number of variables being considered. Examples of such variables are the value of the field, its first derivative, and its second derivative. We will need all three of these variables because we are dealing with extrema at a given potential value.

Following BBKS, we use the notation

$$\eta_i \equiv \frac{\partial F}{\partial x^i} \tag{2.3}$$

$$\zeta_{ij} \equiv \frac{\partial^2 F}{\partial x^i \partial x^j} \tag{2.4}$$

where F is the field and the x's are independent variables. We will also distinguish between V, which is the potential, and Λ, which is the potential at a minimum.

The number of minima N_{min} in a region is:

$$N_{min} = \int d^N x \, \delta^N(\eta_i) |\det(\zeta_{ij})| \theta_H(\lambda_N) \tag{2.5}$$

where N is the number of dimensions, λ_N is the smallest eigenvalue at the minimum,[1]

[1]This foreshadows the notation we will use later: without loss of generality, we order the N

θ_H is the Heaviside step function, and the integration is over all space. This equation follows from first principles. The delta functions for η_i indicate stationarity, since the first derivatives are zero at stationary points. The Heaviside function at the end enforces the requirement that the stationary point is a minimum, since at minima all eigenvalues are positive.[2] If λ_N were negative, the stationary point is no longer a minimum, and the integral gives zero.

The determinant term ensures independence from a change of variables. Remember the delta function is defined as:

$$1 = \int_{-\infty}^{\infty} \delta(x) dx. \tag{2.6}$$

Notably, the integration variable needs to be the same as the argument of the delta function. In Eq. 2.5 the integration variable is x while the argument of the delta function is η_i; a generic change of variables gives:

$$\int dx_1 dx_2 \dots dx_n \delta(f_1(x_i)) \dots \delta(f_n(x_i)) = \int df_1 df_2 \dots df_n J \delta(f_1) \dots \delta(f_n) \tag{2.7}$$

where f is an arbitrary function and the Jacobian J is given by

$$J = \left| \det \frac{\partial x_i}{\partial f_j} \right| = \frac{1}{\left| \det \frac{\partial f_j}{\partial x_i} \right|}. \tag{2.8}$$

In our case f is η, so $\frac{\partial f_j}{\partial x_i}$ is just ζ_{ij}. We therefore need a factor of $|\det(\zeta_{ij})|$ in Eq. 2.5 to cancel this out. Thus far, we have not used the random Gaussian field assumption.

Now we apply the random Gaussian field requirement (Eq. 2.2). Eq. 2.5 becomes:

$$N_{min} = \int dy_1 dy_2 \dots \, \delta^N(\eta_i) |\det(\zeta_{ij})| \theta_H(\lambda_N) \frac{e^{-Q}}{\sqrt{(2\pi)^n \det M}}. \tag{2.9}$$

eigenvalues of the Hessian as $\lambda_1 \geq \lambda_2 \geq \lambda_3 \dots \lambda_N$. For minima, we also have $\lambda_N \geq 0$.

[2]This – minima have positive eigenvalues – is a BBKS convention we also adopt. One could also take minima to have negative eigenvalues; it changes the math slightly but does not affect the conclusions, since it is effectively the same as changing the subject of our research questions from minima above zero to maxima below zero, and these potentials are symmetric about zero.

In our case the y's are η, ζ, and F. The first two are in Eq. 2.5, while the last will eventually be necessary because we are interested in minima with specific field values. Therefore we'll need correlation functions for all of them.

We start with the first one, $\langle FF \rangle$. Physically, this is the average of F^2, the value of the field squared. It is reminiscent of the *two-point correlation function* between two points $\vec{x}, \vec{y}$ of a random Gaussian field F, written as $\langle F(\vec{x})F(\vec{y})\rangle$. The two-point correlation function measures how much knowledge of the field at $\vec{x}$ reveals about the field at $\vec{y}$. Physically, if we know the value of the field at A, we should know something about the value of the field at a nearby point, $A + \delta A$, but we (usually – it is possible for correlation to increase with distance in certain regions of field space, especially at low dimensions) know less of the field value at a more distant point. The correlation function therefore decreases, and physically it must reach zero at an infinitely distant point. $\langle FF \rangle$ corresponds to the two-point correlation function evaluated at the same position, $\langle F(\vec{x})F(\vec{x})\rangle$.

To proceed, we consider the *power spectrum* $P(k)$, which is defined as the Fourier transform of the two-point correlation function:

$$P(k) = \frac{1}{(2\pi)^N} \int d^N k \, \langle F(\vec{x})F(\vec{y})\rangle e^{-i\vec{k}\cdot(\vec{x}-\vec{y})}. \tag{2.10}$$

Here N is the number of dimensions (3 in our 3D world, but 100+ for the inflaton). The inverse Fourier transform then gives the two-point correlation function:

$$\langle F(\vec{x})F(\vec{y})\rangle = \frac{1}{(2\pi)^N} \int d^N k \, P(k) e^{i\vec{k}\cdot(\vec{x}-\vec{y})}. \tag{2.11}$$

The moments of the distribution are defined as

$$\sigma_n^2 = \frac{1}{(2\pi)^N} \int d^N k \, (k^2)^n P(k). \tag{2.12}$$

Therefore $\langle F(\vec{x})F(\vec{x})\rangle = \sigma_0^2$.

For the other correlation functions, we first differentiate Eq. 2.11 and set $\vec{x} = \vec{y}$.

$$\begin{aligned}\langle \eta_i(\vec{x})\eta_j(\vec{y})\rangle &= \frac{1}{(2\pi)^N}\frac{\partial}{\partial x^i}\frac{\partial}{\partial y^j}\int d^N k\, P(k) e^{i\vec{k}\cdot(\vec{x}-\vec{y})}\Big|_{\vec{x}=\vec{y}} \\ &= \frac{1}{(2\pi)^N}\int d^N k\, k^i k^j P(k).\end{aligned} \tag{2.13}$$

The random Gaussian field is isotropic – the correlation between two gradients cannot depend on which directions the gradients are in. In other words, $\langle \eta_i(\vec{x})\eta_j(\vec{y})\rangle$ must be the same regardless of the values of i and j. Therefore the correlation must be proportional to δ_{ij} (or it can be constant for all i and j, but that is physically implausible). So

$$\frac{1}{(2\pi)^N}\int d^N k\, k^i k^j P(k) = K\delta_{ij} \tag{2.14}$$

where K is a constant. Multiplying both sides by δ^{ij} and making use of the fact that in N dimensions $\delta^{ij}\delta_{ij} = \delta_1^1 + \delta_2^2 + \ldots + \delta_N^N = N$, we have

$$\frac{1}{(2\pi)^N}\int d^N k\, k^2 P(k) = NK \rightarrow K = \frac{1}{N}\sigma_1^2. \tag{2.15}$$

A similar prescription works for the correlation functions $\langle F\zeta_{ij}\rangle$ and $\langle \zeta_{ij}\zeta_{kl}\rangle$. For $\langle F\zeta_{ij}\rangle$ we get

$$\begin{aligned}\langle F\zeta_{ij}\rangle &= -\frac{1}{(2\pi)^N}\int d^N k\, k^i k^j P(k) \\ &= K\delta_{ij} \\ \Rightarrow K &= -\frac{1}{N}\delta_{ij}\sigma_1^2.\end{aligned}$$

Note the minus sign relative to the $\langle \eta_i(\vec{x})\eta_j(\vec{y})\rangle$ case.

The $\langle \zeta_{ij}\zeta_{lk}\rangle$ case is more complex.

$$\begin{aligned}\langle \zeta_{ij}\zeta_{lm}\rangle &= \frac{1}{(2\pi)^N}\frac{\partial}{\partial x^i}\frac{\partial}{\partial x^j}\frac{\partial}{\partial y^l}\frac{\partial}{\partial y^m}\int d^N k\, P(k) e^{i\vec{k}\cdot(\vec{x}-\vec{y})}\Big|_{\vec{x}=\vec{y}} \\ &= \frac{1}{(2\pi)^N}\int d^N k k^i k^j k^l k^m P(k).\end{aligned}$$

Two things to note. First, the expression on the second line is completely symmetric in i, j, l, m. Second, isotropy means that the correlation is nonzero only for three cases: $\langle\zeta_{ii}\zeta_{jj}\rangle$, $\langle\zeta_{ij}\zeta_{ji}\rangle$ and $\langle\zeta_{ij}\zeta_{ij}\rangle$. Because of the symmetry of i, j, l, m, we must also have that all three correlations are equal to each other, $\langle\zeta_{ii}\zeta_{jj}\rangle = \langle\zeta_{ij}\zeta_{ji}\rangle = \langle\zeta_{ij}\zeta_{ij}\rangle$. This lets us write down the expression the correlation must be proportional to:

$$\langle\zeta_{ij}\zeta_{lm}\rangle = K(\delta_{ij}\delta_{lm} + \delta_{il}\delta_{jm} + \delta_{im}\delta_{jl}). \tag{2.16}$$

Multiplying both sides by $\delta_{ij}\delta_{lm}$, we get

$$\begin{aligned} \sigma_2^2 &= K(N \times N + \delta_{jm}\delta_{jm} + \delta_{jm}\delta_{jm}) \\ &= K(N^2 + 2N) \\ &\Rightarrow K = \sigma_2^2 \frac{1}{N(N+2)}. \end{aligned} \tag{2.17}$$

Aggregated, the results are the N-dimensional generalization of BBKS equation A1,

$$\begin{aligned} \langle FF\rangle &= \sigma_0^2, \\ \langle\eta_i\eta_j\rangle &= \frac{1}{N}\delta_{ij}\sigma_1^2, \\ \langle F\zeta_{ij}\rangle &= -\frac{1}{N}\delta_{ij}\sigma_1^2, \\ \langle\zeta_{ij}\zeta_{lm}\rangle &= \frac{1}{N(N+2)}\sigma_2^2(\delta_{ij}\delta_{lm} + \delta_{il}\delta_{jm} + \delta_{im}\delta_{jl}). \end{aligned} \tag{2.18}$$

See Section 7.1 in the Appendix for an alternative way to derive these relations.

Now we define the vector y:

$$\begin{aligned} y = \{F, \eta_1, \eta_2, \ldots, \zeta_{11}, \zeta_{22}, \ldots, \zeta_{NN}, \zeta_{N-1,N}, \zeta_{N-2,N}, \ldots, \zeta_{1N}, \zeta_{N-2,N-1}, \\ \ldots \zeta_{1,N-1}, \ldots, \zeta_{12}\} \end{aligned} \tag{2.19}$$

The elements of this vector are the y's in Eq. 2.9. With this ordering of y, we can write down the covariance matrix. The general expression is complicated, but as an example we have the following 10×10 matrix in 3-dimensions:

$$M = \begin{bmatrix} \sigma_0^2 & 0 & 0 & 0 & -\frac{\sigma_1^2}{3} & -\frac{\sigma_1^2}{3} & -\frac{\sigma_1^2}{3} & 0 & 0 & 0 \\ 0 & \frac{\sigma_1^2}{3} & 0 & 0 & 0 & 0 & 0 & 0 & 0 & 0 \\ 0 & 0 & \frac{\sigma_1^2}{3} & 0 & 0 & 0 & 0 & 0 & 0 & 0 \\ 0 & 0 & 0 & \frac{\sigma_1^2}{3} & 0 & 0 & 0 & 0 & 0 & 0 \\ -\frac{\sigma_1^2}{3} & 0 & 0 & 0 & \frac{\sigma_2^2}{5} & \frac{\sigma_2^2}{15} & \frac{\sigma_2^2}{15} & 0 & 0 & 0 \\ -\frac{\sigma_1^2}{3} & 0 & 0 & 0 & \frac{\sigma_2^2}{15} & \frac{\sigma_2^2}{5} & \frac{\sigma_2^2}{15} & 0 & 0 & 0 \\ -\frac{\sigma_1^2}{3} & 0 & 0 & 0 & \frac{\sigma_2^2}{15} & \frac{\sigma_2^2}{15} & \frac{\sigma_2^2}{5} & 0 & 0 & 0 \\ 0 & 0 & 0 & 0 & 0 & 0 & 0 & \frac{\sigma_2^2}{15} & 0 & 0 \\ 0 & 0 & 0 & 0 & 0 & 0 & 0 & 0 & \frac{\sigma_2^2}{15} & 0 \\ 0 & 0 & 0 & 0 & 0 & 0 & 0 & 0 & 0 & \frac{\sigma_2^2}{15} \end{bmatrix}$$

This matrix can be constructed directly from Eq. 2.18. The $(1,1)$ element is the correlation of the first element of y with itself, i.e. $\langle FF \rangle = \sigma_0^2$. The $(1,2)$ element is the correlation of the first element of y with the second element of y, i.e. $\langle F\eta_1 \rangle = 0$, and so on. To simplify the upcoming analysis, we wish to make this matrix as diagonal as possible. To that end, we adopt the basis transform:

$$\begin{aligned} x_1 &= -\frac{1}{\sigma_2} \sum_i \zeta_{ii}, \\ x_n &= -\frac{1}{\sigma_2} \sum_{i=1}^{n-1} \left(\zeta_{ii} - \zeta_{nn}\right), \ (2 \leq n \leq N) \end{aligned} \tag{2.20}$$

The x_n here are analogous, but not identical, to BBKS's x, y, z in BBKS's Appendix A1. Following BBKS, we also rescale F, introducing $\nu = F/\sigma_0$. With this choice of basis the non-zero elements in the covariance matrix become

$$\begin{aligned} \langle \nu^2 \rangle &= 1 \\ \langle x_1^2 \rangle &= 1 \\ \langle \nu x_1 \rangle &= \gamma \\ \langle x_n^2 \rangle &= \frac{2n(n-1)}{N(N+2)}, \ (2 \leq n \leq N) \end{aligned} \tag{2.21}$$

where $\gamma = \sigma_1^2/(\sigma_2\sigma_0)$. For an explicit proof of this result, see Section 7.2. The only non-diagonal correlation left is between ν and x_1. For the vector

$y = \{\nu, x_1, x_2 \ldots, x_n \ldots \eta_i \ldots \zeta_{ij}\}$ (where $i > j$ in the ζ_{ij} term; note also the shift in the ordering compared to Eq. 2.19), the covariance matrix M now looks like this:

$$M = \begin{bmatrix} 1 & \gamma & 0 & 0 & 0 & 0 & 0 & 0 & 0 \\ \gamma & 1 & 0 & 0 & 0 & 0 & 0 & 0 & 0 \\ 0 & 0 & \frac{4}{N(N+2)} & 0 & 0 & 0 & 0 & 0 & 0 \\ 0 & 0 & 0 & \frac{12}{N(N+2)} & 0 & 0 & 0 & 0 & 0 \\ 0 & 0 & 0 & 0 & \ddots & 0 & 0 & 0 & 0 \\ 0 & 0 & 0 & 0 & 0 & \frac{\sigma_1^2}{N} & 0 & 0 & 0 \\ 0 & 0 & 0 & 0 & 0 & 0 & \ddots & 0 & 0 \\ 0 & 0 & 0 & 0 & 0 & 0 & 0 & \frac{\sigma_2^2}{N(N+2)} & 0 \\ 0 & 0 & 0 & 0 & 0 & 0 & 0 & 0 & \ddots \end{bmatrix}$$

where the terms in columns 3–5 are for the x's, and the last two terms are for η and ζ_{ij} with $i \neq j$. There are N $\frac{\sigma_1^2}{N}$ terms and ${}_NC_2$ $\frac{\sigma_2^2}{N(N+2)}$ terms.

Taking the inverse of the covariance matrix and multiplying with the new vector y, the Q factor in equation (2.2) becomes

$$2Q = \nu^2 + \frac{(x_1 - \gamma\nu)^2}{1-\gamma^2} + \sum_{n=2}^{N} \frac{N(N+2)}{2n(n-1)} x_n^2 + \frac{N\boldsymbol{\eta}\cdot\boldsymbol{\eta}}{\sigma_1^2} + \sum_{i,j;i>j}^{N} \frac{N(N+2)(\zeta_{ij})^2}{\sigma_2^2}. \tag{2.22}$$

This is the equivalent of BBKS equation (A4) for N-dimensions. Note that the first two terms remain constant for all N, but the remaining terms are N dependent.

Two further simplifications are possible: we are interested in extrema, which by definition have $\eta = 0$. Also, we can choose our axes such that $\zeta_{ij} = 0$ if $i \neq j$.[3] This eliminates the last two terms in Eq. 2.22.

[3]This corresponds to picking the principal axes of the system in classical mechanics. Alternatively, this corresponds to transforming the symmetric Hessian (the matrix of ζ's) into a diagonal matrix, which is always possible because symmetric matrices S can be expressed as $S = PDP'$, where D is a diagonal matrix and P is a unitary matrix.

2.1.1 The Jacobian

Although we have made progress, we are not yet done. For clarity, we reproduce the crucial Eq. 2.9:

$$N_{min} = \int dy_1 dy_2 \ldots \delta^N(\eta_i)|\det(\zeta_{ij})|\theta_H(\lambda_N)\frac{e^{-Q}}{\sqrt{(2\pi)^n \det M}} \tag{2.23}$$

The analysis in the previous section handles M and Q,[4] but there are still terms in the integral that need to be evaluated. Recall that the y's (the variables being integrated over in Eq. 2.9) in our case are F, η, and ζ. The F integral will be evaluated in the final step.[5] The integral over η is trivial: since we do not need the last two terms of Q (in Eq. 2.22), the only terms in the integrand that depend on η are the δ-functions, and the η integrals evaluate to 1. That leaves the integrals over ζ, which we deal with in this subsection.

We claim that

$$\prod d\zeta_{11} d\zeta_{12} d\zeta_{13} \ldots = A\big(\prod_{i<j} |\lambda_i - \lambda_j|\big) \prod_i^N d\lambda_i \tag{2.24}$$

where A is some constant and the λ's are the eigenvalues of the Hessian. Note this is a simplification, since the $\frac{N(N+1)}{2}$ dimensional vector space (because there are ${}_NC_2$ ζ's) has dropped to N dimensions. To prove Eq. 2.24 we note that given the $\frac{N(N+1)}{2}$ dimensions, we can span the vector space with $\frac{N(N+1)}{2}$ orthogonal vectors. We also note that we only have $\frac{N(N+1)}{2}$ ζ's because we are in the space of symmetric matrices (in turn a consequence of the fact that the Hessian must be symmetric).

In this space we define an inner product between two symmetric matrices S_1, S_2 as $S_1 \cdot S_2 = \mathrm{Tr}(S_1 S_2)$. Inner products must satisfy three properties [38]:

1. It must obey conjugate symetry, i.e. $\langle x, y\rangle = \overline{\langle y, x\rangle}$. Our Hessians are real, so the conjugate is equal to itself. Meanwhile $\mathrm{Tr}(S_1 S_2) = \mathrm{Tr}(S_2 S_1)$ because the trace is invariant under cyclic permutations. So this item is satisfied.

[4] We do not actually need M for our research questions, since $\det M$ is effectively a constant for a given random Gaussian field. We will see more about this in the next section and in section 3.

[5] Remember for the first research question we're interested in $\int_0^\infty N_{min} dF / \int_{-\infty}^\infty N_{min} dF$.

2. It must be linear in the first argument, $\langle a(x+y), z\rangle = a\langle x, z\rangle + a\langle y, z\rangle$. This is easy to see since $a(S_1+S_2)S_3 = aS_1S_3 + aS_2S_3$ is a basic property of matrix multiplication.

3. It must be positive definite, $\langle x, x\rangle > 0$ for $x \neq 0$. This is not hard to see. If a matrix is symmetric, then it is diagonalizable, $S = PDP'$, where D is a diagonal matrix and P is a unitary matrix. Then $\mathrm{Tr}(S_1S_1) = \mathrm{Tr}(PDP'PDP') = \mathrm{Tr}(PD^2P') = \mathrm{Tr}(D^2P'P) = \mathrm{Tr}(D^2) = \sum \lambda_i^2 \geq 0$, where we've used the defining property of unitary matrices and the fact that the trace is invariant under cyclic permutations.

Therefore the trace is a valid inner product. The inner product simultaneously defines a distance: the distance between two points is simply equal to the length of the vector between the two points. In other words,

$$ds^2 = \mathrm{Tr}(dS^2). \tag{2.25}$$

BBKS calls the quantity ds^2 the "metric".

Next, since S is symmetric, it is always diagonalizable with a unitary matrix, and we can take $S = R^\dagger \lambda R$ where λ is the matrix of eigenvalues after rotation. Since R is unitary, we must have $R^\dagger R = I$. Differentiating and using the chain rule, we get:

$$dR^\dagger R + R^\dagger dR = 0 \rightarrow dR^\dagger = -R^\dagger dR R^\dagger. \tag{2.26}$$

We also have, by differentiating $S = R^\dagger \lambda R$,

$$\begin{aligned} dS &= dR^\dagger \lambda R + R^\dagger d\lambda R + R^\dagger \lambda dR \\ &= -R^\dagger dR R^\dagger \lambda R + R^\dagger d\lambda R + R^\dagger \lambda dR \\ &= R^\dagger (d\lambda + [\lambda, dRR^\dagger]) R. \end{aligned} \tag{2.27}$$

The square brackets denote the commutator. Note this is different from BBKS's expression in their appendix B (below Eq. B2); the BBKS expression contains a typo.

Now we can compute the value in Eq. 2.25.

$$\begin{aligned} ds^2 &= \mathrm{Tr}[(R^\dagger(d\lambda + [\lambda, dRR^\dagger])R)^2] \\ &= \mathrm{Tr}[(R^\dagger(d\lambda + [\lambda, dRR^\dagger])^2 R] \\ &= \mathrm{Tr}[(d\lambda + [\lambda, dRR^\dagger])^2]. \end{aligned} \tag{2.28}$$

The second line follows because $R^\dagger R = I$, and the third line follows by invariance of the trace under cyclic permutation. Expanding the square we get

$$ds^2 = \mathrm{Tr}(d\lambda^2 + d\lambda[\lambda, dRR^\dagger] + [\lambda, dRR^\dagger]d\lambda + [\lambda, dRR^\dagger]^2). \tag{2.29}$$

The trace of the middle two terms turns out to be zero, if we exploit 1) the cyclic property and 2) the fact that λ and dλ commute (because they are both diagonal). This leaves the first and last terms. The trace of the first term is of course $\sum d\lambda_i^2$. For the second term, note that $dRR^\dagger$ is a matrix, so its elements can be indexed by two indices which we can write as $(dRR^\dagger)_{ij}$. It is also antisymmetric: $RR^\dagger = 1$, and differentiating this shows $dRR^\dagger = -RdR^\dagger$ (compare Eq. 2.26). Defining $(dRR^\dagger)_{ij} \equiv w_{ij}$ for ease of notation, we have the commutator become

$$\begin{aligned} [\lambda, dRR^\dagger]_{ij} &= (\lambda dRR^\dagger)_{ij} - (dRR^\dagger\lambda)_{ij} \\ &= \sum_k \lambda_{ik} w_{kj} - \sum_{k'} w_{ik'}\lambda_{k'j} \\ &= \lambda_{ii} w_{ij} - \lambda_{jj} w_{ij} \\ &= (\lambda_i - \lambda_j) w_{ij}. \end{aligned} \tag{2.30}$$

The third line follow from the fact that λ is diagonal, and because these are no longer matrix multiplications, therefore they comute. We are interested in the commutator squared, which leads to

$$\begin{aligned} M_{ij} &= [\lambda, dRR^\dagger]^2_{ij} \\ &= \sum_k (\lambda_i - \lambda_k) w_{ik} (\lambda_k - \lambda_j) w_{kj} \\ &= \sum_k (\lambda_i - \lambda_k) w_{ik} (\lambda_j - \lambda_k) w_{jk}. \end{aligned} \tag{2.31}$$

where the second line follows from matrix multiplication, and the third line uses the antisymmetric property $w_{ik} = -w_{ki}$. We want the trace of this, so we set $i = j$ and sum over i.

$$\mathrm{Tr}M = \sum_i \sum_k (\lambda_i - \lambda_k)^2 w_{ik}^2. \tag{2.32}$$

Keeping in mind that since w is antisymmetric, it is nonzero only if $i \neq k$, and we can write $\mathrm{Tr}M = \sum_{i \neq j} (\lambda_i - \lambda_j)^2 w_{ij}^2$. Therefore

$$ds^2 = \sum (d\lambda_i)^2 + \sum_{i \neq j} (\lambda_i - \lambda_j)^2 w_{ij}^2. \tag{2.33}$$

Next, we note that there are $\frac{N(N+1)}{2}$ elements in the above: N of the first term, and $\frac{N(N-1)}{2}$ of the second. Therefore we can take the $d\lambda$'s and $|\lambda_i - \lambda_j| w_{ij}$ as our basis vectors, they span our space, and their product is equal to the product of the $d\zeta$'s.

We are almost at Eq. 2.24. For the rest, keep in mind that the w's are elements of a rotation matrix. If we have statistical isotropy, then integrating over all angles yields a constant (which BBKS calls $d\mathrm{vol}[SO(3)]$), and we arrive at Eq. 2.24.

2.1.2 Putting it together

We again reproduce the crucial Eq. 2.9, in the variables we are now using:

$$N_{min} = \int dF (d\eta_1 d\eta_2 \dots d\eta_N)(d\zeta_{11} d\zeta_{12} \dots d\zeta_{NN}) \\ \delta^N(\eta_i) |\det(\zeta_{ij})| \theta_H(\lambda_N) \frac{e^{-Q}}{\sqrt{(2\pi)^n \det M}} \tag{2.34}$$

with Q given by Eq. 2.22. As argued in the previous subsection, the η integrals evaluate to unity. Furthermore, the results of the previous subsection allow us to write:

$$N_{min} = A \int dF (d\lambda_1 d\lambda_2 \dots d\lambda_N) \prod_{i<j} |\lambda_i - \lambda_j| |\det(\zeta_{ij})| \theta_H(\lambda_N) \frac{e^{-Q}}{\sqrt{(2\pi)^n \det M}} \tag{2.35}$$

A few more simplifications are possible. Because have chosen the principal axes (Sec. 2.1.1), ζ_{ij} is now nonzero only for $i = j$, where its value is the eigenvalue of the Hessian, λ_i. Therefore $\det(\zeta_{ij}) = \prod_i \lambda_i$. Also, so far, no assumptions have been made about the eigenvalues λ_i. Without loss of generality, we can order the eigenvalues such that $\lambda_1 \geq \lambda_2 \geq \lambda_3 \ldots \geq \lambda_N$. For minima, we must also have $\lambda_N \geq 0$. Because there are $N!$ possible orderings that could have been chosen instead, imposing this ordering divides the result by a constant, $N!$, which we can absorb into A. Finally, $\det M$ is a constant[6] and so is 2π, which we can also absorb into A. The final result for minima is:

$$N_{min} = A \int_0^\infty d\lambda_1 \int_0^{\lambda_1} d\lambda_2 \ldots \int_0^{\lambda_N} d\lambda_N \int dF \prod_{i<j} |\lambda_i - \lambda_j| \prod_i |\lambda_i| e^{-Q} \tag{2.36}$$

where the integration limits enforce the ordering $\lambda_1 \geq \lambda_2 \geq \ldots \geq \lambda_N > 0$, and Q is given by (compare Eq. 2.22)

$$\begin{aligned} 2Q &= \nu^2 + \frac{(x_1 - \gamma\nu)^2}{1-\gamma^2} + \sum_{n=2}^{N} \frac{N(N+2)}{2n(n-1)} x_n^2 \\ &= x_1^2 + \frac{(\nu - \gamma x_1)^2}{1-\gamma^2} + \sum_{n=2}^{N} \frac{N(N+2)}{2n(n-1)} x_n^2. \end{aligned} \tag{2.37}$$

We can see eigenvalue repulsion[7] in Eq. 2.36: if $\lambda_i = \lambda_j$, the integrand becomes zero. In other words, there are fewer minima as eigenvalues get closer to each other, and there are no minima for which two eigenvalues are exactly equal.

To modify this equation for saddles, we adapt the integration limits. For example, if we are interested in 1-saddles, we consider instead the equation:

$$N_{sad} = A \int_0^\infty d\lambda_1 \int_0^{\lambda_1} d\lambda_2 \ldots \int_0^{\lambda_{N-1}} d\lambda_{N-1} \int_{-\infty}^{0} d\lambda_N \int dF \prod_{i<j} |\lambda_i - \lambda_j| \prod_i |\lambda_i| e^{-Q}. \tag{2.38}$$

[6] Although $\det M$ contains variables that depend on the properties of the random Gaussian field, none of those variables are being integrated over.

[7] Eigenvalue repulsion was also mentioned in the Introduction of this thesis, in relation to Aazami & Easther's [7] and Marsh *et al.*'s work. [26] It refers to the tendency of eigenvalues of random matrices to "repel" one another, such that no two eigenvalues are likely to be the same.

The integration limits now enforce the order $\lambda_1 \geq \lambda_2 \geq \lambda_3 \ldots \geq \lambda_{N-1} \geq 0 \geq \lambda_N$. Note the absolute value signs around the λ's – these ensure the result is always positive, even though λ_N is negative.

Eqs. 2.36 and 2.38 are key equations for answering our research questions. Because of the unknown constant A in front of the equation, they are not actually the number density of minima/saddles. The integrands are, however, an unnormalized probability density for minima/saddles: if they are relatively large, then minima/saddles are more likely, and vice versa if they are small. Evaluating these equations for different limits on the F integral is the focus of much of this thesis.

2.1.3 The role of γ

At this point it is worth noting that the only parameter of the random Gaussian field remaining in Eqs. 2.36 and 2.38 is γ. In other words, although three parameters were used in the covariance matrix M (σ_0, σ_1 and σ_2, see Eqs. 2.12 and 2.18), only the combination $\sigma_1^2/\sigma_0\sigma_2$ is relevant for the number of minima/saddles. The intuitive explanation for this is that σ_0 is roughly related to the average of the square of the field value (see Eq. 2.18). Multiplying the field value by a constant would change σ_0 (Fig. 2.1), but it would not change the number of minima/saddles. Similarly, σ_1 is the average of the square of the first derivative. Multiplying the first derivative by a constant – equivalent to rescaling the axes – would change σ_1, but again doesn't affect the relative number of minima/saddles in a fixed volume. Therefore two of the three degrees of freedom do not affect the statistics, and we are left with only one parameter γ.

It can be shown that $0 \leq \gamma \leq 1$. We know $\gamma = \sigma_1^2/\sigma_0\sigma_2 \geq 0$ because the σ_i are positive (from their definition, Eq. 2.12, every term in the integrand is positive; one can also see from Eq. 2.18 that the σ's correspond to the average of squares, and must therefore be positive). For the other bound, we know[8]

$$\int (k^2 - \frac{\sigma_1^2}{\sigma_0^2})^2 P(k) dk \geq 0 \tag{2.39}$$

[8]This proof is due to Shaun Hotchkiss.

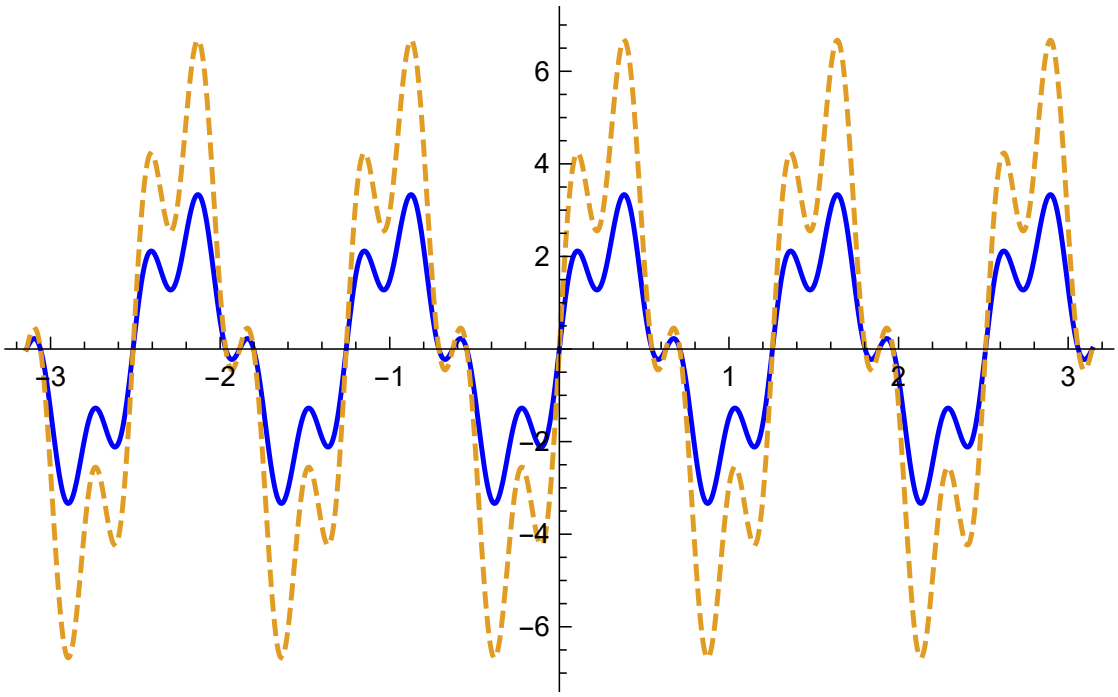

Figure 2.1: In this 1D realization of a random Gaussian field, multiplying the field value by 2 (dashed line) changes σ_0, but does not affect the number or sign of minima.

because the integrand is positive. Expanding the square leads to

$$\begin{aligned}
&\int k^4 P(k)dk - 2\int k^2 \frac{\sigma_1^2}{\sigma_0^2} k^2 P(k)dk + \int \frac{\sigma_1^4}{\sigma_0^4} P(k)dk \\
&= \sigma_2^2 - 2\frac{\sigma_1^4}{\sigma_0^2} + \frac{\sigma_1^4}{\sigma_0^2} \\
&= \sigma_2^2 - \frac{\sigma_1^4}{\sigma_0^2} \geq 0 \\
&\rightarrow \sigma_2^2\sigma_0^2 - \sigma_1^4 \geq 0 \\
&\rightarrow \sigma_2\sigma_0 \geq \sigma_1^2 \\
&\rightarrow 1 \geq \gamma.
\end{aligned} \tag{2.40}$$

Q.E.D.

The exact value γ takes depends on the power spectrum. Because the string landscape is so complicated, there is no canonical answer to the question "what is the landscape's power spectrum?" and therefore no canonical value for γ either. Nonetheless, we will consider two simple power spectra: the Gaussian power spectrum and the power-law power spectrum, for which we can calculate analytical results. In the next subsections, we will calculate γ for both these power spectra.

Gaussian power spectrum

The specific form of the Gaussian power spectrum we adopt is $P(k) = U_0^2 e^{-k^2/2L^2}$, where U_0 is the amplitude of the Gaussian and L is the correlation length.[9] The two-point correlation function is a Gaussian (since the Fourier transform of a Gaussian is another Gaussian), and we can write, by definition (c.f. Eq. 2.11),

$$U_0^2 e^{-\phi^2/2L^2} = \frac{1}{(2\pi)^N}\int d^N k P(k) e^{ik\phi\cos\theta} \tag{2.41}$$

where ϕ is the Fourier conjugate of k and we have written $k \cdot \phi$ as $k\phi\cos\theta$.

[9]The correlation length is a rough estimate for the distance at which the correlation function drops to zero. Its meaning will be discussed in greater detail in Section 5.4.1.

Differentiate twice w.r.t ϕ,

$$U_0^2 e^{-\phi^2/2L^2}\frac{\phi^2-L^2}{L^4} = \frac{1}{(2\pi)^N}\int d^N k(-k^2\cos^2(\theta))P(k)e^{ik\phi\cos\theta}$$
$$= -\frac{1}{(2\pi)^N}\int dk\int d\theta\int d\Omega' k^2 P(k)e^{ik\phi\cos\theta}\cos^2(\theta)\sin^{N-2}(\theta)\omega_{N-2} \tag{2.42}$$

where Ω' is over all non-θ angles, and ω are the non-θ angular terms. ω is obviously N-dependent, hence the subscript. If we set $\phi = 0$ then this simplifies to

$$-\frac{U_0^2}{L^2} = -\frac{1}{(2\pi)^N}\sqrt{\pi}\frac{\Gamma[\frac{N-1}{2}]}{2\Gamma[1+\frac{N}{2}]}\int dk\int d\Omega' k^2 P(k)\omega_{N-2} \tag{2.43}$$

where we have evaluated the integral over θ analytically. On the other hand, σ_1^2 is by definition (see Eq. 2.12)

$$\sigma_1^2 = \frac{1}{(2\pi)^N}\int dk\int d\theta k^2 P(k)\sin^{N-2}(\theta)\omega_{N-2}$$
$$= \frac{1}{(2\pi)^N}\sqrt{\pi}\frac{\Gamma[\frac{1}{2}(N-1)]}{\Gamma[\frac{N}{2}]}\int_0^\infty dk k^2 P(k)\omega_{N-2}. \tag{2.44}$$

Comparing the two equations, we get

$$\frac{U_0^2}{L^2} = \frac{\Gamma[\frac{N-1}{2}]}{2\Gamma[1+\frac{N}{2}]}\frac{\Gamma[\frac{N}{2}]}{\Gamma[\frac{1}{2}(N-1)]}\sigma_1^2 \tag{2.45}$$

or

$$\sigma_1^2 = \frac{2U_0^2}{L^2}\frac{\Gamma[1+\frac{N}{2}]}{\Gamma[\frac{N}{2}]}. \tag{2.46}$$

This is exactly the same result as Yamada and Vilenkin's Eq. 2.4 for σ_1 [34]. A

similar calculation yields expressions for σ_0 and σ_2,

$$\begin{aligned}\sigma_0^2 &= U_0^2 \frac{\Gamma[\frac{N}{2}]}{\Gamma[\frac{N}{2}]} = U_0^2 \\ \sigma_2^2 &= \frac{4U_0^2}{L^4} \frac{\Gamma[2+\frac{N}{2}]}{\Gamma[\frac{N}{2}]}\end{aligned} \tag{2.47}$$

from which we get, after using the expression $\Gamma(N) = (N-1)!$,

$$\gamma = \sqrt{\frac{N}{N+2}}. \tag{2.48}$$

For $N = 100$, this evaluates to $\gamma \approx 0.990$.

Power-law power spectrum

The other commonly-used power spectrum is the power-law power spectrum. These take the form $P(k) = Ak^{-n}$. They come with either and red or blue cutoff,[10] to avoid infinities. For a red cutoff, $P(k) = 0$ for $k < k_{cut}$. The Fourier transform of this power-law power spectrum is, up to some constant factors:

$$\int_{k_{cut}}^{\infty} k^{N-n-1} (\phi k)^{1-N/2} J_{N/2-1}(\phi k) dk \tag{2.49}$$

where N is the number of dimensions and J is the Bessel function [39]. We can substitute this into the definition for the σ's and integrate. Mathematica is able to evaluate the integrals:

$$\begin{aligned}\sigma_0^2 &= \left(\frac{1}{2\pi}\right)^N \int_{k_{cut}}^{\infty} k^{N-1} A k^{-n}; \\ \sigma_0 &= \sqrt{\frac{A k_{cut}^{N-n} (2\pi)^{-N}}{n-N}} \qquad\qquad (n > N)\end{aligned} \tag{2.50}$$

[10] We use 'red' and 'blue' in the cosmological sense, denoting spectra with more power on large scales (small k) as red and small scales (large k) as 'blue'.

$$\sigma_1^2 = \left(\frac{1}{2\pi}\right)^N \int_{k_{cut}}^{\infty} k^2 k^{N-1} A k^{-n};$$
$$\sigma_1 = \sqrt{\frac{A k_{cut}^{2+N-n} (2\pi)^{-N}}{n-N-2}} \qquad (n > N+2) \tag{2.51}$$

$$\sigma_2^2 = \left(\frac{1}{2\pi}\right)^N \int_{k_{cut}}^{\infty} k^4 k^{N-1} A k^{-n};$$
$$\sigma_2 = \sqrt{\frac{A k_{cut}^{4+N-n} (2\pi)^{-N}}{n-N-4}} \qquad (n > N+4) \tag{2.52}$$

Combined, this yields:

$$\gamma = \frac{\sqrt{(n-4-N)(n-N)}}{n-N-2} \tag{2.53}$$

This expression is valid only if $n > 4 + N$.[11]

Alternatively, we can impose a blue cutoff, $P(k) = 0$ for $k > k_{cut}$. The same analysis holds. The moments of the power spectrum are now

$$\sigma_0 = \frac{1}{(2\pi)^{N/2}} \sqrt{\frac{A k_{cut}^{N-n}}{N-n}} \quad (n < N)\,, \tag{2.54}$$

$$\sigma_1 = \frac{1}{(2\pi)^{N/2}} \sqrt{\frac{A k_{cut}^{2+N-n}}{N-n+2}} \quad (n < N+2)\,, \tag{2.55}$$

$$\sigma_2 = \frac{1}{(2\pi)^{N/2}} \sqrt{\frac{A k_{cut}^{4+N-n}}{N-n+4}} \quad (n < N+4)\,, \tag{2.56}$$

And the final expression for γ is:

$$\gamma = \frac{\sqrt{(n-4-N)(n-N)}}{N-n+2} \tag{2.57}$$

valid only if $n < N$. Note that in both Eq. 2.53 and Eq. 2.57, γ does not depend on A or k_{cut}. However, this does not mean these parameters are not physically meaningful. A is related to the root mean square energy of the landscape via $\langle FF \rangle = \sigma_0^2$ (Eq. 2.18), while we will encounter k_{cut} again in Chapter 5.

[11] If $n < 4 + N$, the integral of the power spectrum over all space will not converge.

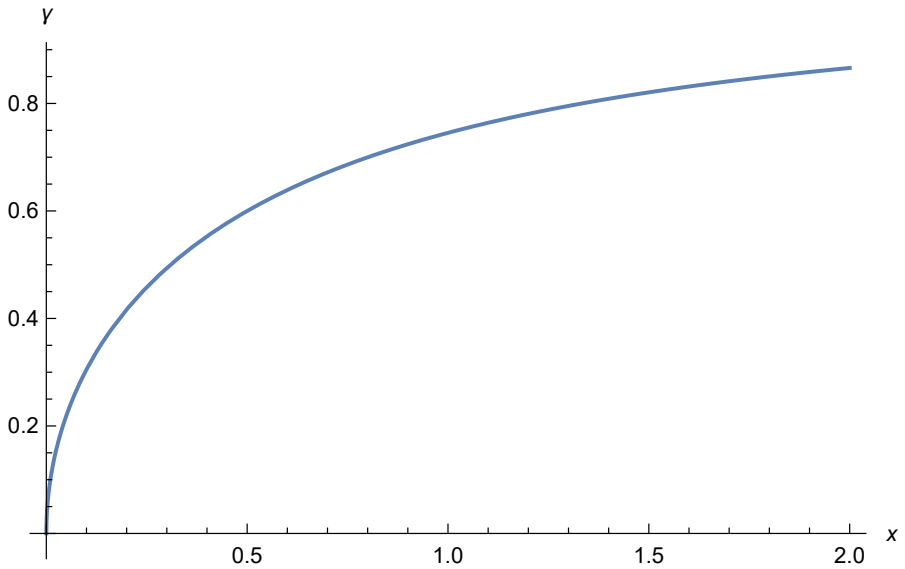

Figure 2.2: γ for the power-law power spectrum $P(k) = Ak^{-n}$ as a function of x, where x is an arbitrary positive number that relates n and N (see text). This result applies for both a red cutoff and a blue cutoff. γ is very close to 1 for moderate values of x, but for sufficiently small x it can also be close to 0.

To illustrate how these expressions for γ work, we substitute $n = 4 + N + x$ in Eq. 2.53 and $n + x = N$ in Eq. 2.57, where x is a positive number. Both expressions then simplify to $\gamma = \sqrt{4x + x^2}/(2 + x)$. A plot of this expression is shown in Fig 2.2. It asymptotes to 1 for large x, but small γ is possible for small x. In other words, the power-law power spectrum is capable of producing all values of γ for appropriate values of n.

2.2 Implementation details

The results of the previous section hold for all N. However, the complexity of Eqs. 2.36 and 2.38 rise quickly with N. We are interested in $N \sim \mathcal{O}(100)$, a number large enough that analytic treatments are very complex, especially for the N-dimensional variables we study such as the eigenvalue distributions at very rare saddles. However, it might not be large enough for a large-N limit to be applicable, either. Consequently, in what follows we will rely heavily on numerical methods. In performing these analyses, some details turn out to be critical to computational

performance.

Firstly (and most importantly), Eq. 2.36 and 2.38 are formulated in terms of λ, the eigenvalues of the Hessian at the point. This turns out to be a bad idea in practice because the λ's can be very small, in which case the product and difference terms make the integrand in Eq. 2.36 and 2.38 infinitesimal, in turn leading to numerical difficulties.

The solution to this problem is to use the difference of eigenvalues as the integration variable. We define

$$\begin{aligned} y_1 &= \lambda_1 - \lambda_2 \\ y_2 &= \lambda_2 - \lambda_3 \\ &\dots \\ y_{N-1} &= \lambda_{N-1} - \lambda_N \\ y_N &= \lambda_N. \end{aligned} \tag{2.58}$$

The choice made earlier to order the eigenvalues $\lambda_1 \geq \lambda_2 \geq \lambda_3 \dots \geq \lambda_N$ therefore becomes $y_i \geq 0 \quad \forall i$ (this applies for minima where all $\lambda_i \geq 0$. For saddles where some number of $\lambda_i \leq 0$, the relation for y_i is trivial to derive).

Secondly, for some questions, we will be dealing with the single most likely minimum/saddle. To find the most likely minimum/saddle, we do not need to perform the integration in Eq. 2.36 and 2.38. Instead we maximize the integrand (recall that Eqs. 2.36 and 2.38 are unnormalized probability densities for minima/saddles.)[12] To do this, we make use of Mathematica's FindMaximum command. It turns out that this command evaluates fastest when there are no constraints on the integration variables. In other words, Mathematica is slower if we ask it to optimize y_i subject to the constraint that $y_i \leq 0$. To get around this, we implement another transform

$$y_i \to \frac{1}{2N}\left(z_i^2 - \sqrt{4 + z_i^2}\right) \tag{2.59}$$

where N is the number of dimensions. For the case of saddles where $y_N \geq 0$, we

[12]There are some subtleties involved with maximizing the integrand instead of performing the full integration, see Fig. 5.1.

also use

$$y_N \to \frac{1}{2N}\left(z_N^2 + \sqrt{4 + z_N^2}\right). \tag{2.60}$$

These two transforms remove the constraints on y_i, since all real values of z_i are acceptable. This leads to a significant speedup.

Finally, FindMaximum requires a starting point to initiate the search. The one we use is $z_i = \sqrt{i} \quad \forall i$, a semi-empirical choice based on the approximate values of z at the maxima. It is conceivable that a different starting point will lead to a different optimum; however we checked this for various starting points without finding a different maximum. We can check the probability distribution for $N = 2$ graphically, as in Fig. 2.3. The probability distribution is smooth, and there is clearly only one maximum. This ties in with the Gaussian approximation, a detail we will encounter in Section 3.4.

2.3 Summary

In this chapter, we have derived the key equations Eq. 2.36 and 2.38 that represent, up to a constant factor, the number density of minima/saddles in a random Gaussian landscape. We have shown that, although random Gaussian fields in general depend on three parameters σ_0, σ_1 and σ_2, only the combination $\sigma_1^2/\sigma_0\sigma_2$, or γ, matters for the number density of minima/saddles. We have further calculated γ for two simple power spectra, the Gaussian power spectrum (Eq. 2.48) and the power-law power spectrum (Eqs. 2.53 and 2.57). These tools form the foundation for our analysis of the research questions in the upcoming chapters.

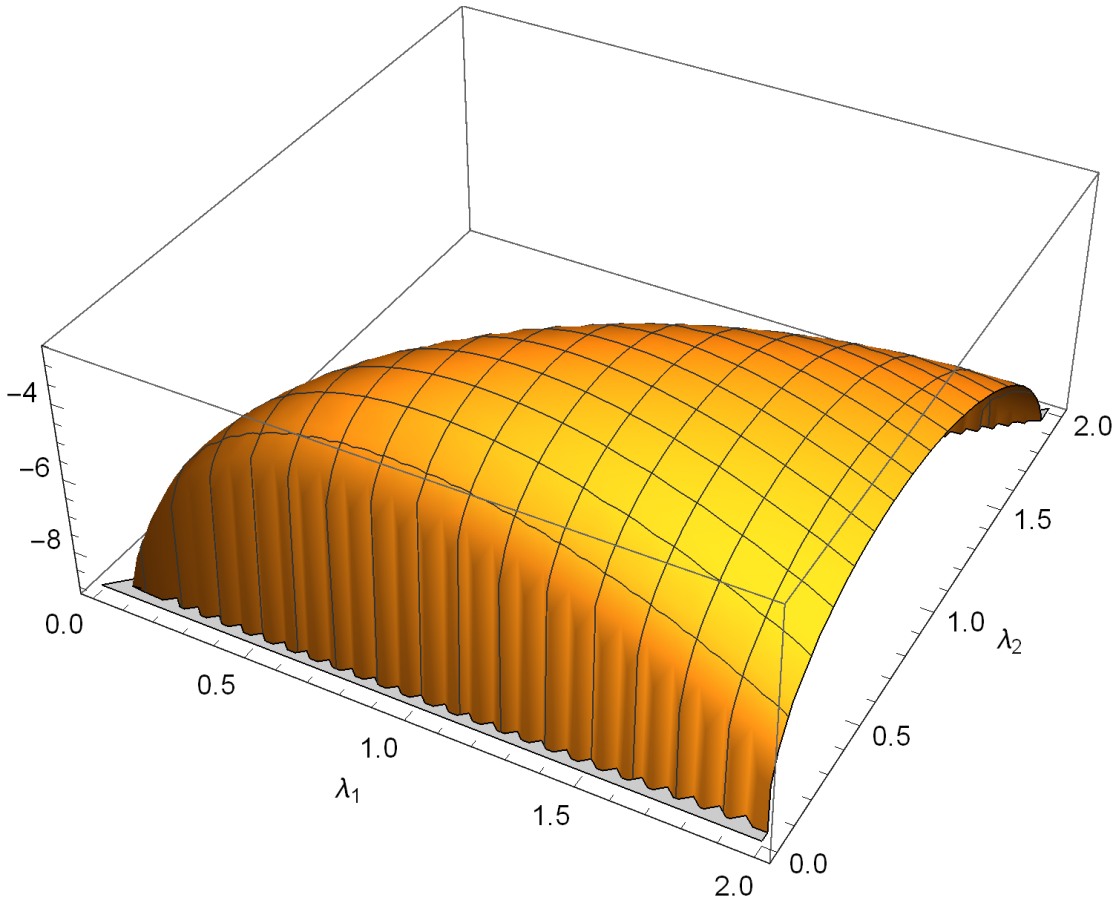

Figure 2.3: Plot of the logarithm of the probability distribution (the integrand of Eq. 2.36) for $N = 2, \gamma = 0.9$. We see deep troughs at $\lambda_2 \approx \lambda_1$, illustrating eigenvalue repulsion, and at $\lambda_2 \approx 0$. As can be seen, the probability distribution is smooth, and there is only one maximum.

Chapter 3

Question One: Distribution of Cosmological Constants in a Gaussian Landscape

Observations indicate we live in a universe with dark energy. Assuming dark energy is due to a cosmological constant, then empirically, the cosmological constant is very small (about $10^{-123}E_P$, where E_P is the Planck energy density, or M_P^4 in natural units with $c = \hbar = 1$), but nonzero. Explaining this small value poses a problem for physics, because it would have been so much simpler for the cosmological constant to be exactly zero.

From the perspective of string theory, the string landscape can potentially support a dense discretuum of cosmological constants[1] [50]. This allows for an anthropic explanation of the cosmological constant's value. However, this still requires $P(\Lambda)$, the probability for each individual value of Λ, which has not been calculated in detail for string landscape proposals.

Our first research question investigates this probability. Mathematically, we are interested in $p(\Lambda > 0|min)$.[2] It should be clear that this probability can be written

[1]This means the value of the cosmological constant must take specific values as opposed to varying continuously.

[2]Beginning from this point, we use Λ to refer to the value of the field at our minimum. This notation compares to V, which refers to the more general case of the field value, not necessarily at our minimum.

as:

$$p(\Lambda > 0|min) = \frac{\int_0^\infty d\Lambda N_{min}}{\int_{-\infty}^\infty d\Lambda N_{min}} \tag{3.1}$$

where N_{min} is the probability density of minima (Eq. 2.36). If this probability turns out to be very small, then it is possible that every minimum of the landscape is "below the waterline", posing a challenge for landscape explanations of the cosmological constant. More generally, we can also calculate $P(\Lambda|min)$ for different values of Λ, in our trial landscape.

Here we make a technical note: we do not evaluate $p(\Lambda = 10^{-123}E_P|min)$ because this probability depends on the power spectrum used. Put differently, this probability is dimensionful while the probability we calculate is dimensionless. This is because $V = \nu\sigma_0$ by definition, and while the machinery of Chapter 2 allows us to calculate the probability of finding a minimum with a given ν, we cannot translate ν into an energy density without the power spectrum-dependent quantity σ_0. Nonetheless, $\nu > 0$ if and only if $V > 0$,[3] and hence if $p(\Lambda > 0|min)$ is small, it will remain small regardless of what the power spectrum is.

3.1 Expectations

Before we evaluate Eq. 3.1, we briefly discuss what we expect to see, on both intuitive and mathematical levels.

3.1.1 Variation with Λ

The greater the value of Λ, the higher up the potential we are. The higher up the potential we are, the more likely the stationary points we encounter will be maxima. This is intuitive, because if a (rare) stationary point very high up the potential is not a maximum, then there must be (even rarer) points nearby with higher Λ.[4] Accordingly, we expect that the fraction of minima N_{min}/N_{max} decreases as Λ increases.

[3] By definition, σ_0 is always positive since it corresponds to the average of squares, see Eq. 2.18.

[4] As mentioned in the Introduction, this result was also derived by Bray and Dean [12].

Mathematically, we can see this from the definition of Q (Eq. 2.37). As ν increases, Q increases, e^{-Q} decreases, and N_{min} decreases, as expected. Furthermore, because x_1 is directly proportional to the negative of the sum of eigenvalues, it is always negative for minima.[5] Examining the expression for Q (Eq. 2.37), we see that it contains the term $(\nu - \gamma x_1)^2$. For negative x_1, this term is zero (i.e. Q maximal, and by extension N_{min} maximal) for a negative value of ν, consistent with the expectation that there are more minima with negative ν than positive ν. Comparatively, for maxima, this term is zero for a positive ν. We therefore see that N_{min}/N_{max} decreases with ν, as expected.

3.1.2 Variation with N

The number N denotes the dimension of the random Gaussian field, or equivalently, the number of component fields. The fields are typically assumed to be string theoretic moduli. Like much of the landscape, the precise value of N is uncertain. Estimates range from dozens [56] to hundreds of thousands in the most complex compactifications [3], with the most common value cited as "hundreds".

It stands to reason that the more fields there are, the less likely *all* of them reach a minimum at the same point (which they must, for there to be an overall minimum). Therefore we expect N_{min} to decrease with N relative to the number of saddles. This is clear also from the definition of Q: as N increases, Q increases, the exponential term is smaller, and N_{min} decreases.

What is not immediately clear is if $p(\Lambda > 0|min)$ decreases with N. We can get a sense of whether it should by examining Eq. 2.36. As N increases, so does the number of eigenvalues. This, together with the fact that the polynomial term favors large λ, causes x_1 to become more negative for minima.[6] This causes the second term in Eq. 2.37, which contains the term $(x_1 - \gamma\nu)^2$, to favor smaller values of ν. Accordingly, we expect the probability distribution to move, but its shape to be unchanged. Since we are interested in the part of the distribution that is greater than 0 as a proportion of the entire distribution, we must have that $p(\Lambda > 0|min)$ decreases with N.

[5] Keep in mind our convention where minima have positive eigenvalues.

[6] Recall that x_1 is the sum of eigenvalues, see Eq. 2.20.

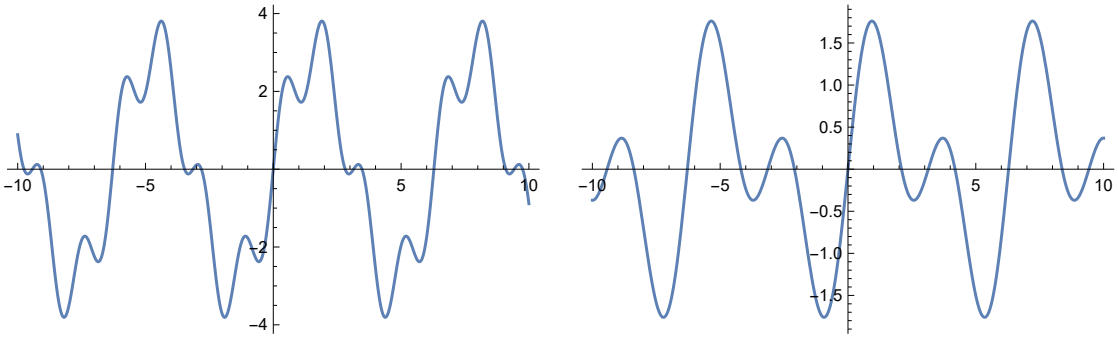

Figure 3.1: Two 1D realizations of a random Gaussian field. The field on the left has smaller γ and is therefore more "turbulent", with more minima as well as more minima above zero.

3.1.3 Variation with γ

Intuitively, γ is a measure of how "turbulent" the potential is. A power spectrum that extends over a narrower range of scales yields a potential with large γ, and there are fewer minima and maxima for a given region of space (see Fig. 3.1).

However, the number we are actually after is $p(\Lambda > 0|min)$, and it's not obvious how this number varies as N_{min} decreases. To get an idea, we again look at the expression for Q in Eq. 2.37. A larger γ decreases the width of the second term, which is the only place where ν enters into the expression. Larger γ also drives the most likely ν to more negative values (bear in mind that x_1 is negative for minima). Therefore, we expect the distribution to both become more sharply peaked *and* move to lower ν, which means that there are proportionately fewer minima above 0, and $p(\Lambda > 0|min)$ decreases.

We will see these heuristics bear out in the upcoming sections.

3.2 ν integral

Before proceeding further, we note that the integrals over ν in Eq. 2.36 can be performed analytically. The only dependence of the integrand on ν is via the first

two terms of Q. Consequently, we can write the denominator of Eq. 3.1 as

$$\begin{aligned}
\text{denom} &= \int_{-\infty}^{\infty} d\nu \int_{\lambda_1 \geq \lambda_2 \ldots \geq 0} d^N x \prod_{i<j} |\lambda_i - \lambda_j| \prod_i |\lambda_i| \times e^{-Q} \\
&= \int d^N x \; f(x_1, x_2 \ldots) \int_{-\infty}^{\infty} d\nu \; \exp\left(-\frac{(\nu - \gamma x_1)^2}{2(1-\gamma^2)}\right) \\
&= \sqrt{2\pi(1-\gamma^2)} \int d^N x \; f(x_1, x_2 \ldots) \qquad (3.2)
\end{aligned}$$

with

$$f(x_1, x_2 \ldots) = \prod_{i<j} |\lambda_i - \lambda_j| \prod_i |\lambda_i| \times \exp\left(-\frac{x_1^2}{2} - \sum_{n=2}^{N} \frac{N(N+2)}{4n(n-1)} x_n^2\right).$$

Similarly, we can evaluate the ν integral in the numerator of Eq. 3.1:

$$\begin{aligned}
\text{numer} &= \int_{0}^{\infty} d\nu \int_{\lambda_1 \geq \lambda_2 \ldots \geq 0} d^N x \; \prod_{i<j} |\lambda_i - \lambda_j| \prod_i |\lambda_i| \times e^{-Q} \\
&= \sqrt{\frac{\pi(1-\gamma^2)}{2}} \int d^N x \; f(x_1, x_2 \ldots) \times \left(1 + \text{erf}\left(\frac{\gamma x_1 \sqrt{1-\gamma^2}}{\sqrt{2}}\right)\right) \qquad (3.3)
\end{aligned}$$

The desired integral is then numer/denom.

3.3 Results for $1 < N \lesssim 12$

For small values of N, up to about $N = 12$, we can directly evaluate the integrals Eq. 3.2 and Eq. 3.3 numerically using Mathematica. We first investigate how $p(\Lambda|min)$ varies with N and γ, in conjunction with the heuristics above. Figure 3.2 plots the resulting unnormalized probability density against the potential value. We see that the heuristics are obeyed: larger γ makes the distribution more tightly peaked as well as shifts most minima to negative values, while larger N moves the distribution to more negative values but does not affect the shape.

Keep in mind we are interested in the fraction of the curve that is greater than zero. In other words, if the area under the curve is normalized to 1, the desired probability is the area under the curve above $V = 0$. The two figures make it clear

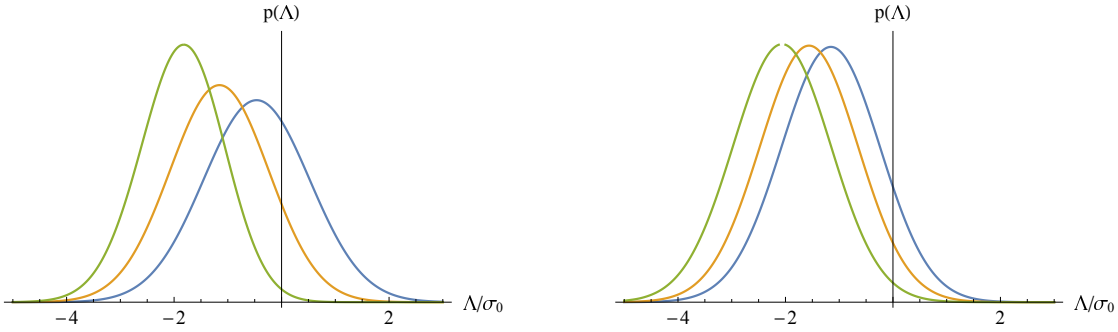

Figure 3.2: [Left] The unnormalized probability density $p(\Lambda|min)$ for $N = 3, \gamma = 0.2$, 0.5 and 0.8 (blue, orange, green respectively) and [Right] $p(\Lambda|min)$ for $\gamma = 0.5, N = 3$, 5 and 8 (blue, orange, green respectively). The distribution moves leftward with increasing N and increasing γ. Keep in mind we are interested in the part of the curve that is greater than zero, so in both figures the green line represents a smaller $p(\Lambda > 0|min)$ than the blue line.

that as γ and N increase, $p(\Lambda > 0|min)$ decreases. A plot of this probability for three different N's is in Fig. 3.3.

3.3.1 Comparison with numerical realization

To get an intuitive feel for the results, one can compare the results for $N = 2$ with a numerical realization of a random Gaussian field. We create the numerical realization by summing a Fourier series of arbitrary dimensions, amplitude and frequency, then searching for stationary points.[7] As a very simple illustrative example, for $N = 2, n_{max} = 2$, where N is the number of dimensions and n_{max} is the maximum frequency, we can expand the field F as this Fourier series:

$$F = \lambda_1 \cos(x + y + c_1) + \lambda_2 \cos(x - y + c_2) + \lambda_3 \cos(2x + c_3) + \lambda_4 \cos(2y + c_4) + \lambda_5 \cos(x + c_5) + \lambda_6 \cos(y + c_6) \quad (3.4)$$

[7]We acknowledge the use of code written by Ali Masoumi.

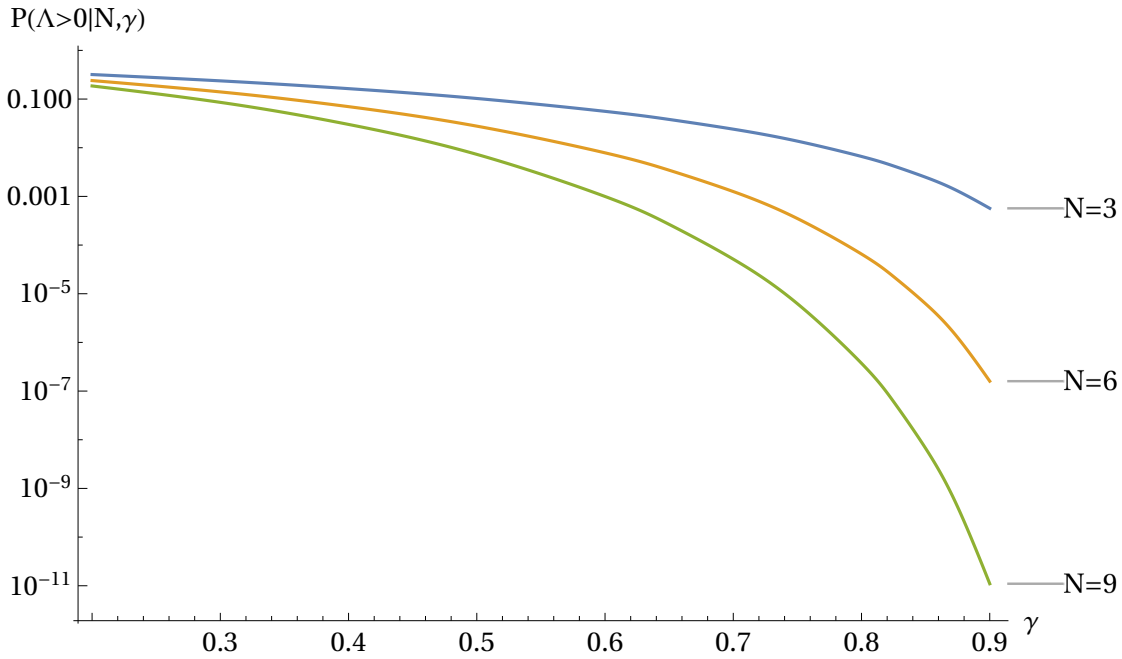

Figure 3.3: The probability that a given minimum has $\Lambda > 0$ as a function of γ, for $N = 3, 6, 9$. We see that both the heuristics are obeyed: the probability decreases with N, and γ.

where the λ's and c's are random constants, and x, y are the two dimensions.[8] We can then search a given realization for maxima and minima. This method does not generate a random Gaussian field with a specific $\gamma = \sigma_1^2/\sigma_0\sigma_2$, but it yields a field with calculable γ.

For the realization in Eq. 3.4, $\sigma_0^2 = \langle F^2 \rangle$ (see Eq. 2.18). There are 36 terms in F^2, but most of them are zero because the average of the cross terms[9] is zero, a basic property of Fourier series. Of the remaining terms, the average of a cosine squared is 1/2. Therefore $\sigma_0^2 = \sum_{i=1}^{6} \frac{1}{2}\lambda_i^2$.

The σ_1 term is more complicated. In principle, $\sigma_1^2 = \langle \eta_i^2 \rangle$, where $i = x$ or y. This indifference to direction is a consequence of the isotropy of the field. However, the generated random Gaussian field is not generally isotropic – to be isotropic one would, e.g., need to also include the $\cos(-x + y + c)$ term *and* ensure that this term has the same coefficient λ as the $\cos(x - y + c)$ term. This anisotropy means σ_1, and by extension γ, are not well-defined. However, for sufficiently large n_{max}, the field will still be approximately isotropic, and the calculated γ's approximately the same in every direction.

With this caveat aside, we can calculate σ_1 using either of $\sigma_1^2 \approx \langle \eta_x \eta_x \rangle \approx \langle \eta_y \eta_y \rangle$. As an illustration, η_x is obviously

$$\eta_x = \lambda_1 \sin(x + y + c_1) - \lambda_2 \sin(x - y + c_2) - 2\lambda_3 \sin(2x + c_3) - \lambda_5 \sin(x + c_5) \tag{3.5}$$

from which $\sigma_1^2 = \frac{N}{2}(\lambda_1^2 + \lambda_2^2 + 4\lambda_3^2 + \lambda_5^2)$, where we have left the number of dimensions N in the expression (for this 2D field, of course, $N = 2$).

[8] Superficially there should be more terms – $(2n_{max} + 1)^2$ in fact – but many are discarded. In particular, the $\cos(c)$ term is discarded because it's simply a constant. The $\cos(2x + 2y + c)$ and similar terms are discarded since the norm of the coefficients, $\sqrt{(-2)^2 + 2^2}$, exceeds the length of the box (which is n_{max}, or 2, in this case). This keeps the potential spherically symmetric. Finally, all terms in which the coefficient of the first frequency is negative (such as $\cos(-x+y+c)$) are discarded because the potential is symmetric if it is multiplied by -1.

[9] For example, the average of the $\lambda_1\lambda_2 \cos(x + y + c_1)\cos(x - y + c_2)$ term over a full cycle of x and y is zero.

	Simulated field
γ	~ 0.870
Number of dimensions	2
Number of stationary points (total)	2251
Number of minima	562
Number of minima above zero	5
$P(\Lambda > 0\|min)$ (Simulated)	~ 0.0088968
$P(\Lambda > 0\|min)$ (Calculated)	0.0105489

Table 3.1: Comparison of $P(\Lambda > 0|min)$ between a simulated random Gaussian field and the probability calculated using Eqs. 3.2 and 3.3. The value of γ is approximate because the simulated random Gaussian field is not isotropic; however the calculated γ for the two different directions still agree to three decimal places.

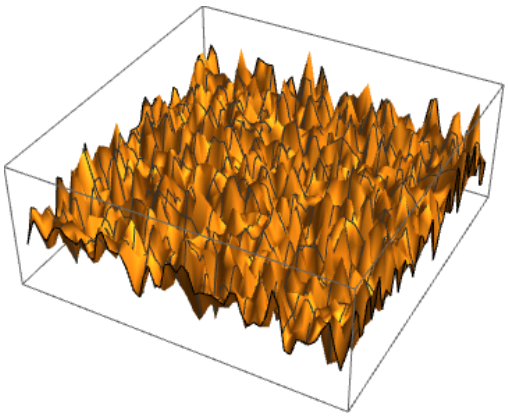

Figure 3.4: A piece of the simulated field in Table 3.1. For this field, $n_{max} = 30$.

Similarly,

$$\zeta_{xx} = \lambda_1 \cos(x + y + c_1) - \lambda_2 \cos(x - y + c_2) - 4\lambda_3 \cos(2x + c_3) - \lambda_5 \cos(x + c_5) \tag{3.6}$$

from which $\sigma_2^2 = \frac{N(N+2)}{2}(\lambda_1^2 + \lambda_2^2 + 16\lambda_3^2 + \lambda_5^2)$.

Taken together, these results let us compute γ, and therefore compare the results from this numerical realization against the theoretical results. We show a simulated 2D field in Fig. 3.4 and its properties in Table 3.1. The simulated $P(\Lambda > 0|min)$ is close to the calculated value.

This method of comparing against a numerically realized random Gaussian field scales poorly with n_{max} and especially with N, restricting its use to simple cases.

3.4 $N \gtrsim 12$

For $N \gtrsim 12$, direct calculation becomes very resource-intensive. To make progress, we use the *Gaussian approximation*. We approximate the integrals Eqs. 3.2 and 3.3 as Gaussian integrals centered on the point of maximum likelihood:

$$\text{integral} \approx I_p \sqrt{\frac{(2\pi)^N}{\det H}} \tag{3.7}$$

where I_P is the value of the integrand at its peak, and H is the Hessian at the peak. To use this approximation, we first find the x's that maximize the integrand, calculate I_P using those values, and finally calculate the Hessian with respect to those x's using the finite difference method. This is a standard technique.[10] The first-order approximation to a derivative is:

$$f'(x) \approx \frac{f(x+h) - f(x-h)}{2h} \tag{3.8}$$

To second order, the approximation is

$$f'(x) \approx \frac{1}{12h} f(x-2h) - \frac{2}{3h} f(x-h) + \frac{2}{3h} f(x+h) - \frac{1}{12h} f(x+2h) \tag{3.9}$$

The Hessian is the matrix of second derivatives. There are N directions, so it is a $N \times N$ matrix. The second order approximation for the Hessian is therefore

$$f''(x,y) \approx \left[\frac{1}{12h} f(x-2h,y) - \frac{2}{3h} f(x-h,y) + \frac{2}{3h} f(x+h,y) - \frac{1}{12h} f(x+2h,y)\right] \circ \left[\frac{1}{12h} f(x,y-2k) - \frac{2}{3h} f(x,y-k) + \frac{2}{3h} f(x,y+k) - \frac{1}{12h} f(x,y+2k)\right]$$

[10] See e.g. https://geometrictools.com/Documentation/FiniteDifferences.pdf. One could in principle calculate the analytic Hessian, but it is very complex.

which results in 16 terms. The first four are:

$$\frac{f(x-2h,y-2k)}{144h^2} - \frac{f(x-2h,y-k)}{18h^2} + \frac{f(x-2h,y+k)}{18h^2} - \frac{f(x-2h,y+2k)}{144h^2} \quad (3.10)$$

which is simply the $\frac{1}{12h}f(x-2h,y)$ term composite with the four terms in the second brackets. The remaining terms are now straightforward to derive.

In the notation of our problem, the x, y correspond to $x_1, x_2, x_3 \ldots x_N$.[11] There are N^2 terms in the Hessian, each of which need to be summed. Once done, we can take the determinant, and calculate the Gaussian integral. The values of h and k can affect the final value of the approximation. It turns out that the second-order Hessian allows a relatively large h, k without loss of numerical precision. We typically take $h = k = 0.0001$, and verified that changing this value does not substantially alter the final results.

How good is this approximation? For $N < 12$, we can compare against the numerical integrals. An illustrative comparison is in Fig. 3.5. The Gaussian approximation turns out to be very good: it produces a curve with roughly the same shape and peak. It slightly overestimates the numerical value of the integral, but the factor is roughly independent of Λ and close to unity. Given that we are dealing with numbers on the order of 10^{-500} and focus on large differences in the logarithms of the probabilities, this $\mathcal{O}(1)$ factor is completely negligible. We also plot a comparison of $P(\Lambda > 0|min)$, obtained using the Gaussian approximation and direct evaluation of the integrals, in Fig. 3.6. The plot only goes up to $N = 8$ because for $8 < N <\sim 12$, although we are still able to numerically calculate the "exact" value of $P(\Lambda > 0|\gamma, N, min)$, for reasonable computational costs the result is only accurate to within a few % (see Fig. 3.6). Hence, for $N > 8$ the dominant error is in the "exact" numerical result as opposed to the Gaussian approximation. We already see hints of this at $N = 8$: the relative error for $N = 8$ is much choppier than for lower dimensions. The plot does indicate that the relative error increases slowly with N. If we extrapolate to $N \sim 150$, it appears that the Gaussian

[11] Or y_i, z_i defined in Section 2.2 – it is equivalent to maximize any of the three variables.

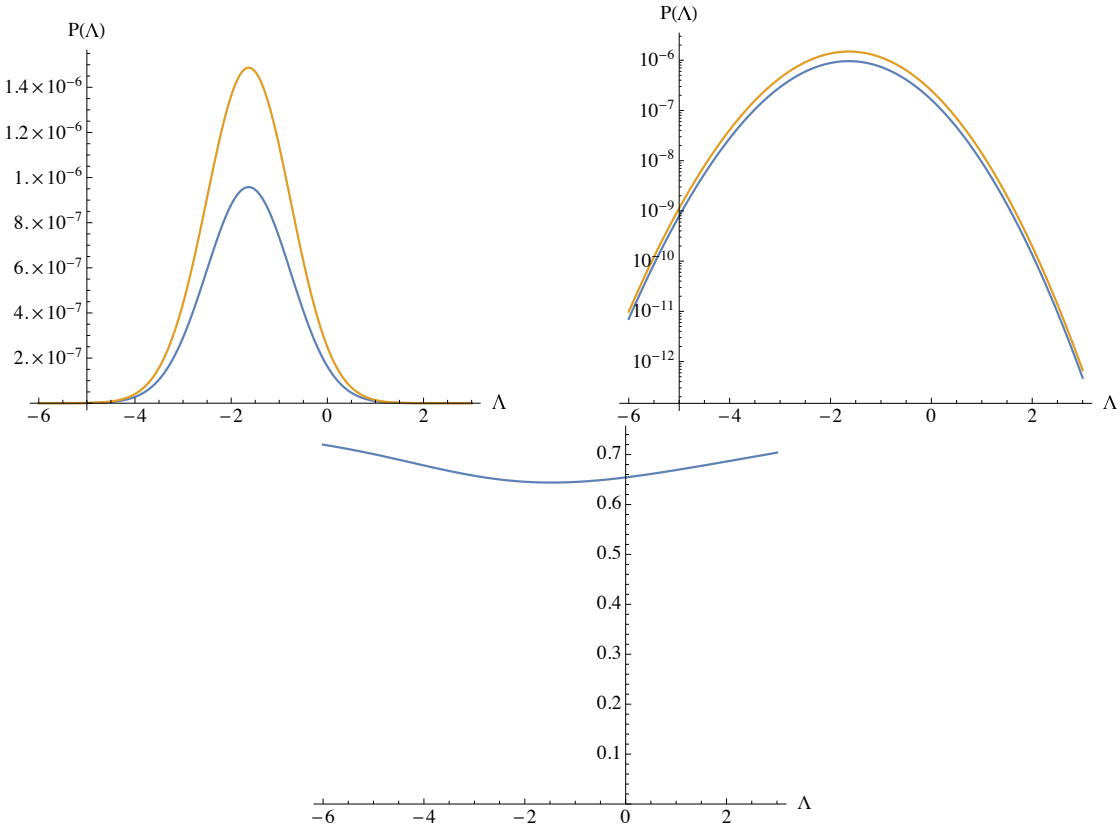

Figure 3.5: Top: A comparison of the unnormalised exact $p(\Lambda)$ (blue line) with the Gaussian approximation (orange line), for $\gamma = 0.6$ and $N = 4$. The left and right plots show the exact result and the Gaussian approximation, on linear and logarithmic axes. Bottom: the ratio of the two curves. The Gaussian approximation always over-estimates the integral, but the ratio is roughly independent of Λ and remains close to unity.

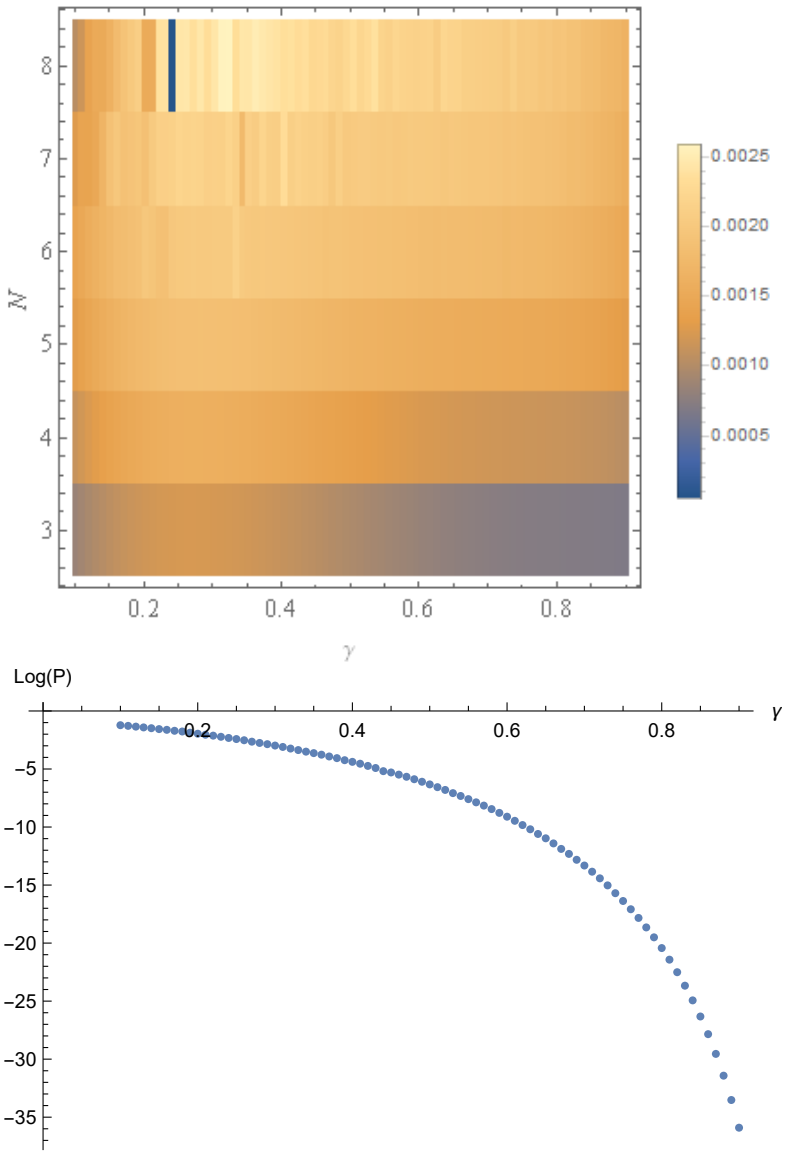

Figure 3.6: Top: Plot of the relative error in $\log(\mathrm{P}(\Lambda > 0|\gamma, \mathrm{N})$ obtained from calculating P using the Gaussian approximation versus the exact numerical result. The error never exceeds 0.3% over the whole range, but see discussion in the text for expectations when extrapolated out to $N \sim \mathcal{O}(100)$. Bottom: Plot of $\log(\mathrm{P}(\Lambda > 0|\gamma, \mathrm{N})$ as a function of γ, for $N = 12$. The values are the "exact" results, calculated using Mathematica's NIntegrate command. Although the result is quite smooth, one can see tiny fluctuations where the "exact" result calculated by Mathematica is slightly different from the value if the curve is smooth. We therefore conclude that the "exact" result is accurate to a few %, a conclusion consistent with the error estimate reported by Mathematica.

approximation can be off by ~ 3 in this log plot, or three orders of magnitude. Although this sounds like a lot, we are dealing with probabilities on the order of 10^{-500}, and three orders of magnitude will have only a small effect on the result. Therefore, we continue to use the Gaussian approximation even for large N.

We make a final comment here on the Gaussian approximation: if we accept the Gaussian approximation as sound, then we would expect there to be only one overall maximum in the likelihood (i.e. the peak of the Gaussian). This non-existence of other maxima is indirectly supported by the fact that we do not find different optima when calling FindMaximum with different starting points for the search (see Section 2.2).

3.5 Results for $N > 12$

The results for $12 < N < 150$, calculated using the Gaussian approximation for different values of γ, are shown in Fig. 3.7 and Fig. 3.8. For $N > 150$, the computations required are expensive, even with the Gaussian approximation.

As can be seen from the figures, as N increases, the probability of a minimum having $\Lambda > 0$ decreases quickly, and for sufficiently large values of γ, it can drop below 10^{-500}. On its own, this result is not surprising – surely for a sufficiently smooth random Gaussian field we would expect very few minima, and of those minima, most of them would be below zero. Therefore, the next question is, what value of γ is reasonable?

To answer this question, we make use of the results from Section 2.1.3 for the γ of simple power spectra. The **Gaussian power spectrum** has $\gamma = \sqrt{N/(N+2)}$, or about 0.990 at $N = 100$. Fro these parameter values, $P(\Lambda > 0|min)$ evaluates to 10^{-1197}. This probability is so minute that even with 10^{500} minima in the landscape, the probability of a single minimum having $V > 0$ is roughly 10^{-700}, and thereby poses a challenge for landscape cosmology. Nonetheless, for the high end estimate of 10^{27200} vacua (see the introduction and Ref. [3]) there are still more than enough minima to go round.[12]

The **power-law power spectrum** has $\gamma = \sqrt{4x + x^2}/(2 + x)$, where $x =$

[12]This last conclusion might fail if N turns out to be much larger than 100. Like many other things about the string landscape, its exact value is not known.

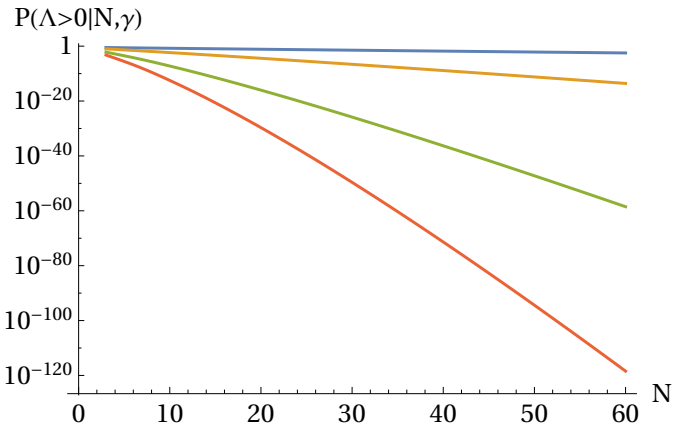

Figure 3.7: The probability that a given minimum has $\Lambda > 0$, as a function of N for $\gamma = 0.2$, 0.5, 0.8 and 0.9 (top to bottom) calculated using the Gaussian approximation.

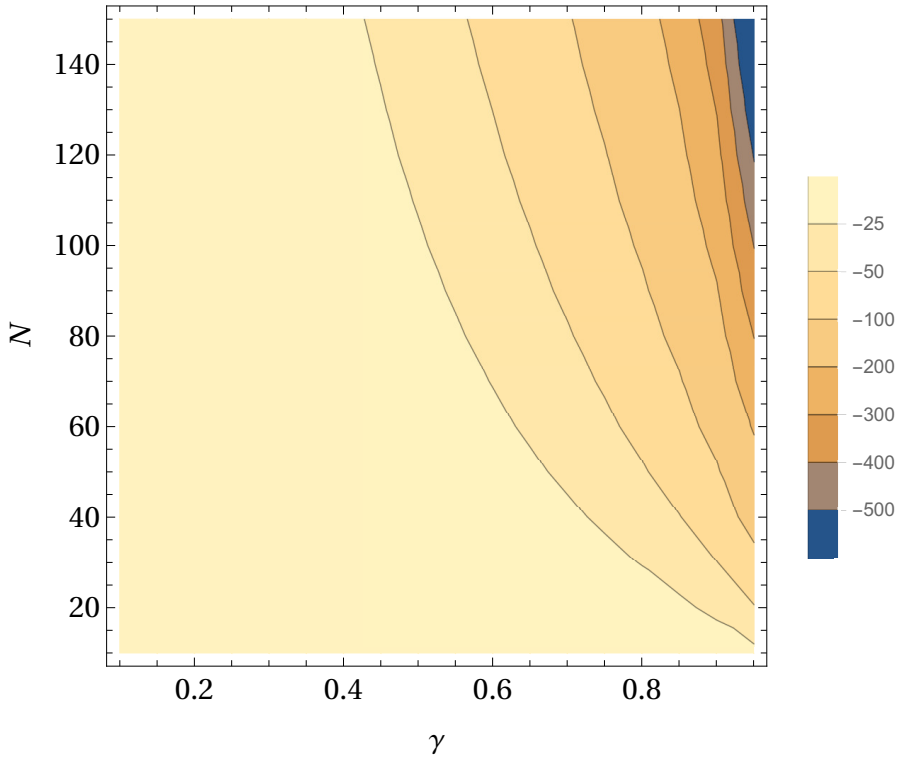

Figure 3.8: $\log_{10}(P(\Lambda > 0|N, \gamma))$ as a function of N and γ. For moderately large N and γ close to unity, fewer than 1 in 10^{500} minima have $\Lambda > 0$.

$n - 4 - N$ for a red cutoff or $x = N - n$ for a blue cutoff. This expression can generate all possible values of γ. It can be shown that in order to have $P(\Lambda > 0|min) > 10^{-500}$ at $N = 100$, we need $\gamma < \sim 0.96$, corresponding to $x \lesssim 5.14$ (Fig. 3.8).

3.6 Summary

In this chapter, we have calculated $P(\Lambda > 0|min)$, thus answering the first research question. We began with direct integration of Eq. 2.36, which can be efficiently computed for small N, then introduced the Gaussian approximation to compute the integrals up to $N \sim 150$. The key result is Fig. 3.8, which plots $P(\Lambda > 0|min)$ as a function of the two free parameters in the landscape, N and γ. We see that for much of the parameter space there are comparatively many minima with $\Lambda > 0$, but the fraction decreases with increasing N and γ. For $N \sim 100$ and γ close to unity, this fraction can decrease to the point where fewer than 1 in 10^{500} minima have $\Lambda > 0$, potentially posing a problem for landscape cosmology.

Chapter 4

Question two: eigenvalues at minimum

In the landscape picture of our universe's history, prior to inflation, the universe was (loosely speaking) located at a saddle. It inflated out of the saddle and eventually settled in a minimum, where it is currently located. This makes it desirable to know the properties of the minimum: it would tell us about the end of inflation, give some indication of the surrounding potential heights,[1] and also help inform quintessence models. In quintessence, dark energy is not due to a cosmological constant, but rather a scalar field analogous to the inflaton. The slope of this scalar field would then tell us about how fast dark energy is changing.

From the perspective of our calculations, what we are trying to find are the eigenvalues at the most probable minimum, which we will use as a proxy for 'our' minimum. To do this, we recall that Eqs. 2.36 and 2.38 are unnormalized probability densities for the number of minima and saddles. Accordingly, it is easy to calculate what the most probable eigenvalues are: simply find the values of λ_i and Λ that maximize the integrand. We do this using Mathematica's FindMaximum function. This yields all N eigenvalues simultaneously.

Before going into the results, we note several things. First, the distribution of eigenvalues at the most probable Λ is independent of γ. This can be seen from Eq. 2.37. The only place in which γ enters the expression is in the term $(\nu - \gamma x_1)^2$.

[1] If the minimum is not the global minimum, this is potentially relevant in quantum tunneling scenarios where our universe continues its evolution by tunneling out of the current minimum.

Therefore the most likely Λ ($= \nu\sigma_0$ by definition) is the value that minimizes this term, or $\gamma x_1 \sigma_0$. Choosing this Λ eliminates the only γ dependence from Q. Secondly, the x's are intimately related to the eigenvalues, but they also include a factor of σ_2 (see Eq. 2.20). Therefore, all the results we derive in this section are actually for the dimensionless eigenvalues λ/σ_2. Thirdly, three parameters in Eqs. 2.36 and 2.38 need to be input by hand: N, γ and Λ. The first two are (unknown) properties of the random Gaussian field, but the last can be constrained from observations: it is the value of the potential at our minimum, which in turn is related to the observed value of dark energy. This value is about $6.3 \times 10^{-27} kg/m^3$ today.[2] If we take the natural guess[3] that σ_0 is approximately the Planck energy density $c^5/\hbar G \approx 5.1550 \times 10^{96} kg/m^3$, then $\Lambda = V/\sigma_0 \approx \mathcal{O}(10^{-123})$. This is a vanishingly small number. Therefore, in the plots to follow, we consider the point $\Lambda = 0$ in addition to the most probable value of Λ.

A final detail is that we want the expected distribution of eigenvalues $\rho(\lambda)$, but the method above of maximizing the integrand only finds the most probable eigenvalues. For any given N there will be N eigenvalues. We turn this into a distribution $\rho(\lambda)$ by first considering $n(\lambda)$, defined as the number of eigenvalues smaller than λ. This function is related to the desired $\rho(\lambda)$ – recall that by definition, $\int_{\lambda_2}^{\lambda_1} \rho(\lambda) d\lambda$ yields the number of eigenvalues between λ_2 and λ_1. Therefore $n(\lambda) = \int_0^{\lambda_1} \rho(\lambda) d\lambda$, or $\rho(\lambda) = dn(\lambda)/d\lambda$. Our results do not actually produce a smooth function $n(\lambda)$ – we only have 100 discrete eigenvalues which we have to interpolate to get $n(\lambda)$ for all values of λ. Accordingly, the approximation fails in any region in which there are few λ: in other words, it will fail to resolve sharp features in the distribution, and it will not work well in regions which contain almost no eigenvalues ($\rho(\lambda) \sim 0$).

In Fig. 4.1 we plot the expected distribution of eigenvalues $\rho(\lambda)$ for $N = 100$, at both the peak likelihood when Λ is allowed to vary,[4] and at the peak likelihood assuming $\Lambda = 0, \gamma = 0.9$. With no restrictions whatsoever on λ, the distribution of eigenvalues is well-known: it is the Wigner semicircle [8, 9]. The eigenvalue distribution in Fig. 4.1 is different because we have the extra constraint that we

[2] Calculated using $\Omega_\Lambda = 0.69$, as in the Planck results [40], with $H_0 = 70 km/s/Mpc$.

[3] This guess is based on the idea that the string theory landscape only comes into play at Planckian energies; at lower energies the Standard Model of Particle Physics works well.

[4] Recall that this distribution is independent of γ.

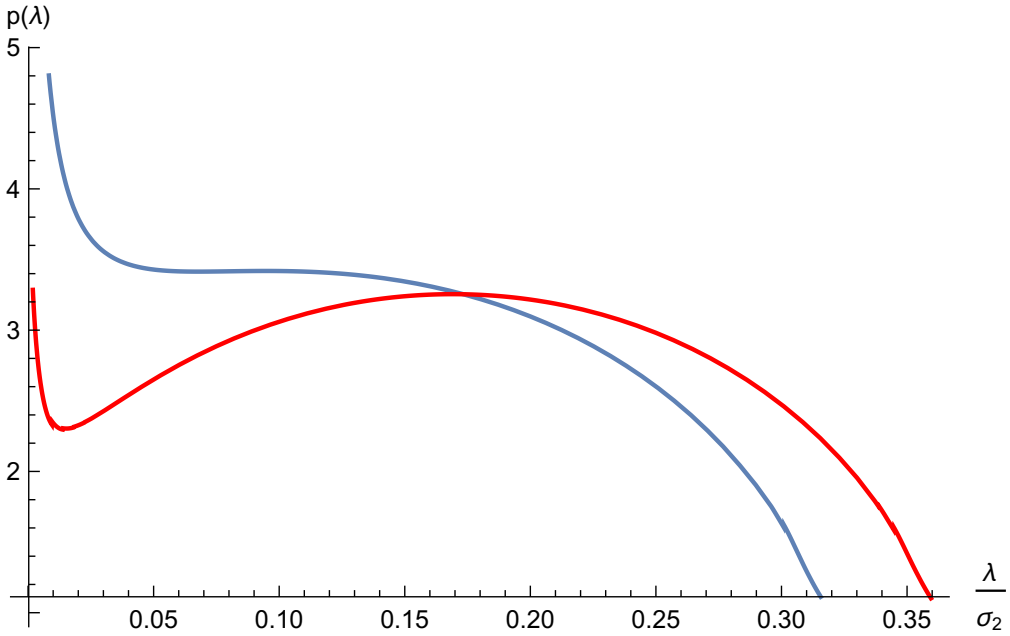

Figure 4.1: The expected distribution of eigenvalues at most likely value of Λ (numerically calculated to have $\Lambda/\sigma_0 = -15.64$, red curve) and at $\Lambda = 0$ (blue curve) for $N = 100, \gamma = 0.9$. The horizontal axis corresponds to the eigenvalues at that point, while the vertical axis is the expected number density of each eigenvalue. Note the red curve is independent of γ (see text). Compare Figures 8 and 9 in Yamada and Vilenkin [34].

are at a minimum, i.e. all eigenvalues must be > 0. The result is that, for the most probable Λ, we see what looks like a Wigner semicircle but with deviations at small eigenvalues. The deviations occur at larger eigenvalues if we impose the constraint that $\Lambda = 0$.

This shape of $\rho(\lambda)$ is in broad agreement with the results derived by Yamada & Vilenkin [34] using a different method. There is some deviation with Yamada & Vilenkin's results at the very smallest eigenvalues, where their curve turns around and goes to zero. The discrepancy arises because we lack the resolution at those values – we only have a few eigenvalues in that regime which makes the interpolation miss the sharp feature – which is in turn because we only have N eigenvalues. We cannot simply increase N, both because of the computational costs and because the expected turnaround in the eigenvalue distribution decreases with N [34]. We note, however, that the distribution must go to zero because the value of the integrand

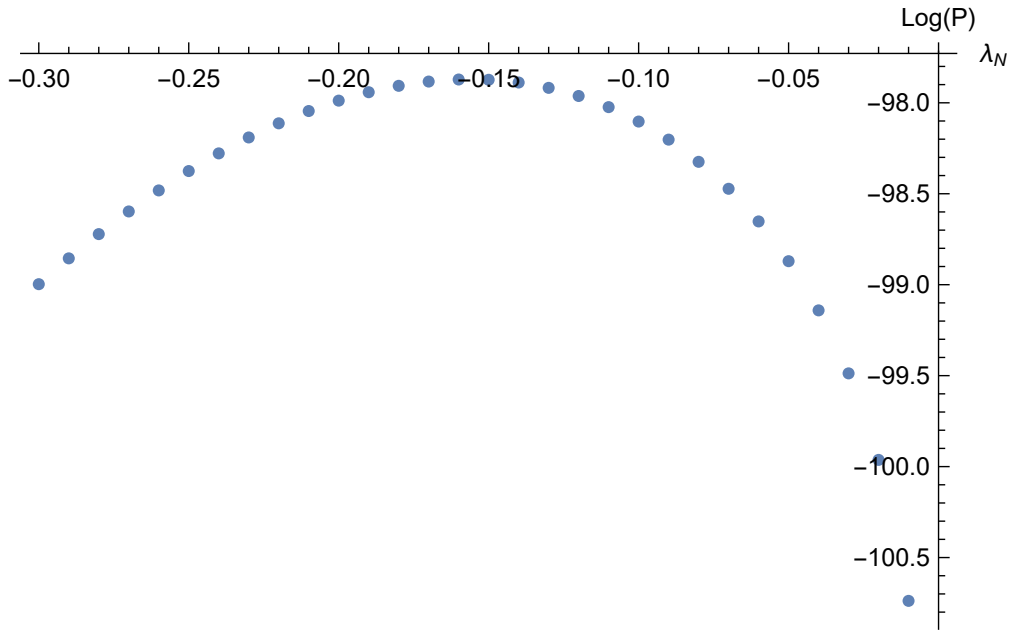

Figure 4.2: Plot of the unnormalized log-likelihood (vertical axis) against the dimensionless eigenvalue of the downward direction (horizontal axis), for $\gamma = 0.9, N = 10$ and Λ integrated over. The probability increases as λ increases, up to about $\lambda_N = -0.15$, before decreasing again. From this, we confirm that the likelihood goes to zero as $\lambda_N \to 0$, in agreement with Yamada & Vilenkin's results.

in Eq. 2.36 goes to zero as the smallest eigenvalue λ_N goes to zero, a feature we verified in our code by fixing all eigenvalues except λ_N and confirming that $\lambda_N = 0$ is excluded (Fig. 4.2).

Some other results for the eigenvalues are in Figs 4.3, 4.4 and 4.5, where we investigate the variation with γ, the values of the biggest and smallest eigenvalues, and the ratio of the two smallest eigenvalues. The ratio of the smallest eigenvalues is especially intriguing, because if each dimension is associated with one quintessence field, it raises the possibility that more than one quintessence field is active around a minimum. Another interesting effect is that the smallest eigenvalues decrease as γ increases (Fig. 4.4). If the refined de Sitter swampland conjecture [62] turns out to be valid, then there would be no minima with $\Lambda > 0$. This would require dark energy to be explained in some other way, such as quintessence. In this case the region of parameter space we are interested in is $\gamma \sim 1$,[5] and Fig. 4.4 indicates that

[5]This is the region of parameter space for which most minima have $\Lambda < 0$. See Chapter 3.

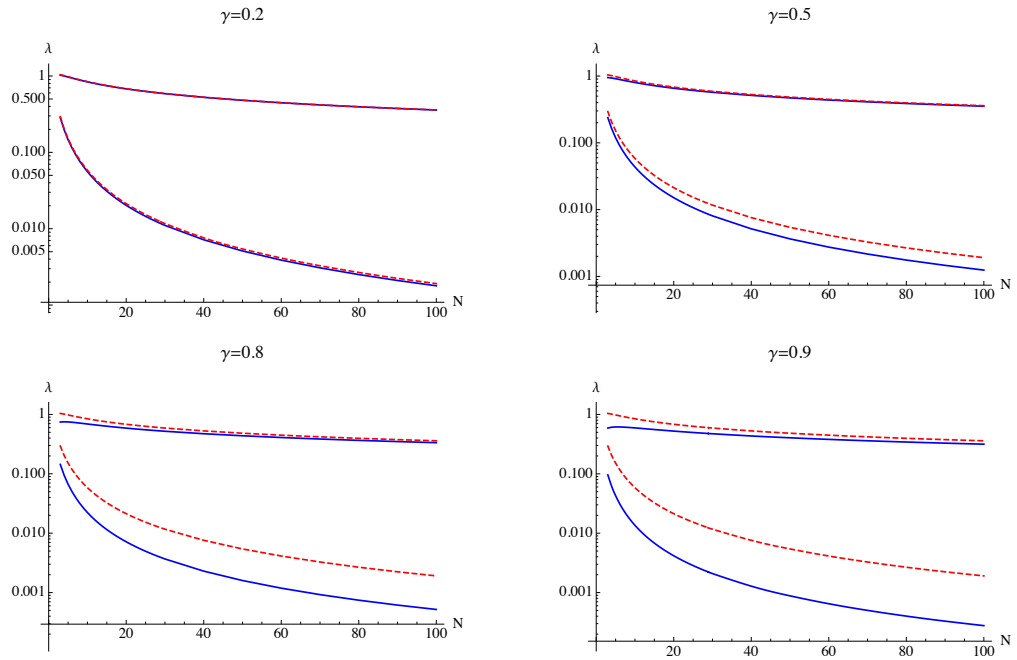

Figure 4.3: The expected minimum and maximum eigenvalues of the Hessian at a local minimum, as a function of N for four values of γ. Dashed lines denote eigenvalues at the most likely value of Λ; solid lines indicate values at $\Lambda = 0$. The expected values of the smallest eigenvalue decreases as N increases, while the maximum value is roughly unchanged.

the smallest eigenvalues of the minima with $\Lambda = 0$ approach zero in this limit. This suggests that random Gaussian random functions naturally generate minima with a very gentle incoming slope which could provide possible quintessence potentials. We will say more on this in Chapter 6.

In this section, we have shown that the most probable eigenvalues at minima of the landscape can be investigated using Eq. 2.36. We have shown that the single most-probable minimum, which has $V < 0$, has eigenvalues that are independent of γ. Our results are consistent with previous work by Yamada and Vilenkin [34], but also go further, since we are able to calculate the most probable eigenvalues for minima with different V or γ. The small eigenvalues we find at rare minima are especially interesting, with implications for both inflation and quintessence.

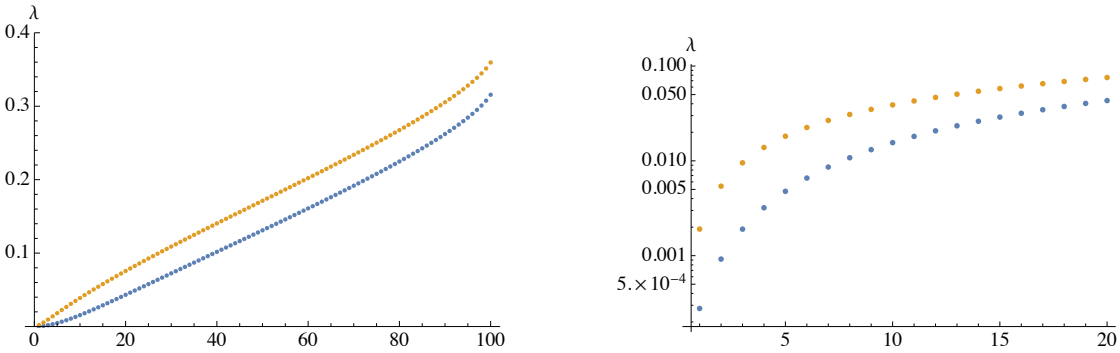

Figure 4.4: A plot of the most probable eigenvalues for $\gamma = 0.9$ and $N = 100$. The left hand plot shows the most likely value of each of the 100 λ_i; the right hand plot shows the smallest eigenvalues on a log scale. The orange points correspond to the most probable eigenvalues when Λ is allowed to vary, while the blue points correspond to the most probable eigenvalues with $\Lambda = 0$.

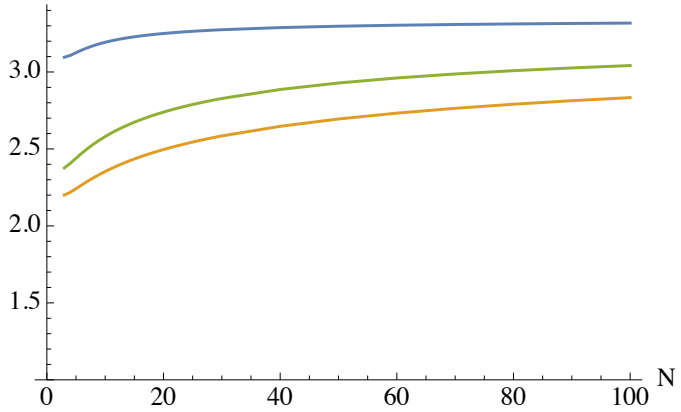

Figure 4.5: The expected ratio of the two smallest eigenvalues as a function of N. The orange line is the ratio at the most probable point (which does not depend on γ), while the green and blue lines are for $\Lambda = 0$ and $\gamma = 0.5$ & 0.9 respectively.

Chapter 5

Question three: steepness of outward slopes for saddles

The final research question is arguably the most exciting, because it relates directly to inflation. In the landscape picture, before inflation, our universe was presumably located at a saddle with at least one downhill direction. Our universe then "rolls" downhill along this direction. If the gradient of the downhill direction is small, then slow roll inflation results. If we assume that all other directions are upwards,[1] then the saddle can be described with Eq. 2.38.

Slow roll inflation is parameterized by the two slow-roll parameters, η and ϵ (Eq. 1.1; we have used units $c = \hbar = 1$):

$$\epsilon = \frac{M_P^2}{2}\left(\frac{V'}{V}\right)^2 \tag{5.1}$$

$$\eta = M_P^2\left|\frac{V''}{V}\right| \tag{5.2}$$

where M_P is the Planck mass, V is the inflaton, and V' is its derivative.[2] Inflation occurs when these parameters are small.[3] The first parameter ϵ is by definition zero at saddles, so we are primarily interested in the second parameter, η. We

[1] This is an intuitive assumption: if a steeper downhill direction existed, the universe would probably have rolled down that direction instead.

[2] Here we switch once again (with apologies) to the notation in the Introduction where V is the inflaton and ϕ are the parameters of the inflaton. Unfortunately, this notation switch is necessary to make the upcoming equations more immediately recognizable.

[3] But see the caveat raised in the Introduction: strictly speaking only ϵ needs to be small.

note at once that η depends on V'', which in turn is related to the eigenvalues of the Hessian via $\lambda_i = \zeta_{ii}/\sigma_2$ (see Eq. 2.4; ζ_{ii} is the second derivative of the field). Meanwhile, $\nu = \Lambda/\sigma_0$ by definition. Therefore, we can write:

$$\eta = M_P^2 \left| \frac{\lambda \sigma_2}{\nu \sigma_0} \right| \tag{5.3}$$

where λ is the eigenvalue in the downward direction. From here, we can use the methods we used in the last chapter to calculate the most probable value of λ for a given ν. Then, we can calculate σ_0 and σ_2 for a specific power spectrum, and evaluate η. This yields η for the most probable 1-saddle.

Before we proceed, there is a subtlety worth pointing out: while maximizing the integrand of Eq. 2.38 yields the properties of the most probable 1-saddle, we are interested in the properties of *typical* 1-saddles, and the most probable 1-saddle might not be representative of typical 1-saddles. It turns out that the ν_1 at which typical saddles are located is not the same as the ν_2 for single most probable saddle. In particular, we find that $P(\nu|\gamma, \text{1-saddle})$,

$$P(\nu|\gamma, \text{1-saddle}) = \frac{\int \mathcal{L}(\lambda_1, \cdots \lambda_N; \nu, \gamma) d\lambda_1 \cdots d\lambda_N}{\int_\infty^{-\infty} d\nu \int \mathcal{L}(\lambda_1, \cdots \lambda_N; \nu, \gamma) d\lambda_1 \cdots d\lambda_N} \tag{5.4}$$

where $\mathcal{L}$ is the integrand of Eq. 2.38, peaks at a different ν compared to the ν found by maximizing the integrand without integrating over ν (Fig. 5.1). Physically, this means that although the single most probable 1-saddle has $\nu = \nu_2$, there are a lot of almost-as-probable 1-saddles at a nearby value of $\nu = \nu_1$, such that collectively one is more likely to find a 1-saddle at ν_1. In principle, ν_1 is the value we want – it is the ν at which 1-saddles are most likely to be located. Nonetheless, ν_1 and ν_2 are very similar. We therefore calculate ν_2, which is computationally much cheaper.

Here we make another comment: while the results for the first two research questions only depend on the power spectrum via the parameter γ, this third research question is different – it depends on the ratio σ_2/σ_0. Nonetheless, γ remains relevant because it determines if we are likely to find 1-saddles with $V > 0$. In the following sections, we will state as many dimensionless results (meaning power spectra-independent) as possible for ν and λ first, before dealing with dimensionful properties later.

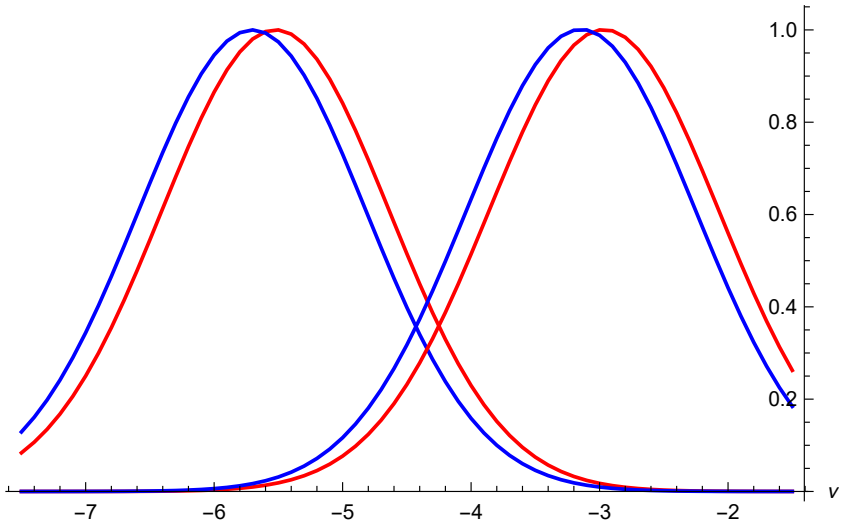

Figure 5.1: The normalized likelihood for the most probable 1-saddle (red) obtained by maximizing the integrand of Eq. 2.38, and the result after evaluating Eq. 5.4 using the Gaussian approximation (blue). $\gamma = 0.5, N = 20$ (right curves) and $\gamma = 0.5, N = 50$ (left curves). The peaks of the red (blue) curve correspond to ν_2 (ν_1) in the text. The two values of ν are very close to one another, hence we focus on calculating the much-cheaper ν_2.

5.1 The number of 1-saddles

A first estimate for the number of 1-saddles is $N \times N_{min}$ [28]. Since the number of minima in the landscape has variously been estimated as 10^{500} to 10^{27200} [3], for $N \sim \mathcal{O}(100)$, this translates to 10^{502} to 10^{27202} 1-saddles, which are close enough to the original value as to be effectively the same. It is a sign of just how large the numbers involved are that a two-order magnitude of difference has virtually no impact on the results. It is also worth noting that the intrinsic error in the Gaussian approximation (Section 3.4), at $N = 100$, is expected to be greater than two orders of magnitude.

The first question to ask is if the number of 1-saddles with $V > 0$ follows the same relation as minima. This is a straightforward problem to attack using the same methods as with minima. The short answer is 'yes' (Fig. 5.2), 1-saddles with $V > 0$ also get rarer as γ increases. This should not be surprising – since they have only one downhill direction, 1-saddles are 'almost minima', and they will be rare in situations where minima are rare.

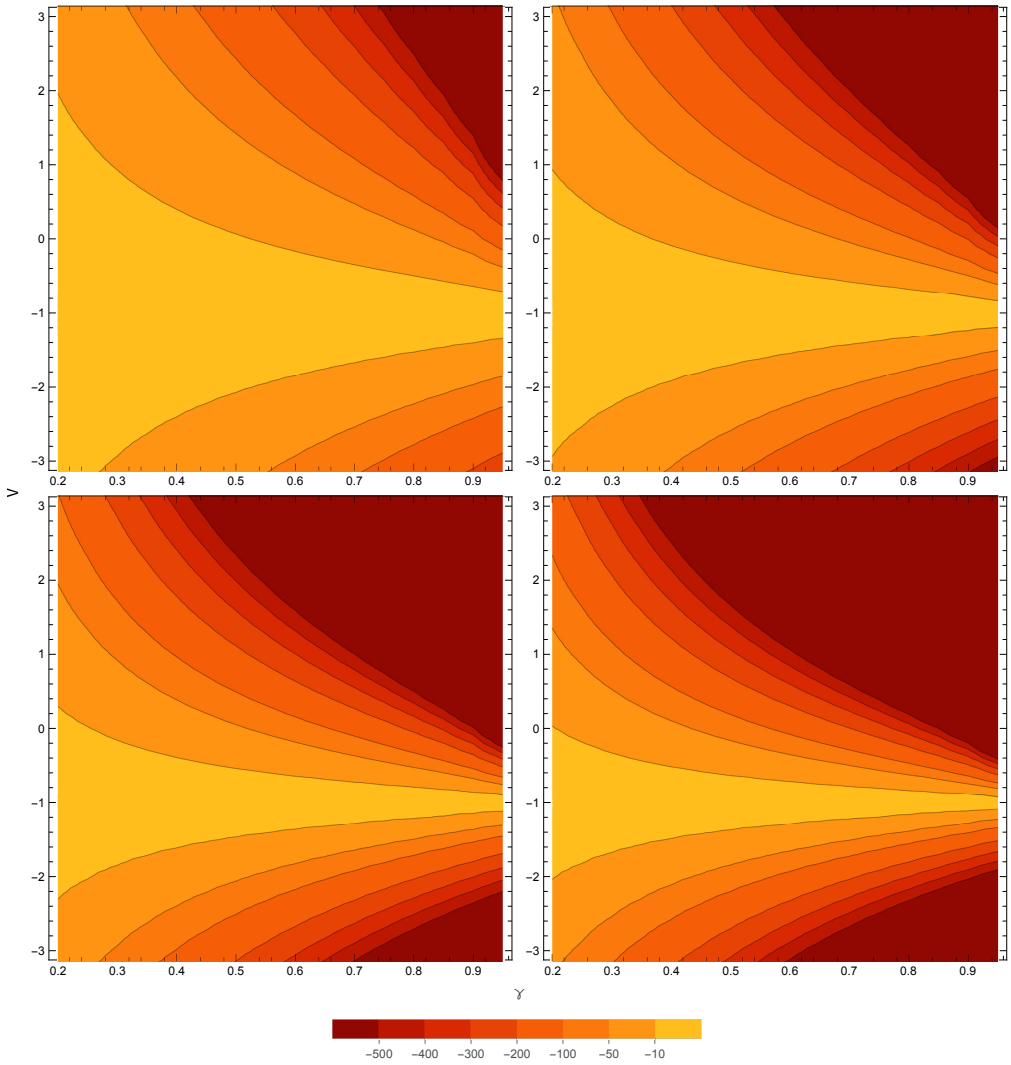

Figure 5.2: The likelihood of 1-saddles as a function of γ and V/V_{max}, where V_{max} is the V at which most 1-saddles are located, for $N = 50$ (top left), 100, 200, and 300 (bottom right). The contours show the log of the likelihood. As can be seen, 1-saddles are more probable for small values of γ, and the fraction that is above 0 decreases with N. This is the same behavior seen for minima (Fig. 3.8).

5.2 The value of ν

By definition, $\nu = V/\sigma_0$. In turn, σ_0 is closely related to the root mean square energy of the landscape ($\sigma_0^2 = \langle FF \rangle$, see Eq. 2.18), and is therefore something that can in principle be fixed experimentally. However, the energies required are so high that no conceivable experiment will be able to probe them.[4] The only experimental detail available is that the average energy of the landscape is greater than LHC scale, which still leaves a wide range of possibilities for σ_0.

A first guess for σ_0 is Planck energy, $c^5/\hbar G$, or M_P^4 in units where $c = \hbar = 1$.[5] Quantum gravity effects are expected around Planck energy, and the string landscape would presumably have a roughly similar energy range. This guess implies that ν corresponds to the energy of the pre-inflation saddle in Planck units – so for example $\nu = 0.1 \rightarrow V = 0.1 M_P^4$.

A theoretical issue with this guess for σ_0 is that the peak of the likelihood – the ν at which most minima (maxima) are located – decreases (increases) with N (see Fig. 3.2). In fact, most of the minima for $N = 3$ already have $\nu < -1$. This implies that most of the maxima and minima are not classically accessible. To avoid this, one could choose a σ_0 that decreases with N. Calculations show that the the most probable ν varies as $\sqrt{N}$ (Fig. 5.3), which suggests that we could choose $\sigma_0 = M_P^4/\sqrt{N}$. This sets M_P^4 to be the energy density at which most maxima are located, $-M_P^4$ to be the equivalent energy density for minima, and the root mean square energy of the landscape to $M_P^4/\sqrt{N}$ – a value still far above the LHC scale for any likely N.

Another question to address is the value of V for typical inflationary saddles. If we ascribe dark energy to a cosmological constant, then V for our current universe is about $6.3 \times 10^{-27} kg/m^3$.[6] The value of V before inflation must be greater than this, but this value is small enough that it is not much of a constraint.

Surprisingly enough, although our universe is no longer at the saddle of inflation,

[4] Actually attaining those energies, and thereby potentially moving from one minimum in the landscape to another, will very likely annihilate us all. This is because it would change the laws of physics.

[5] This convention is widely adopted in cosmology, and we will also adopt these units in subsequent equations throughout this section.

[6] This number, first encountered in Section 4, was calculated using $\Omega_\Lambda = 0.69$ [40] with $H_0 = 70 km/s/Mpc$.

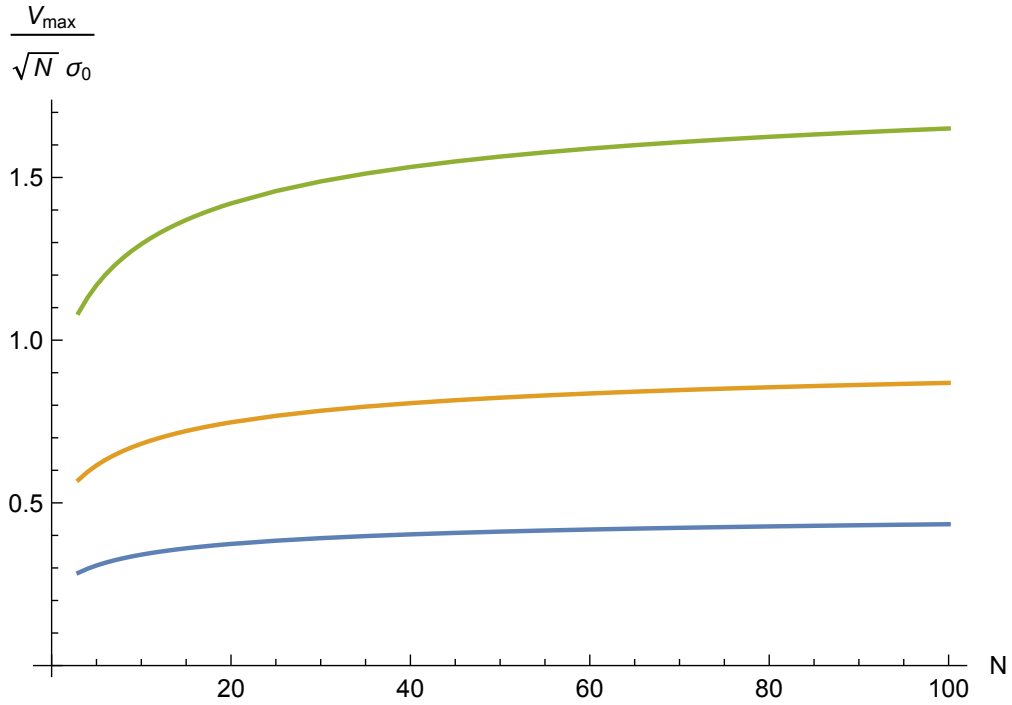

Figure 5.3: (Left) The value of V at the point of maximum likelihood for maxima as a function of N, for (from bottom to top) $\gamma = 0.25$, 0.5 and 0.95. The results have been divided by $\sqrt{N}$ to illustrate their scaling behaviour.

the inflationary V is potentially observable. Inflation takes the quantum fluctuations in matter density in the early universe and blows them up to cosmological scales. These fluctuations are small perturbations to the metric and fields, and are of two kinds: scalar perturbations and tensor perturbations. Tensor perturbations are especially interesting for our purposes, because inflation predicts a power spectrum for them ([41], Eq. 7.147):

$$P_h \simeq \frac{2}{M_p^2}\left(\frac{H}{2\pi}\right)^2 |_{k=aH} \tag{5.5}$$

where H is the Hubble parameter when the mode in question leaves the horizon. Since the Hubble parameter is related to the potential of the field by ([41], Eq. 3.7)

$$H^2 \simeq \frac{V(\phi)}{3M_P^2} \tag{5.6}$$

a detection of tensor mode perturbations would also fix V, and by extension ν.

In practice, results are expressed in terms of the tensor-to-scalar ratio r, which is related to the energy scale of the inflationary saddle by

$$V \sim \frac{r}{0.7} \times \left(1.8 \times 10^{16}\text{GeV}\right)^4 \sim \frac{r}{0.7} \times (0.0014 M_P)^4 \tag{5.7}$$

(see [42] Eq. 5). Measuring a nonzero tensor-to-scalar ratio would be evidence of physics at an energy scale only a few orders of magnitude below the Planck scale.

The only problem with this is that tensor mode perturbations have not been detected. The best current constraints place the maximum value of r at about ~ 0.044 [57], which puts the energy scale of the inflationary saddle at not more than about $(0.0007 M_P)^4$.

If we take $\sigma_0 \approx M_P^4$, then the non-detection of tensor mode perturbations implies ν is at most $0.0014^4 \times 0.63 \sim 2.4 \times 10^{-13}$. If we take $\sigma_0 \approx M_P^4/\sqrt{N}$, then ν is at most $\sim 2.4 \times 10^{-12}$ for $N = 100$. Accordingly, for our calculations of η, we take $\nu = 1 \times 10^{-12}$; the results are virtually identical for either value of ν.

5.3 The dimensionless eigenvalue λ

By definition, $\lambda = V''/\sigma_2$. Its position in the numerator of Eq. 5.3 indicates that inflation is more probable with small λ. Figure 5.4 shows how the value of λ varies with N, both at the overall peak (which has $\nu < 0$) and at the cosmologically relevant energy density $\nu = 10^{-12}$. The most probable λ decreases as N increases or γ decreases. This result does not mean the dimensionful eigenvalue, $\lambda\sigma_2$, exhibits the same behavior with N and γ, since that depends on the power spectrum used. However, calculations show that the dimensionless downhill eigenvalue decreases when compared to the dimensionless uphill eigenvalues as N increases or γ decreases (Fig. 5.5). In other words, the downhill direction is quite gentle when compared to the uphill directions, and it gets gentler for large N and small γ.

This result suggests that the random Gaussian landscape might offer a natural solution to the so-called η *problem*: inflation needs $|\eta| \approx 0.01$, but its natural value is closer to unity. In random Gaussian landscapes, one naturally gets a small downhill direction relative to the uphill directions. This does not imply a small

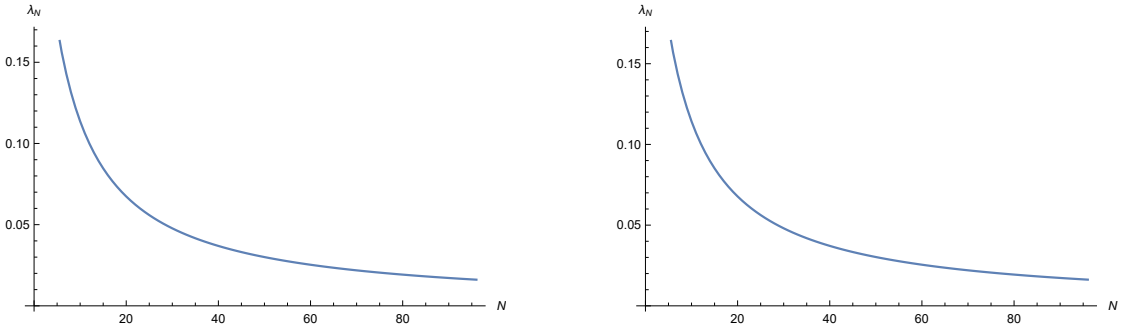

Figure 5.4: A plot of the most probable downward dimensionless eigenvalue for $\gamma = 0.1$. The left hand plot is for the overall peak (which has $V < 0$), while the right hand plot is at $\nu = 10^{-12}$. The most probable downward dimensionless eigenvalue decreases with N,

η – that again depends on the power spectrum – but it does mean that random Gaussian landscapes might be able to soften the η problem independently of how the landscape is constructed. In Fig. 5.6 we plot the most probable distribution of eigenvalues for 1-saddles at various ν, illustrating its size relative to the other eigenvalues.

The variation with γ is also notable: small γ corresponds to the region of parameter space for which large numbers of 1-saddles have $V > 0$ (see Fig. 5.2). If our universe is but one of many possible universes with a positive cosmological constant, this would be the region to look at.

5.4 Gaussian power spectrum

We now proceed to results for explicit power spectra. As a reminder, the specific form of the Gaussian power spectrum we adopt is $P(k) = U_0^2 e^{-k^2/2L^2}$. A caveat for all the Gaussian power spectrum results in this section is that, if the number of vacua in the landscape is $\sim 10^{500}$, the Gaussian power spectrum probably does not yield any 1-saddles above zero (see Section 2.1.3).

If we nonetheless have a 1-saddle above zero (with $\sim 10^{502}$ 1-saddles, the odds of this for a 100-dimensional landscape are roughly 1-in-10^{700}), then we have that $\gamma = \sqrt{N/(N+2)}$ as derived in section 2.1.3, while σ_2/σ_0 can be calculated using

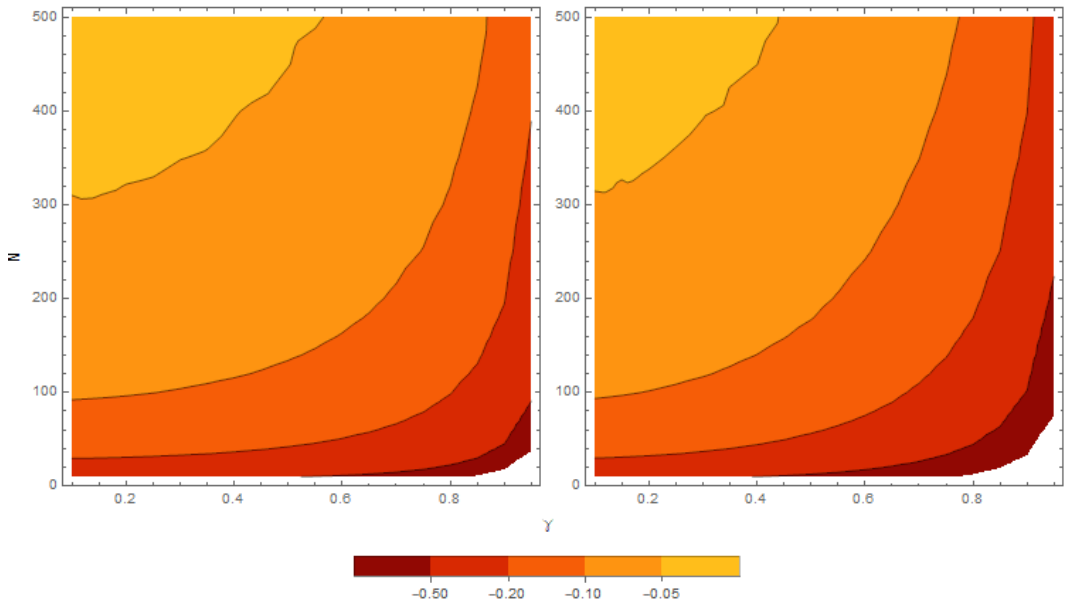

Figure 5.5: The ratio of the downhill eigenvalue to the average of the uphill eigenvalues, as a function of N and γ, for the most probable 1-saddle. (Left) The plot for $V = 0$. (Right) The plot for $V = V_{max}$, where V_{max} is the value of V at which most 1-saddles are located. For small γ and large N, the downhill slope gets gentler relative to the uphill slopes.

Eq. 2.47:

$$\frac{\sigma_2}{\sigma_0} = \frac{1}{L^2}\sqrt{N(2+N)} \tag{5.8}$$

We can immediately plot η as a function of N using Eq. 5.3. There is only one detail: the σ_2/σ_0 ratio involves the unknown L, whose values need to be input by hand. We will briefly discuss the physical interpretation of this parameter now.

5.4.1 The correlation length L

In these equations, L is the correlation length. It is closely related to the two-point correlation function, first mentioned in the text above Eq. 2.10. By definition, the two-point correlation function is the Fourier transform of the power spectrum:

$$F(|\phi_1 - \phi_2|) = \frac{1}{(2\pi)^N}\int d^N k P(k) e^{ik\cdot(\phi_1-\phi_2)} \tag{5.9}$$

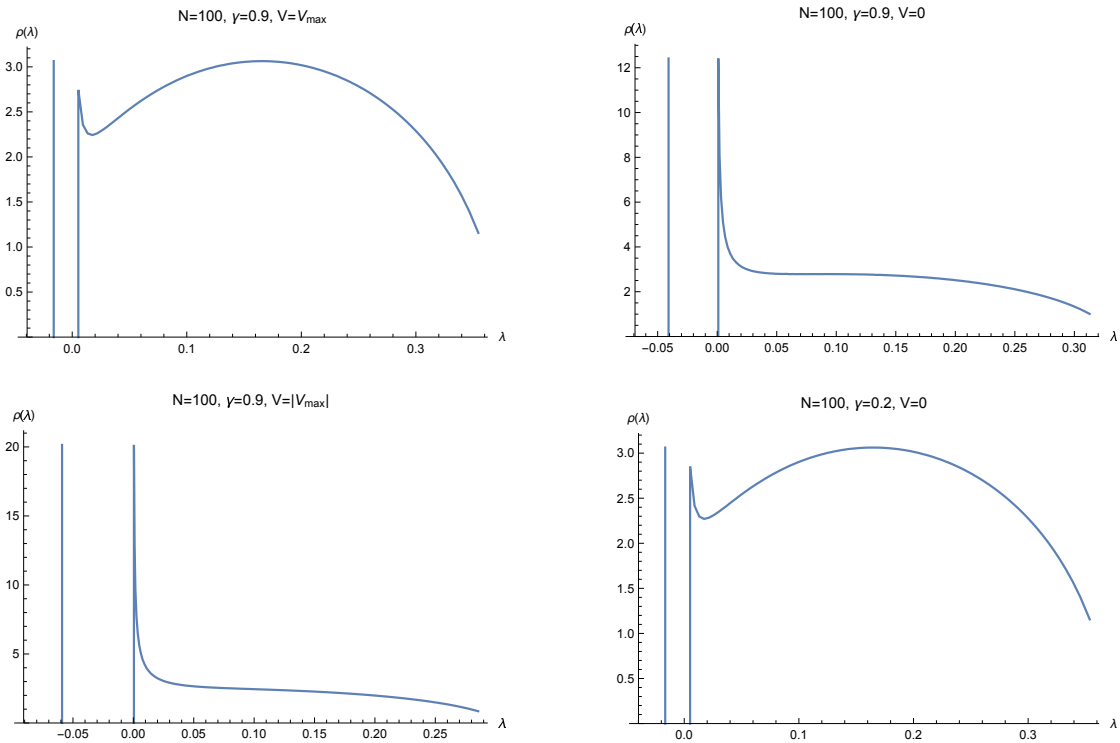

Figure 5.6: The most probable eigenvalue distributions for 1-saddles for various parameters. The most probable downhill eigenvalue is generally quite small relative to the uphill ones. Compare Fig. 4.1, which is the corresponding eigenvalue distribution for minima.

where we have used $F(|\phi_1 - \phi_2|)$ as shorthand for $\langle F(\vec{x})F(\vec{y})\rangle$, with ϕ_1 being the value of the potential at $\vec{x}$ and ϕ_2 being the value of the potential at $\vec{y}$.

The two-point correlation function is a measure of how much knowledge at one point in the potential tells us about neighbouring points. Broadly speaking, given knowledge of the potential at our current location, we are able to make statements about the value of the potential at a point up to L away. A large correlation length therefore implies that the potential is more predictable.

A large correlation length $L \gg 1/M_P$ also implies correlation drops more slowly. This is undesirable from a theoretical perspective, for two reasons:

- The very existence of correlation implies the presence of predictive power. In turn, predictive power implies that some kind of underlying physics, presumably string theory, is producing the correlation. It would then be

necessary for multiple short-range ($\sim$ Planck length) terms to add up to long-range correlations, which is unlikely.

- If the correlation drops slowly, the potential has a similar value at long distances from the original point. Accordingly, a large L makes small η trivial. Mathematically, it is clear that $\sigma_0^2 = F(0)$, or the peak of the correlation function. Differentiating this equation with respect to ϕ, we also have that $\sigma_1^2 \propto -d^2F/d\phi^2$. A correlation function that decreases quickly (corresponding to larger $d^2F/d\phi^2$, or smaller σ_1) would also have a shorter correlation length. Because $\gamma = \sigma_1^2/\sigma_0\sigma_2 < 1$, for fixed γ, a smaller σ_1 necessarily implies a smaller σ_2.[7] By extension this also leads to a smaller η, since η is directly proportional to σ_2 (Eq. 5.3).

  Note this is not a necessary conclusion: conceivably, the correlation function could dip slightly before increasing, and the correlation length might not be related to $d^2F/d\phi^2$ at the origin. However, such correlation functions would be highly contrived, and we can in general expect η to decrease as L is increased.

The upshot is: we want a small η at small ν, but not large L.

5.4.2 Results

After accounting for L above, the resulting η for $\nu = 0.1, 0.5$ and 0.9 is shown in Fig. 5.7. We do not plot the curve for $\nu = 10^{-12}$ because it is "off the charts" – the calculated downhill eigenvalue λ decreases only slightly with increasing ν, and cannot compensate for the factor of ν in the denominator of Eq, 5.3. Note that $\eta L^2/M_P^2$ is much greater than 1 unless $L \gg M_P$ – exactly the type of correlation length we do not want. Furthermore, $\eta L^2/M_P^2$ increases with N for constant L, which means the most probable minima of landscapes with more than ~ 100 moduli are still not likely to support slow-roll inflation.

It is in principle possible that a less-probable minimum will have a smaller η. Therefore we would like to calculate exactly how much less probable this scenario

[7] σ_0 cannot vary by much because it is fixed to the root mean square energy of the landscape. See Section 5.2.

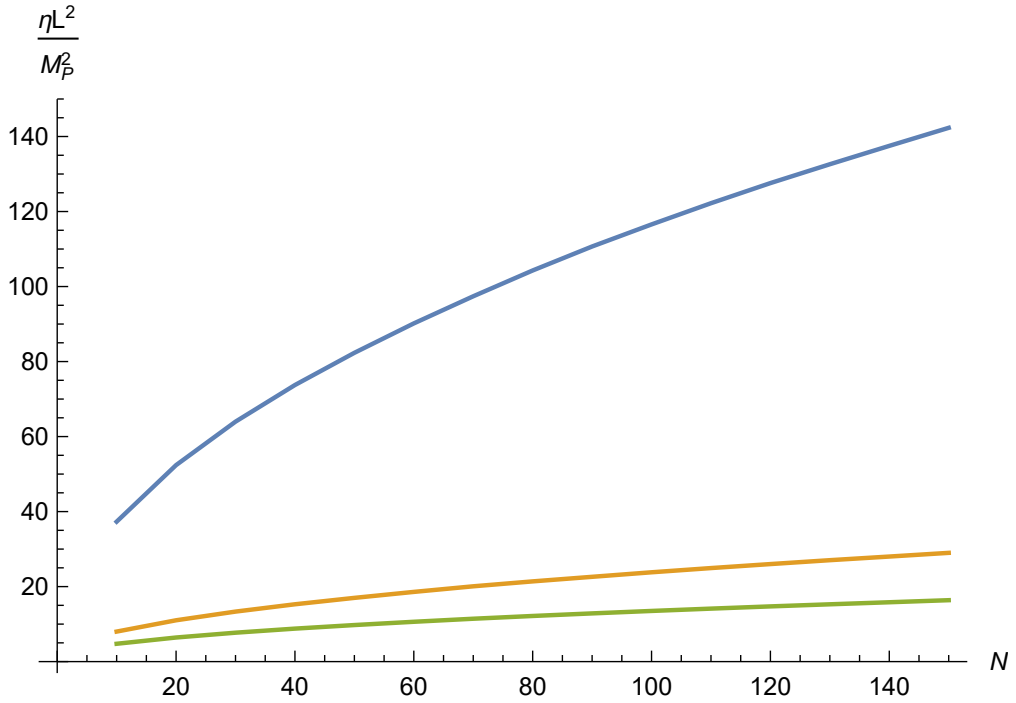

Figure 5.7: The value of the slow-roll inflation parameter $\eta L^2/M_P^2$, where L is the correlation length and M_P is the Planck mass, as a function of the number of dimensions N for a Gaussian power spectrum, at the most probable 1-saddle. From top to bottom, $\nu = 0.1, 0.5$ and 0.9. It can be seen that for these parameters, η is greater than 1 unless $L > M_P$. η also increases with N, which does not bode well for inflation.

is. We can do this by examining how the likelihood (the integrand of Eq. 2.38) varies as the downhill eigenvalue is varied. This likelihood is plotted in Fig. 5.8. It can be inferred from Fig. 5.7 and Eq. 5.3 that, for $\nu \sim 10^{-12}$, we need a downhill eigenvalue that is $\sim 10^{-15}$ to get $\eta \sim 0.01$. From Fig. 5.8, we see that this is roughly 60 orders of magnitude less probable than the most probable downhill eigenvalue at this value of ν, which is about ~ 0.1. If we take the number of minima in the landscape as 10^{500}, then with the probability of even having a 1-saddle with $V > 0$ in the first place already roughly 10^{-700},[8] this makes the probability of having a viable slow-roll inflation saddle roughly 10^{-760}. Note this is not a precise estimate, because we have not calculated the probability that this 1-saddle with $V > 0$ also has $\nu \sim 10^{-12}$. Nonetheless, it is likely to be fairly close, because the scarcity of

[8]See Section 3.5.

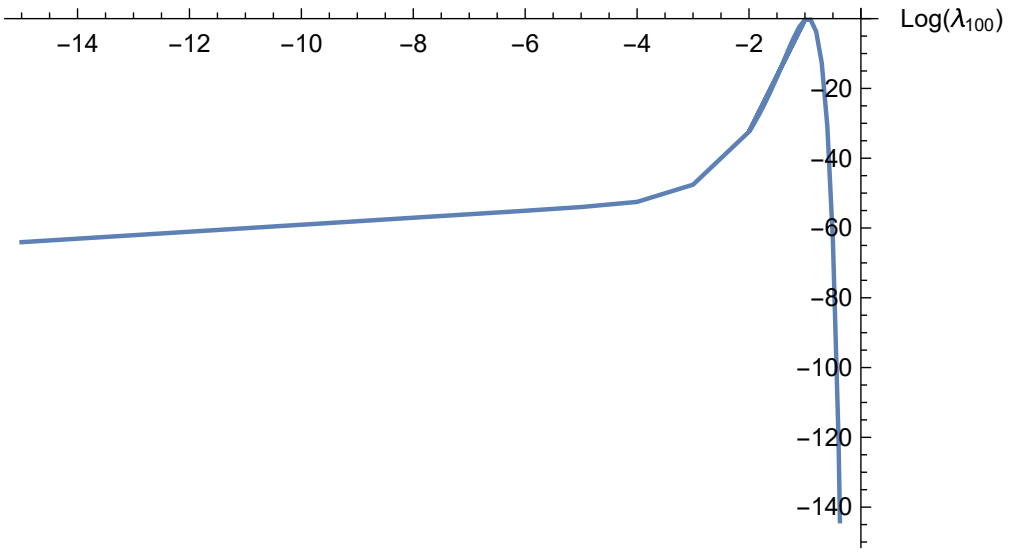

Figure 5.8: The likelihood of a 1-saddle with fixed downward eigenvalue for $\nu = 10^{-12}, \gamma = 0.990, N = 100$. On the horizontal axis is $\log(\lambda_{100})$, the log of the downhill eigenvalue in dimensionless units. On the vertical axis is the likelihood with the most probable eigenvalue normalized to 0. The most probable dimensionless downhill eigenvalue is about 0.1, while a downhill eigenvalue of 10^{-15} is about 60 orders of magnitude less probable.

1-saddles with $V > 0$ implies that any 1-saddle "above the waterline" will almost surely have very small ν. This minute probability makes it very improbable that slow-roll inflation can occure in a landscape with 10^{500} minima. On the other hand, the high-end estimate of 10^{272000} minima still has more than enough vacua to support slow-roll inflation.

5.5 Power-law power spectrum

We next consider the power-law power spectrum. We will start by considering a power spectrum with a red cutoff. In this case the power spectrum is $P(k) = Ak^{-n}$ for $k > k_{cut}$, and 0 otherwise. As shown earlier, the σ_i's for this power spectrum are of the form Eq. 2.50–2.52. σ_2/σ_0 is

$$\frac{\sigma_2}{\sigma_0} = k_{cut}^2 \sqrt{1 - \frac{4}{4 - n + N}} \tag{5.10}$$

valid only if $n > 4 + N$. After using the substitution $n = 4 + N + x$ as in the text below Eq. 2.1.3, we get

$$\eta = M_P^2 \frac{\lambda}{\nu} k_{cut}^2 \sqrt{\frac{4+x}{x}}. \tag{5.11}$$

To proceed, we must 1) choose a value for x, and by extension a value for γ; 2) choose a value of ν, corresponding to the energy density of the pre-inflation saddle, and 3) compute the most probable λ. First, however, we will investigate the parameter k_{cut}. As will be shown, this parameter controls the correlation length in the landscape.

The correlation function for the power-law power spectrum is (Eq. 2.49 with different limits on the integral):

$$F(|\phi_1|) = \frac{A}{(2\pi)^N} \int_{k_{cut}}^{\infty} dk k^{N-n-1} (\phi_1 k)^{1-N/2} J_{N/2-1}(\phi_1 k) \tag{5.12}$$

where J is the Bessel function of the first kind, and we have set $\phi_2 = 0$ for simplicity. This integral can now be evaluated analytically,

$$F(|\phi|) = \frac{A}{(2\pi)^N} \frac{1}{\Gamma[n/2]} 2^{-n-N/2} k_{cut}^{-n} \phi^{-N} \Gamma\left[\frac{N-n}{2}\right] (2^N (k_{cut}\phi)^n - 2^n (k_{cut}\phi)^N \times \Gamma[n/2]_1 \tilde{F}_2 \left[\frac{N-n}{2}, \frac{N-n+2}{2}, -\frac{1}{4} k_{cut}^2 \phi^2\right] \tag{5.13}$$

where ${}_1\tilde{F}_2$ is the regularized generalized hypergeometric function [60].

A plot of this function for representative parameter values is given in Fig. 5.9. The normalized correlation function is plotted on the y-axis, while the horizontal axis is ϕ, which can be loosely interpreted as the "distance" in the landscape. From the left-hand figure, if we hold k_{cut} constant, then the correlation function drops off more slowly with large N, corresponding to a correlation length that increases with N. On the other hand, if we adopt $k_{cut} = \sqrt{N}$, then the correlation function asymptotes, and there is a maximum correlation length in the landscape that is independent of N. Hence, we will adopt $k_{cut} = \sqrt{N}$. Note that this choice adds a factor of N to η (Eq. 5.11), a manifestation of the result in Section 5.4.1 that decreasing the correlation length increases η. Nonetheless, this factor of N alone is

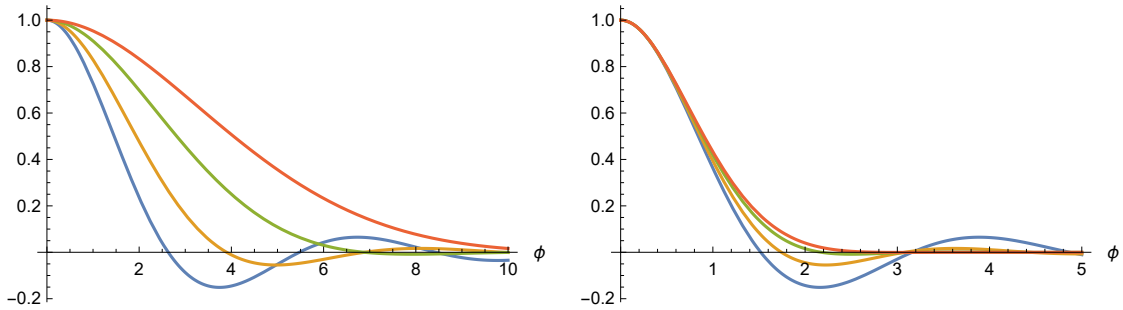

Figure 5.9: The value of the normalized correlation function (y-axis) as a function of ϕ, for four different numbers of dimension N: from bottom to top, $N = 3, 5, 10, 20$ respectively. The plots are for $x = 0.1$. Left: the normalized correlation function with $k_{min} = 1$. Right: the normalized correlation function with $k_{min} = \sqrt{N}$.

not fatal for small η – it is possible the downhill eigenvalue decreases faster than N.

Figure 5.10 shows the values of η calculated using Eq. 5.11 for a red cutoff, at different values of ν, γ, and N. As can be seen, η is much greater than 1 when ν is small – the downward eigenvalue does not decrease fast enough to compensate for the $1/\nu$ factor in η. In the $\nu = 1$ case, η changes relatively quickly with N for small N, but for $N > \sim 20$ it is virtually constant with N – any variations are at the sub-% level. Also plotted are the regions of parameter space where the likelihood of finding a 1-saddle is 10^{-250} and 10^{-500} relative to the likelihood at $\nu = -\sqrt{N}$.[9] The regions above the dotted lines are not likely to have any 1-saddles in the first place.

The analysis for a blue cutoff, where $P(k) = Ak^{-n}$ for $k < k_{cut}$ and $P(k) = 0$ otherwise, is very similar but less satisfactory. This is because the power spectrum imposes long-range correlations in the landscape for small γ.[10] In this case σ_2/σ_0 is (see Eqs. 2.54) the same as in the red case,

$$\frac{\sigma_2}{\sigma_0} = k_{cut}^2 \sqrt{1 - \frac{4}{4 - n + N}} \tag{5.14}$$

[9] $\nu = -\sqrt{N}$ is the approximate peak likelihood, i.e. the value of ν at which most saddles are located. See Section 5.2.

[10] Keep in mind that k is the conjugate variable of ϕ, and ϕ measures the 'distance' in the landscape.

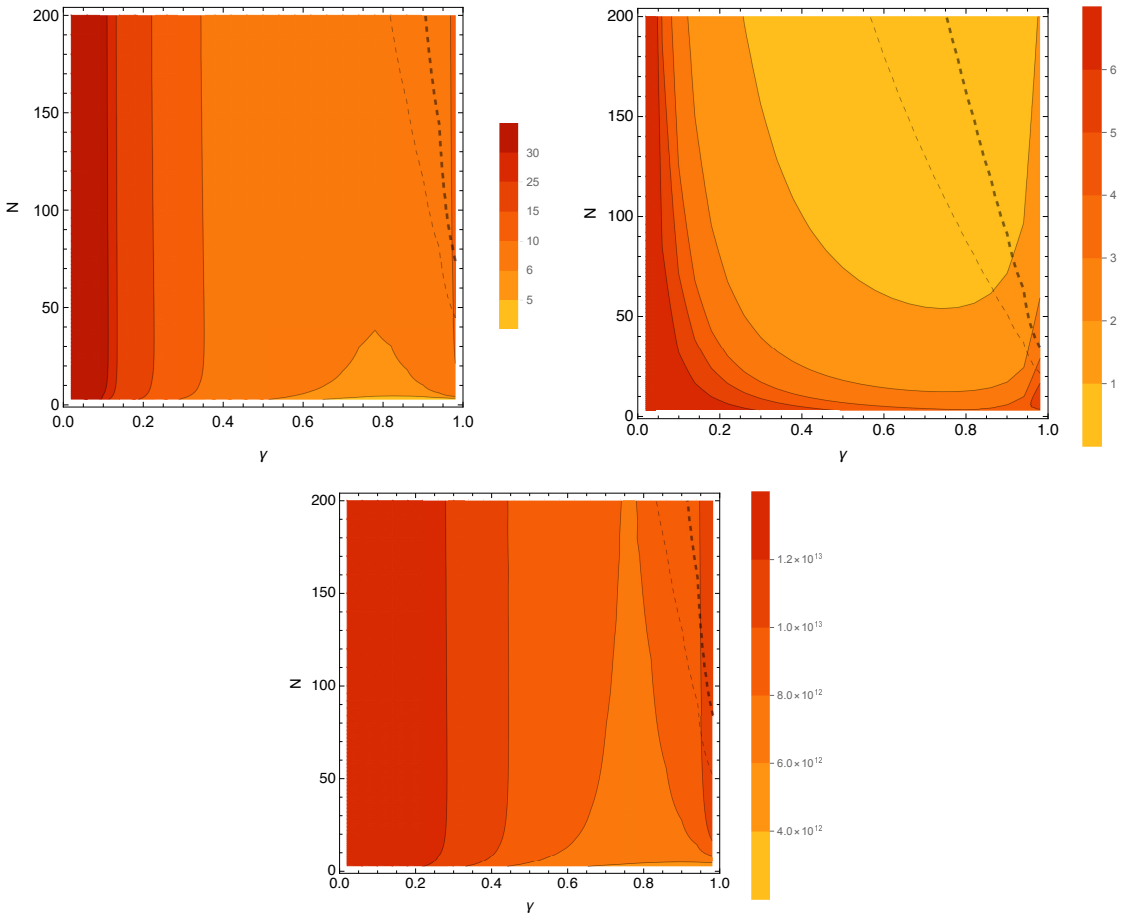

Figure 5.10: Most likely values of η with $\nu = 1$ and $\nu = \sqrt{N}$ (top), and $\nu = 10^{-12}$ (bottom) for a power-law power spectrum with a red cutoff. The light and heavy dashed lines correspond to regions above which the likelihood of finding a 1-saddle is 1 in 10^{250} and 1 in 10^{500} relative to the likelihood for $\nu = -\sqrt{N}$. Above these dashed lines, there are not likely to be any 1-saddles with $V > 0$. Note the slightly different contours in the $\nu = 1$ plot, necessary to show the same feature as in the $\nu = 10^{-12}$ plot.

except this equation is valid only if $n < N$. As with the red cutoff, we substitute $n \to N - \delta$, which yields $\gamma = \sqrt{\delta(4+\delta)}/(\delta+2)$, where $\delta > 0$. This is exactly the same as for the red cutoff. Putting in the expressions for the moments, η becomes

$$\eta = M_P^2 \frac{\lambda}{\nu} k_{cut}^2 \sqrt{\frac{\delta}{4+\delta}}\,. \tag{5.15}$$

The correlation function is

$$F(|\phi|) = \frac{A}{(2\pi)^N} 2^{-N/2} k_{cut}^{N-n} \Gamma\left[\frac{N-n}{2}\right] {}_1\tilde{F}_2\left(\frac{N-n}{2}; \frac{N-n}{2}+1, \frac{N}{2}; -\frac{1}{4}k_{cut}^2\phi^2\right). \tag{5.16}$$

This correlation function is plotted in Fig. 5.11. We again set $k_{cut} = \sqrt{N}/M_P$, as the correlation function shows the same scaling behaviour with N as the red case. However, it does not necessarily asymptote to zero – the terminal value shows a significant dependence on δ, and becomes arbitrarily close to unity as δ approaches zero. This is because small values of δ imply more power at very small k (bear in mind $P(k) = Ak^{-N+\delta}$), introducing long-range coherence into the landscape. To get a meaningful correlation function, we need to either impose a second cutoff at small k, which yields similar results to the red case; increase k_{cut} as δ increases, which increases η per Eq. 5.15;[11] or simply exclude scenarios where δ is small. In the last case, Fig. 5.11 suggests taking $\delta \gtrsim 2$, corresponding to $\gamma \gtrsim \sqrt{3}/2 \approx 0.866$.

The resulting raw η plots are in Fig. 5.12. The dotted lines again indicate the regions of parameter space where one does not expect to find a 1-saddle with $V > 0$. The regions with $\gamma \lesssim \sqrt{3}/2$ are greyed out, indicating the zone that is excluded if one takes $\delta > 2$. Excluding these zones also excludes the regions where the most probable 1-saddle has $\eta < 1$.

Similar to the Gaussian power spectrum, the values of η at $\nu = 10^{-12}$ for the most probable 1-saddle are very large for both the infrared and the ultraviolet cutoff. However, it is possible that a less probable 1-saddle will have $\eta \sim 0.01$. Again similar to the Gaussian power spectrum, we calculate how the integrand of Eq. 2.38 varies as the downhill eigenvalue is varied. This likelihood is plotted in Fig. 5.13 for $\nu = 10^{-12}, \gamma = 0.1, N = 100$. The general shape of the plot is roughly independent of these parameters, but the probability drops off more quickly

[11] Note again the inverse relationship between the correlation length and η.

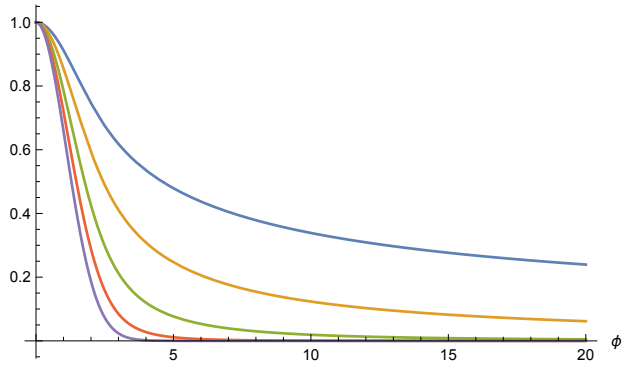

Figure 5.11: The correlation function for a power-law power spectrum with a blue cutoff. $N = 50$ and (from top) $\delta = 0.5, 1, 2, 4$ and 10, with $k_{cut} = \sqrt{50}$. For small δ the correlation function does not asymptote to zero, yielding an arbitrarily-large correlation length, but it does go to zero for sufficiently large δ.

for large γ. We can see from the two bottom plots of Fig. 5.10 and 5.12 that in order to get $\eta \sim 0.01$ for a cosmologically interesting 1-saddle we need a downhill $\lambda_N < \approx 10^{-14}$. Figure 5.13 indicates that such a downhill eigenvalue is ~ 15 orders of magnitude less probable than the most probable downhill eigenvalue, which is of order 0.01. This is clearly not ideal – our inflationary 1-saddle is $\sim 10^{15}$ times less probable than the most probable 1-saddle. On the other hand, $\gamma = 0.1$ is also in the region of parameter space for which a significant fraction of 1-saddles have $V > 0$ (see Fig. 5.2). With $\sim 10^{500}$ minima total in the landscape, this 10^{15} difference is insignificant, and there will be plenty of viable 1-saddles.

Comparing the left hand figure of Fig. 5.13 with Fig. 5.8, the rate at which the probability decreases clearly depends on γ. This dependence on γ is shown in the right hand figure of Fig. 5.13. The probability of anomalously small downhill directions decreases with γ, further emphasizing that the region of parameter space with small γ is also the region most able to support inflationary 1-saddles.

5.6 Summary

In this chapter, we have investigated how the downhill eigenvalue of 1-saddles vary as N, γ and ν are varied. We see that the downhill eigenvalue is naturally much smaller than most uphill eigenvalues, and it gets smaller for large N or

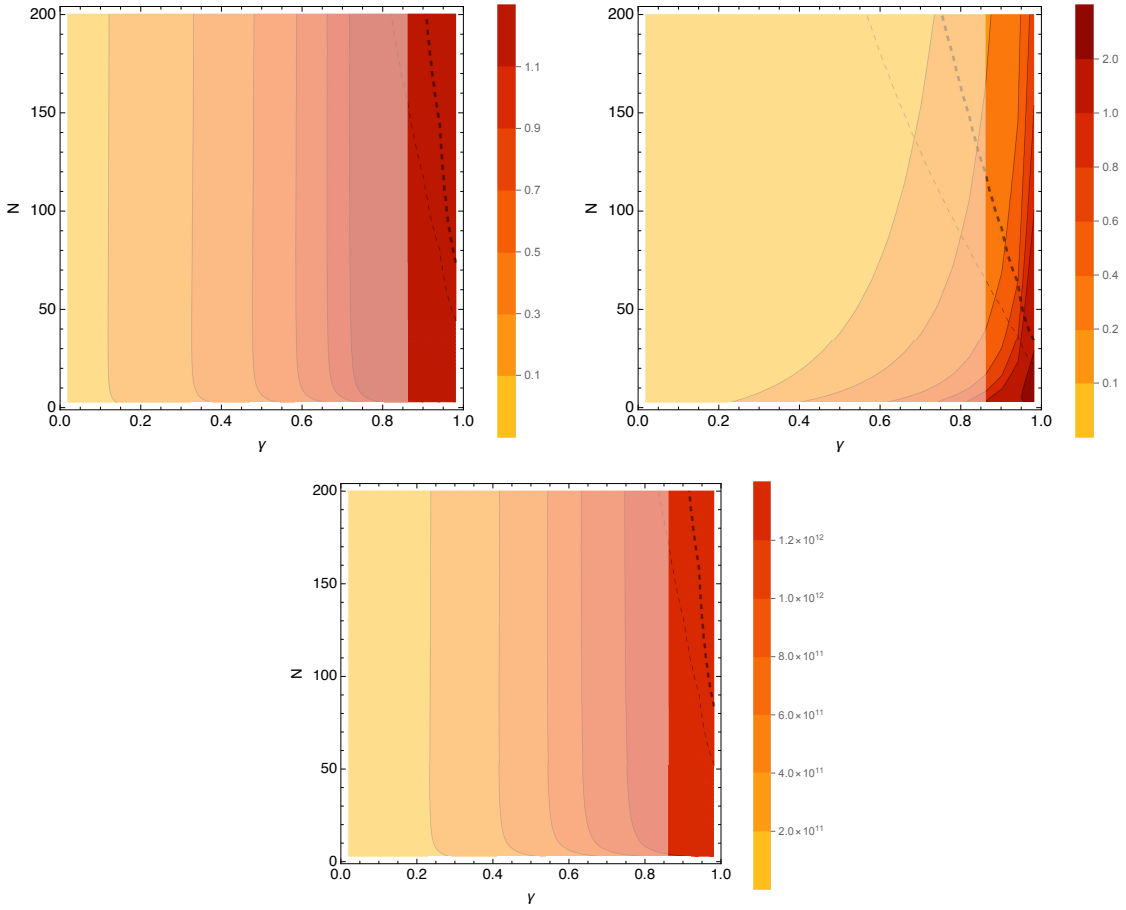

Figure 5.12: Most likely values of η with $\nu = 1$ and $\nu = \sqrt{N}$ (top), and $\nu = 10^{-12}$ (bottom) for a power-law power spectrum with a blue cutoff. The light and heavy dashed lines correspond to regions above which the likelihood of finding a 1-saddle is 1 in 10^{250} and 1 in 10^{500} relative to the likelihood for $\nu = -\sqrt{N}$. Above these dashed lines, there are not likely to be any 1-saddles. The regions with $\gamma < \sqrt{3}/2$ are greyed out: for these values of γ, the correlation length is unbounded.

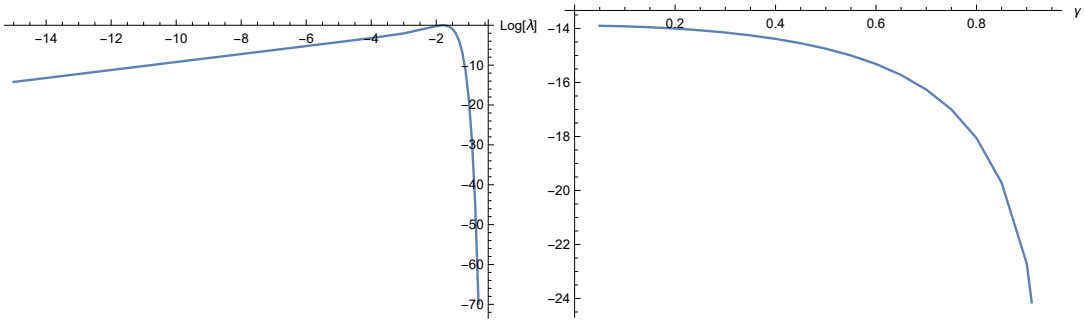

Figure 5.13: (Left) The likelihood of a 1-saddle with fixed eigenvalue for $\nu = 10^{-12}, \gamma = 0.1, N = 100$. On the vertical axis is the log-likelihood with the most probable eigenvalue normalized to 0. On the horizontal axis is $\log(\lambda_{100})$, the log of the downhill eigenvalue in dimensionless units. We can see that a very small eigenvalue of 10^{-15}, sufficient for $\eta \sim 0.01$, is still only ~ 14 orders of magnitude less likely than the most probable 1-saddle. (Right) The log-likelihood of a 1-saddle with $\lambda = 10^{-15}$ relative to the most probable λ, as a function of γ and with $N = 100$, $\nu = 10^{-12}$. For $\gamma = 0.1$, the log-likelihood is 10^{-14}, corresponding to the result in the left-hand figure.

small γ. This suggests that random Gaussian landscapes can naturally solve the η problem by providing a small negative mass term compared to the average mass. We also investigated the inflationary slow-roll parameter η for the power-law power spectrum and the Gaussian power spectrum. We find that η depends on the correlation length, and we investigated how η varies with the correlation length. We find that the Gaussian power spectrum is very unlikely to produce a single viable inflationary 1-saddle unless there are more than $\sim 10^{1400}$ vacua in the landscape, or unless the correlation length is very large. The power-law power spectrum, however, is capable of producing slow-roll inflation while bounding the correlation length, for appropriate choices of its free parameters k_{cut} and n.

Chapter 6

Conclusions and Future Work

In this thesis, we have used the random Gaussian field approach to investigate the string landscape. We derived the number density of minima (Eq. 2.36) and saddles (Eq. 2.38) from first principles. We evaluated these integrals directly (Section 3.3) for $N \leq 12$, then adopted the Gaussian approximation for large N (Section 3.4). These methods form the foundation of all our results. Using this machinery, we reached the following key conclusions:

1. The random Gaussian field has as its parameters the number of dimensions N, and the three moments of the power spectrum $\sigma_0, \sigma_1, \sigma_2$. For the number density of minima and saddles, however, only N and the combination $\sigma_1^2/\sigma_0\sigma_2$, i.e. γ, matters. We showed γ is necessarily between 0 and 1, and roughly measures how turbulent the landscape is – small γ corresponds to a more turbulent landscape, while large γ corresponds to a smoother landscape.

2. For $\gamma \gtrsim 0.96$, the probability of having a minimum with positive energy density ($V > 0$) at $N = 100$ drops below 10^{-500}. A Gaussian power spectrum (and by extension, a Gaussian correlation function) yields $\gamma = \sqrt{N/(N+2)}$, which for $N \sim 100$ evaluates to $\gamma \approx 0.990$, a number firmly in the regime where minima with positive energy densities are an extreme rarity. Conversely, a power-law power spectrum can be configured to yield a landscape with any value of γ. These results are in Section 2.1.3 and Chapter 3.

3. The slopes of the single most probable minimum/saddle are independent of γ.

The eigenvalues resemble a Wigner semicircle with deviations at very small eigenvalues. The slopes of a minimum/saddle with other energy densities depend on γ. These and other results are in Chapter 4.

4. For saddles with one downhill direction (1-saddles), we can directly calculate the expected inflationary slow-roll parameter η for a given power spectrum. For a Gaussian power spectrum, the probability of a 1-saddle with $V > 0$ and $\eta \sim 0.01$ is about 10^{-1400} at $N = 100$, rendering multiverse cosmology highly improbable for landscapes with $\sim 10^{500}$ minima. A power-law power spectrum cannot simultaneously produce a bounded correlation length *and* a most-probable 1-saddle with $\eta < \sim 0.01$, but it is possible for a less-probable 1-saddle to have $\eta \sim 0.01$. With $\sim 10^{500}$ minima in the landscape, there is a region of parameter space in which one can bound the correlation length and still find plenty of 1-saddles with $V > 0$, $\eta < 0.01$. These and other results are in Chapter 5.

5. We find that for saddles with one downhill direction, the eigenvalue of the downward direction is small relative to the uphill directions, and it gets smaller for large N and small γ. This conclusion is independent of the power spectrum, and suggests that the inflationary η-problem may be naturally softened in some landscape scenarios. More details for this result are in Section 5.3.

Our results show that it is possible to extract quantitative predictions for the landscape using the random Gaussian approximation. We now briefly touch on two questions: 1) what could invalidate the above conclusions, and 2) where do we go from here?

6.1 What could go wrong?

We made no approximations when deriving they key equations Eqs. 2.36 and 2.38. However, we did use the Gaussian approximation in calculating our results. If numerical errors exist, this is the most probable source. There are two possibilities: the extrapolation to large N, and the intrinsic error of the Gaussian approximation

itself (Fig. 3.6). This possibility is studied in Section 3.4. We do not expect the approximation to fail, but we have not rigorously proved that it doesn't.

Another possible source of error is if there are multiple maxima in the likelihood. In this scenario, the "most probable" peak we identify is a local maximum as opposed to global maximum. We investigated this in Section 2.2 and found no such behavior for low N. It also seems unlikely there are multiple maxima in the likelihood based on the form of the integrand.

A further, key caveat that applies to all our results is that they are based on the random Gaussian approximation, which only sets the baseline expectation. In other words, the actual string theory landscape can (and almost surely will) have different properties from the system we examine here.

6.2 What next?

The random Gaussian field approach makes minimal assumptions, yet allows us to make quantitative calculations. This makes it an attractive tool to further investigate various questions about landscape cosmology. We briefly outline several such topics.

6.2.1 Topological inflation

Topological inflation was first proposed by Alexander Vilenkin in 1994 [58]. It is distinct from slow-roll inflation in that there is a central peak in the potential which falls off on both sides, which supports a stable field configuration. An example potential is, as originally proposed by Vilenkin,

$$V(\phi) = \frac{1}{4}\lambda(\phi^2 - \eta^2)^2 \tag{6.1}$$

where λ and η are constants.[1] In this case there are two minima at $\phi = \pm\eta$, while $\phi = 0$ is a local maximum. The central peak drives eternal inflation, and there is a *domain wall* separating the two minima at $\pm\eta$.

[1]These are not eigenvalues λ, the Fourier conjugate variable ϕ, or the slow-roll inflation parameter η. The notation is the one used by Vilenkin, but the conflict in notation with the rest of this thesis is unfortunate.

In the terminology of this thesis, the $\phi = 0$ point can be viewed as a 1-saddle.[2] It is therefore possible to investigate the properties of the 1-saddle using Eq. 2.38. To do this, we first need to derive the constraints on λ and ν required for topological inflation. We start by considering the Taylor expansion about the central saddle,

$$V(\phi) = V_0 - \frac{V_0''\phi^2}{2} \tag{6.2}$$

where V_0'' is the second derivative of the field at the origin. The value of ϕ for which the potential drops to zero is $\phi = \pm\sqrt{2V_0/V_0''}$. Meanwhile, the wall's boundaries are where the gradient energy balances the potential energy,

$$\left(\frac{\partial\phi}{\partial x}\right)^2 \sim V_0. \tag{6.3}$$

To calculate the gradient energy, we note that the coordinate ϕ changed by $\sim \sqrt{2V_0/V_0''}$ over a 'distance' that is the width δ of the domain wall. Therefore

$$\frac{\partial\phi}{\partial x} \sim \frac{\sqrt{2V_0/V_0''}}{\delta}, \tag{6.4}$$

and using Eq. 6.2 we get

$$\delta \sim \sqrt{\frac{2}{V_0''}}. \tag{6.5}$$

For topological inflation to occur, we need $\delta > H_0^{-1}$, where H_0^{-1} is the horizon size of the vacuum energy within the wall [58]. This leads to:

$$\begin{aligned}\sqrt{\frac{2}{V_0''}} > \frac{1}{H_0} &= m_P\sqrt{\frac{3}{8\pi V_0}} \\ \Rightarrow V_0'' &\leq \frac{2V_0}{3M_P^2}\end{aligned}$$

where m_p, M_P are the Planck mass and reduced Planck mass respectively. Here V_0'' and V_0 are physical quantities. Substituting $V_0'' \to \lambda\sigma_2$ and $V_0 \to \nu_0\sigma_0$, we

[2] Although there looks like two downhill directions, one towards the minimum at $+\eta$ and the other towards the minimum at $-\eta$, there is only one parameter ϕ varying. There is also only one eigenvalue for the same reason (recall that the eigenvalue is the second derivative of the Hessian).

see that topological inflation requires practically the same condition as slow-roll inflation. The only difference is that the bound on the slow-roll parameter η is slightly different: $\eta < \sim 2/3$. Accordingly, the results from Section 5 carry over smoothly, and within the same region of parameter space where we expect typical 1-saddles to support slow-roll inflation, we can also expect typical 1-saddles with $V \sim M_P^4$ to support topological inflation.

6.2.2 Quintessence

Quintessence has already been mentioned a few times in this Thesis. It is a scalar field(s) similar to the inflaton that drives the accelerating expansion of the universe, except that 1) non-relativistic matter needs to be included in the dynamics, and 2) it is at much lower energy than inflation. [59] Compared to the cosmological constant, it is dynamic; its energy density changes over time. This leads to a dark energy equation of state that also varies with time.

In the same way that inflation occurs when the inflaton is nearly flat, accelerated expansion also requires the quintessence field to be nearly flat. This is hinted at in our results – for minima that have $\Lambda > 0$, the smallest eigenvalues are naturally very close to zero. If each eigenvalue corresponds to one quintessence field, then the slope of the potential in a direction is related to the mass squared of that field by $m_i^2 = \sigma_2 \lambda_i$. The closeness of the eigenvalues then implies that the masses of the fields are similar, but also that no two masses can be exactly equal, because of eigenvalue repulsion. It also raises the possibility that more than one quintessence field might be active near an extremum even if the evolution is dominated by a single field at greater distances. It might be possible to investigate the consequences of this with the relative sizes of the slopes of the scalar fields (Fig. 4.5).

6.2.3 Other properties of the landscape

We have calculated η for several power spectra as well as $P(V > 0|min)$ as a function of γ, but there are other interesting questions to ask of the landscape:

- How far is it to the next minimum? This affects the rates of quantum tunneling between minima. The first step to approaching this problem would

be investigating the constant A in Eqs. 2.36 and 2.38 to get an actual number of minima/saddles in a unit volume.

- How probable is it to have > 60 e-folds of inflation? This depends on the downhill eigenvalue starting small and staying small.

- What does a typical evolutionary track look like? As discussed in the Introduction, there have already been efforts to calculate this [26, 27], but the method used has theoretical problems [27, 28]. It remains a worthy question, however, whose solution will tell us about what to expect during inflation.

- Is it possible to construct a power spectrum for the landscape such that inflation gets more probable with N? This question stems from the fact that the dimensionless downward eigenvalue, λ_N, already decreases as N increases. The 'reason' η does not always decrease with N is because the moments of the power spectrum, σ_2/σ_0 (see Eq. 5.3), increases with N more quickly than λ_N decreases. It is relatively simple to construct a power spectrum such that σ_2/σ_0 does not increase with N (a power-law power spectrum with $k_{cut} = 1/\sqrt{N}$ will do it), but constructing such a power spectrum that also has a bounded correlation length is much harder. In Section 5.4.1 we provided general arguments to believe such a power spectrum should not exist unless highly contrived, but this is not a hard no-go theorem. In this case, the 'ideal' power spectrum for multiverse cosmology will have both η and the correlation length decreasing with N.

- How probable (or improbable) are various swampland conjectures? If the conjectures involve some function of V, V' or V'', it might be possible to investigate them with the random Gaussian approximation. The lack of success at constructing a de Sitter vacua (i.e., a minimum with $V > 0$) in string theory has led some to a conjecture that string theory admits no de Sitter vacua [61] or that de Sitter vacua are in the swampland [19]. If this turns out to be the case, then the corresponding region of parameter space in the random Gaussian approximation is $\gamma \approx 1$.

  Another conjecture is that either $|V'| \geq \mathcal{O}(1)V$, or $\min(V'') \leq -\mathcal{O}(1)V$, where $\min(V'')$ is the smallest eigenvalue [62]. The conjecture is designed

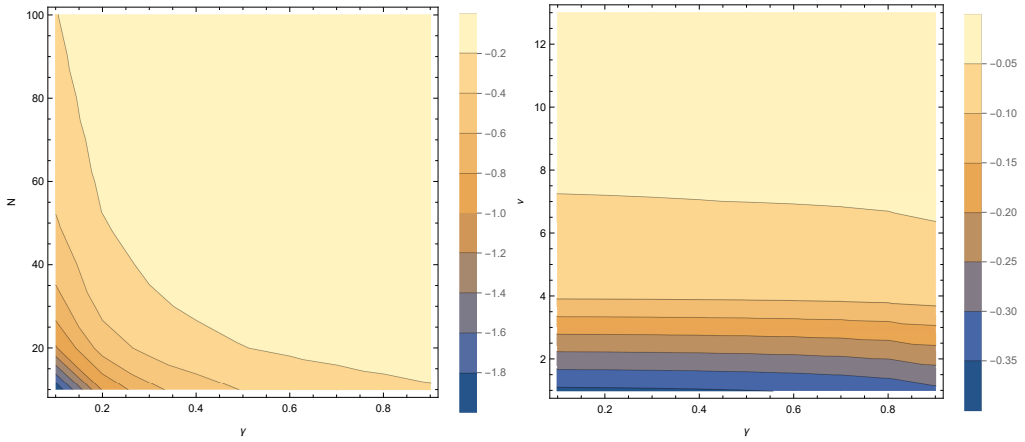

Figure 6.1: A contour plot of the ratio λ_1/ν for maxima, at the most probable ν as a function of N (left), and at fixed ν with $N = 100$ (right). The ratio is $\mathcal{O}(1)$. Since σ_2/σ_0 is $\mathcal{O}(100)$ for both the Gaussian power spectrum and the power-law power spectrum for typical choices of the correlation length and $N \sim 100$, this implies the second condition is usually satisfied for maxima with $V > 0$.

to prohibit de Sitter vacua – it is trivially satisfied for $V < 0$ since the first condition is always true. We can investigate this conjecture by examining maxima with $V > 0$.[3] At these maxima, $V' = 0$, so the first condition is never satisfied; therefore for the conjecture to be true, the second condition must be always satisfied. We can investigate if it is always satisfied using Eq. 2.36. In the notation of this thesis, the second condition is $-\lambda_1\sigma_2 \leq \mathcal{O}(1)\nu\sigma_0$.[4] A contour plot of the ratio $-\lambda_1/\nu$ is in Fig. 6.1. Whether the constraint is satisfied depends on the power spectrum, of course, but the results are encouraging for the conjecture: for $N = 100$, σ_2/σ_0 is $\mathcal{O}(100)$ for both the Gaussian power spectrum and the power-law power spectrum (Eq. 5.8 and Eq. 5.10), given typical choices for the correlation length. This implies the conjecture is indeed satisfied for maxima with $V > 0$.

[3]This is equivalent to examining minima with $V < 0$; see footnote 2 on Page 11.

[4]This formula is written for minima, where λ_1 is positive and ν is negative. Note that we are considering λ_1, which in this thesis is the largest eigenvalue.

Chapter 7

Appendix

7.1 Derivation of BBKS Equation A1

In this section we adopt the notation of BBKS's [54] Appendix A.

The two equations of interest are:

$$\langle \eta_i \eta_j \rangle = \frac{\sigma_1^2}{3} \delta_{ij} \tag{7.1}$$

$$\langle \zeta_{ij} \zeta_{kl} \rangle = \frac{\sigma_2^2}{15} (\delta_{ij}\delta_{kl} + \delta_{ik}\delta_{jl} + \delta_{il}\delta_{jk}) \tag{7.2}$$

BBKS gave these for 3 dimensions, and we want to derive the corresponding expressions in N dimensions. The first equation is relatively easy to derive. By definition,

$$\langle (\nabla F)^2 \rangle = \sigma_1^2 \tag{7.3}$$

This is not in BBKS, but is sensible given Eq. 4.6c in the paper. Each gradient adds a factor of ik in Fourier space, and the power spectrum is proportional to the absolute square of the Fourier coefficients. Adding a factor of k^2 in the integral

then is equivalent to taking the gradient. Then

$$\begin{aligned}\sigma_1^2 &= \left\langle \left[\left(\frac{\partial F}{\partial x}\right)\hat{x} + \left(\frac{\partial F}{\partial y}\right)\hat{y} + \left(\frac{\partial F}{\partial z}\right)\hat{z} \right]^2 \right\rangle \\ &= \left\langle \left(\frac{\partial F}{\partial x}\right)^2 + \left(\frac{\partial F}{\partial y}\right)^2 + \left(\frac{\partial F}{\partial z}\right)^2 \right\rangle \\ &= \left\langle 3\left(\frac{\partial F}{\partial x}\right)^2 \right\rangle \\ &= 3\langle \eta_x^2 \rangle\end{aligned}$$

where the third line follows by isotropy. The correspondence with Eq. 7.1 is now obvious. There are no cross terms, hence the delta function.

The second equation is harder. From the definition,

$$\langle (\nabla^2 F)^2 \rangle = \sigma_2^2 \tag{7.4}$$

The LHS is (in 3D)

$$\begin{aligned}(\nabla^2 F)^2 = \left\langle \left(\frac{\partial^2 F}{\partial x^2}\right)^2 + \left(\frac{\partial^2 F}{\partial y^2}\right)^2 + \left(\frac{\partial^2 F}{\partial z^2}\right)^2 \right\rangle \\ + \left\langle 2\frac{\partial^2 F}{\partial x^2}\frac{\partial^2 F}{\partial y^2} + 2\frac{\partial^2 F}{\partial x^2}\frac{\partial^2 F}{\partial z^2} + 2\frac{\partial^2 F}{\partial y^2}\frac{\partial^2 F}{\partial z^2} \right\rangle\end{aligned} \tag{7.5}$$

i.e. there are nine terms, reducible to six since products commute. Now we claim that

$$\left\langle \left(\frac{\partial^2 F}{\partial x^2}\right)^2 \right\rangle = 3\left\langle \frac{\partial^2 F}{\partial x^2}\frac{\partial^2 F}{\partial y^2} \right\rangle \tag{7.6}$$

To prove this, we define a new direction $\hat{u} = (\hat{x} + \hat{y})\frac{1}{\sqrt{2}}$. Shifting into Fourier space, $k_u = (k_x + k_y)/\sqrt{2}$. Taking the fourth power,

$$4k_u^4 = k_x^4 + k_y^4 + 4(k_x k_y^3) + 4(k_y k_x^3) + 6(k_x^2 k_y^2) \tag{7.7}$$

Taking the expectation value of this, the two terms in the middle disappear because the k's are odd functions, leaving

$$\langle 4k_u^4 \rangle = \langle k_x^4 \rangle + \langle k_y^4 \rangle + \langle 6(k_x^2 k_y^2) \rangle \tag{7.8}$$

Remembering that in Fourier space, taking the derivative is equal to multiplying by k, this is

$$4\left\langle\left(\frac{\partial^2 F}{\partial u^2}\right)^2\right\rangle = \left\langle\left(\frac{\partial^2 F}{\partial x^2}\right)^2\right\rangle + \left\langle\left(\frac{\partial^2 F}{\partial y^2}\right)^2\right\rangle + 6\left\langle\frac{\partial^2 F}{\partial x^2}\frac{\partial^2 F}{\partial y^2}\right\rangle \tag{7.9}$$

We must have $\langle(\frac{\partial^2 F}{\partial u^2})^2\rangle = \langle(\frac{\partial^2 F}{\partial x^2})^2\rangle = \langle(\frac{\partial^2 F}{\partial y^2})^2\rangle$ by isotropy, so

$$\left\langle\left(\frac{\partial^2 F}{\partial x^2}\right)^2\right\rangle = 3\left\langle\frac{\partial^2 F}{\partial x^2}\frac{\partial^2 F}{\partial y^2}\right\rangle \tag{7.10}$$

which is the desired result. Now we are almost done. From Eq. 7.5, we see there are N squared terms and ${}_2{}_N C_2$ cross terms. This means that

$$\begin{aligned}\sigma_2^2 &= \left(N + \frac{N(N-1)}{3}\right)\left\langle\left(\frac{\partial^2 F}{\partial x^2}\right)^2\right\rangle \\ &= N(N+2)\left\langle\frac{\partial^2 F}{\partial x^2}\frac{\partial^2 F}{\partial y^2}\right\rangle \quad (x \neq y)\end{aligned}$$

Note there's nothing special about the x's and y's, and they could equally have been any other dimension.

7.2 Proof of Eq. 2.20

We reproduce the original correlations, Eq. 2.18.

$$\begin{aligned}\langle FF\rangle &= \sigma_0^2 \\ \langle\eta_i\eta_j\rangle &= \frac{1}{N}\delta_{ij}\sigma_1^2 \\ \langle F\zeta_{ij}\rangle &= -\frac{1}{N}\delta_{ij}\sigma_1^2 \\ \langle\zeta_{ij}\zeta_{lm}\rangle &= \frac{1}{N(N+2)}\sigma_2^2(\delta_{ij}\delta_{lm} + \delta_{il}\delta_{jm} + \delta_{im}\delta_{jl})\end{aligned}$$

as well as the basis transform Eq. 2.20,

$$\begin{aligned} x_1 &= -\frac{1}{\sigma_2}\sum_i \zeta_{ii} \\ x_n &= -\frac{1}{\sigma_2}\sum_{i=1}^{n-1}\left(\zeta_{ii}-\zeta_{nn}\right), (2 \le n \le N) \end{aligned}$$

We wish to derive Eq. 2.21,

$$\begin{aligned} \langle \nu^2 \rangle &= 1 \\ \langle x_1^2 \rangle &= 1 \\ \langle \nu x_1 \rangle &= \gamma \\ \langle x_n^2 \rangle &= \frac{2n(n-1)}{N(N+2)},\ (2 \le n \le N) \end{aligned} \tag{7.11}$$

The first of these four equations is trivial because $\nu \equiv F/\sigma_0$ by definition. For the second,

$$\begin{aligned} \langle x_1 x_1 \rangle &= \frac{1}{\sigma_2^2}\left(\sum_i \langle \zeta_{ii}\zeta_{ii}\rangle + 2\sum_{i\neq j}\langle \zeta_{ii}\zeta_{jj}\rangle\right) \\ &= \frac{1}{\sigma_2^2}\left(\frac{1}{N(N+2)}\sigma_2^2(3)\times N + \frac{2}{N(N+2)}\sigma_2^2(1)\times_N C_2\right) \\ &= \frac{1}{N(N+2)}\left(3N + N(N-1)\right) \\ &= 1 \end{aligned} \tag{7.12}$$

as desired. The second line follows from the fact that there are N $\langle \zeta_{ii}\zeta_{ii}\rangle$ terms and ${}_NC_2$ $\langle \zeta_{ii}\zeta_{jj}\rangle$ terms. Similarly, for the third equation,

$$\begin{aligned} \langle \nu x_1 \rangle &= -\frac{1}{\sigma_0\sigma_2}\left(\sum_i \langle F\zeta_{ii}\rangle\right) \\ &= \frac{1}{\sigma_0\sigma_2}\frac{1}{N}\sigma_1^2 \times N \\ &\equiv \gamma \end{aligned} \tag{7.13}$$

Finally, for the fourth equation,

$$\langle x_n x_n \rangle = \frac{1}{\sigma_2^2} \langle \left(\sum_{i=1}^{n-1} (\zeta_{ii} - \zeta_{nn}) \right)^2 \rangle \tag{7.14}$$

Bear in mind that n is not a dummy index – it is also in x_n on the left hand side of the equation. We need to handle the square of a sum, which is tricky. The easiest way to approach it is to write out some examples for low n. If $n = 3$, then the term in the brackets is $[(\zeta_{11} - \zeta_{33}) + (\zeta_{22} - \zeta_{33})]^2$, which evaluates to

$$(\zeta_{11} - \zeta_{33})^2 + (\zeta_{22} - \zeta_{33})^2 + 2(\zeta_{11} - \zeta_{33})(\zeta_{22} - \zeta_{33})$$

Similarly, for $n = 4$, we get three terms $(\zeta_{11} - \zeta_{44})^2 + (\zeta_{22} - \zeta_{44})^2 + (\zeta_{33} - \zeta_{44})^2$ and the cross terms $2(\zeta_{11} - \zeta_{44})(\zeta_{22} - \zeta_{44}) + 2(\zeta_{11} - \zeta_{44})(\zeta_{33} - \zeta_{44}) + 2(\zeta_{22} - \zeta_{44})(\zeta_{33} - \zeta_{44})$. This is indicative of what the general formula might look like,

$$\begin{aligned} \left(\sum_{i=1}^{n-1} (\zeta_{ii} - \zeta_{nn}) \right)^2 &= \sum_{i=1}^{n-1} (\zeta_{ii} - \zeta_{nn})^2 + \sum_{i,j;i \neq j}^{n-1} (\zeta_{ii} - \zeta_{nn})(\zeta_{jj} - \zeta_{nn}) \\ &= \sum_{i=1}^{n-1} (\zeta_{ii}^2 - 2\zeta_{ii}\zeta_{nn} + \zeta_{nn}^2) + \sum_{i,j;i \neq j}^{n-1} (\zeta_{ii}\zeta_{jj} - \zeta_{ii}\zeta_{nn} - \zeta_{jj}\zeta_{nn} + \zeta_{nn}^2) \end{aligned} \tag{7.15}$$

Applying Eq. 2.18,

$$\begin{aligned} \langle x_n x_n \rangle = &\frac{1}{\sigma_2^2} \times (n-1) \left(\frac{1}{N(N+2)} \sigma_2^2(3) \times 2 - \frac{2}{N(N+2)} \sigma_2^2(1) \right) \\ &+ \frac{1}{\sigma_2^2} \times 2 \times_{n-1} C_2 \left(-\frac{1}{N(N+2)} \sigma_2^2(1) + \frac{1}{N(N+2)} \sigma_2^2(3) \right) \end{aligned} \tag{7.16}$$

where the first line corresponds to the first sum, and the second line corresponds to the second sum. Note the total number of terms in the second sum is $2 \times_{n-1} C_2$, since there are ${}_{n-1}C_2$ ways to choose two values for i, j, but any choice for i, j is

equivalent to making the same choice for j, i. Simplifying this equation yields.

$$\begin{aligned}\langle x_n x_n \rangle &= (n-1)\left(\frac{4}{N(N+2)}\right) + (n-1)(n-2)\left(\frac{2}{N(N+2)}\right) \\ &= \frac{2n(n-1)}{N(N+2)}\end{aligned} \tag{7.17}$$

as desired.

Bibliography

[1] Planck 2018 results, X. Constraints on inflation. Astronomy and Astrophysics, 641, A10 (2020)

[2] W. H. Kinney, Physical Review D, 72, 023515 (2005)

[3] M. Douglas, Universe, 5(7), 176 (2019)

[4] https://www.universetoday.com/36302/atoms-in-the-universe/ Retrieved 19 October 2020.

[5] A. Vilenkin, *Many Worlds in One*, Hill and Wang, 2007. ISBN: 9780809067220

[6] N. Arkani-Hamed, L. Motl, A. Nicolis, and C. Vafa, Journal of High Energy Physics, 2007, 060 (2007)

[7] A. Aazami and R. Easther, Journal of Cosmology and Astroparticle Physics (0603:013), 2006

[8] E. Wigner, Annals of Mathematics, 62, 548-564, 1955.

[9] E. Wigner, Annals of Mathematics, 67, 325-328, 1958.

[10] X. G. Chen, G. Shiu, S. Yoske and S.H. Henry Tye, Journal of High Energy Physics, 26, 2012

[11] D. Battefeld, T. Battefeld, S. Schulz, Journal of Cosmology and Astroparticle Physics, 06:034, 2012

[12] A. J. Bray and D. S. Dean, Physical Review and Letters, 98, 150201, 2007

[13] D. S. Dean and S. N. Majumdar, Physical Review and Letters, 97, 160201, 2006

[14] D. S. Dean and S. N. Majumdar, Physical Review E, 77, 041108, 2008

[15] S. N. Majumdar, C. Nadal, A. Scardicchio and P. Vivo, Physical Review and Letters, 103, 220603, 2009

[16] S.-H. Henry Tye, J. J. Xu and Y. Zhang, Journal of Cosmology and Astroparticle Physics, 04:018, 2009

[17] J. Frazer and A. R. Liddle, Journal of Cosmology and Astroparticle Physics, 02:026, 2011

[18] H. Ooguri and C. Vafa, Nuclear Physics B, 766, 1–3, 2007

[19] G. Obied, H. Ooguri, L. Spodyneiko, and C. Vafa, arXiv:1806.08362, 2018

[20] P. Agrawal, G. Obied, P. J.Steinhardt and C. Vafa, *Physics Letters B*, 784, 2018

[21] S. K. Garg, and C. Krishnan, Journal of High Energy Physics, 75, 2019

[22] N. Agarwal, R. Bean, L. McAllister and G. Xu, Journal of Cosmology and Astroparticle Physics, 09:002, 2011

[23] T. Bjorkmo and M.C. David Marsh, Journal of Cosmology and Astroparticle Physics, 02:037, 2018

[24] T. Bjorkmo and M.C. David Marsh, Journal of Cosmology and Astroparticle Physics, 12:022, 2018

[25] Y. H. He, V. Jejjala, L. Pontiggia, Y. Xiao and D. Zhou, International Journal of Modern Physics A, 34, 17, 1950084, 2019

[26] M. C. D. Marsh, L. McAllister, E. Pajer and T. Wrase, Journal of Cosmology and Astroparticle Physics 11:040, 2013

[27] B. Freivogel, R. Gobbetti1, E. Pajer and I.S. Yang, arXiv:1608.00041, 2016

[28] A. Masoumi, A. Vilenkin and M. Yamada, Journal of Cosmology and Astroparticle Physics, 12:035, 2017

[29] F. J. Dyson, Journal of Mathematical Physics, 3, 1191, 1962.

[30] B. Greene, D. Kagan, A. Masoumi, D. Mehta, E. J. Weinberg and X. Xiao, Physical Review D, 88, 026005, 2013

[31] A. Masoumi and A. Vilenkin, Journal of Cosmology and Astroparticle Physics, 03:054, 2016

[32] R. Easther, A. Guth and A. Masoumi, arXiv:1612.05224, (2016)

[33] D. Marsh, L. McAllister, and T. Wrase, Journal of High Energy Physics, 2012, 102, 2012

[34] M. Yamada and A. Vilenkin, Journal of High Energy Physics, 2018, 29, 2018

[35] M. Dias, J. Frazer and M.C.D. Marsh, Physical Review and Letters, 117, 141303, 2016

[36] M. Dias, J. Frazer and M.C.D. Marsh, Journal of Cosmology and Astroparticle Physics, 01:036, 2018

[37] S. Winitzki, *Eternal Inflation*, World Scientific. (2009) ISBN 978-0-359-79133-0

[38] P. K. Jain and K. Ahmad, *Functional Analysis* (2nd ed.). (1995) New Age International. p. 203. ISBN 81-224-0801-X.

[39] Chappers (https://math.stackexchange.com/users/221811/chappers), Computing Fourier transform of power law, URL (version: 2019-11-27): https://math.stackexchange.com/q/2174387

[40] Planck 2018 results, VI. Cosmological parameters. Astronomy and Astrophysics, 641, A6, 2020

[41] A. R. Liddle & D. H. Lyth, *Cosmological Inflation and Large-Scale Structure.* (2000) Cambridge University Press, ISBN 0-521-66022-X

[42] W. H. Kinney, New Astronomy Reviews, 47, 11–12, 2003

[43] P.A.R Ade et al., BICEP2/Keck and Planck collaborations, Physical Review Letters, 114, 101301, 2015

[44] W. Taylor and N. Y. Wang, Journal of High Energy Physics, 2015, 164, 2015

[45] Y. V. Fyodorov and C. Nadal, Physical Review Letters, 109, 167203, 2012

[46] Y. V. Fyodorov, P. L. Doussal, A. Rosso and C. Texier, Annals of Physics, 397, 1-64, 2018

[47] G. Wainrib and J. Touboul, Physical Review Letters, 110, 118101, 2013

[48] J. R. Ipsen and A. D. H. Peterson, Physical Review E, 101, 052412, 2020

[49] M. R. Douglas, B. Shiffman, and S. Zelditch, Communications in Mathematical Physics, 252, 325-358, 2004

[50] R. Bousso and J. Polchinski, Journal of High Energy Physics, 06 006, 2000

[51] R. Feng, Transactions of the American Mathematical Society, 371, 5247-5265, 2019

[52] A. Weinrib, and B. I. Halperin, Physical Review B, 26, 1362-1368, 1982

[53] M. R. Dennis, European Physical Journal: Special Topics, 145, 191-210, 2007

[54] J. M. Bardeen, J. R. Bond, N. Kaiser, and A. S. Szalay, Astrophysical Journal, 304, 15-61, 1986

[55] Y. V. Fyodorov and I. Williams, Journal of Statistical Physics, 129, 1081-1116, 2007

[56] B. Schellekens, The String Theory Landscape, Hannover, 5 February 2014. https://www.nikhef.nl/ t58/Presentations/Hannover.pdf

[57] M. Tristram et al., Astronomy and Astrophysics, 647, A128, 2021

[58] A. Vilenkin, Physical Review Letters, 72, 20, 3137-3140, 1994

[59] S. Tsujikawa, Classical and Quantum Gravity, 30, 214003, 2013

[60] Wolfram Research (1996), HypergeometricPFQRegularized, Wolfram Language function, https://reference.wolfram.com/language/ref/HypergeometricPFQRegularized.html. Accessed April 2021.

[61] U. H. Danielsson and T. Van Riet, International Journal of Modern Physics D, 27, 12, 1830007, 2018

[62] H. Ooguri, E. Paltic, G. Shiu and C. Vafa, Physics Letters B, 788, 2019